Department of Precision and Microsystems Engineering

Machines with high accuracy on factory floors

M.A. Boogaard

Report no : EM 12.005
Coach : dr.ir. G.W. van der Poel
Professor : prof.dr.ir. D.J. Rixen
Specialisation : Engineering Dynamics
Type of report : Master of Science thesis
Date : 2 March 2012

Machines with high accuracy on factory floors
Prediction of the coupled dynamics, using dynamic substructuring

Master of Science Thesis

For obtaining the degree of Master of Science in Engineering
Dynamics at Delft University of Technology

M.A. Boogaard

2 March 2012

Faculty of Mechanical, Maritime and Materials Engineering (3mE) · Delft University of Technology

The work in this thesis was supported by Philips Innovation Services.

Abstract

This thesis will propose a new method to predict the response of sensitive equipment, once it is installed on the factory floor.

Currently, only the stiffness of the floor is taken into account when the dynamic response of a machine on a floor is predicted. To improve these methods, a short literature survey is done about the dynamics of factory floors. From this survey it follows that a floor is better characterised by an SDOF oscillator. To use this characterisation in practice, dynamic substructuring will be used. With dynamic substructuring it is possible to predict the coupled response of a machine, when the dynamic response of the floor is known. This could either follow from a detailed model or from a measurement. In this thesis it is shown how this should be done with measurements.

This dynamic substructuring can be easily extended to improve the method to predict the response of the machine to the vibrations of the floor. It is found that an equivalent system can be defined which predicts the floor vibrations more accurately. This method is again based on a dynamic measurement of the floor, as well as the free vibration level of the floor.

In the second part of this thesis, the theory is validated with an experiment. First it is shown how to obtain the dynamic response of the floor from impact measurements. It is found that a floor typically has a lot of damping, which damps the response quickly. This limits the achievable frequency resolution. Also problems are encountered with harmonic vibrations of a floor, which appear as a resonance, and the combination of the low response and an exponential window, which might cause an artificial anti-resonance.

These measurements are than used to predict the coupled response of a test case. This prediction is also validated with a validation measurement. It was found that these floor measurements together with the dynamic substructuring predicts the coupling very well. The proposed method to predict the coupled vibration level of the floor could however not be validated with this experiment.

When the results obtained with the dynamic subtructuring are compared with the results as obtained with the existing methods, it is found that dynamic substructuring improves the prediction very much.

Acknowledgements

When I started working on this thesis, I did not know where it would end exactly. Now that it is finished, I am convinced that a proper solution is proposed for the problem I started with. Looking back, I wonder why I did not follow this route from the beginning, but I learned that doing research is an iterative process. That is why I want to thank Tjeerd van der Poel, who guided me through this process and returned my focus to the original problem, everything I came up with something fancy. Although you think you did not spend enough time on my project, I think you have been a great supervisor.

I would also like to thank prof. Daniel Rixen. I would not only thank you for all the time you spend on this project and answering the numerous questions I had, but I would also like to thank you for your inexhaustible enthusiasm about the topic of dynamics. During my minor I was lucky that you replaced prof. Van Keulen as a lecturer and since than I decided that I want to learn more about dynamics.

Furthermore I would like to thank Gert van Schothorst at Philips for providing the opportunity to do this project. I wish to thank also Chris Basten en Krijn Bustraan, for helping me with the realisation of the experiments. Furthermore I would like to thank everyone who has shown interest in what I was doing and provided me some sort of advice, both at the TU Delft and at Philips.

I would like to thank my family and especially my wife Jolien for their support and loving. Although he went missing in the end, I want to thank Pi Li for welcoming me almost every morning and providing bright ideas throughout the day.

Delft, The Netherlands — M.A. Boogaard
17 February 2012

Contents

Nomenclature

List of Symbols

$\boldsymbol{M}$	Mass matrix
$\boldsymbol{C}$	Damping matrix
$\boldsymbol{K}$	Stiffness matrix
$\boldsymbol{Y}$	Dynamic flexibility
$\boldsymbol{Z}$	Dynamic stiffness
$\boldsymbol{u}$	Dynamic response
$\boldsymbol{q}$	Generalized dynamic response
$\boldsymbol{f}$	External forces
$\boldsymbol{g}$	Internal connection forces
$\boldsymbol{B}$	Signed Boolean matrix
$\boldsymbol{L}$	Boolean localisation matrix
$\boldsymbol{\lambda}$	Lagrange multiplier

Abbreviations

DOF	Degree Of Freedom
FBS	Frequency Based Substructuring
FEA	Finite Element Analysis
FRF	Frequency Response Function
HFF	High Frequency Floor
LFF	Low Frequency Floor
OMA	Operational Modal Analysis
SCI	Steel Construction Institute

SDOF	Single Degree Of Freedom
TPA	Tranfer Path Analysis

Chapter 1

Introduction

In 1965 Gordon Moore stated that the number of transistors that can be placed inexpensively on an integrated circuit doubles approximately every two years. This trend has continued for more than half a century and although it is expected that this growth will slow at the end of 2013, the transistor density will still increase. This growth is made possible by the increasing accuracy of photolithographic machines.

This puts high demands on the performance of the photolithographic machines. The performance might be jeopardized by the disturbances from the factory floor it is placed on. On one hand, the internal dynamics of the machine will be different on different floors, such that the controller might not operate optimally. On the other hand, the performance will be disturbed by vibrations of the floor.

To further improve the performance of these machines, it is important to predict the dynamic coupling with the floor in an early stage of the design phase. Currently the floor is assumed to behave like a simple spring for each mount. This way, the mounting stiffness of the machine will change and the apparent floor stiffness depends on the number of mounts. Sometimes, even more mounts are added to the machine when it is found that the stiffness of the floor is too small.

For the vibrations of the floor, a maximum vibration level is specified. To analyse the response of the machine to these vibrations, they are simply applied to the mounts of the tool. At this stage the floor is assumed to be rigid.

1.1 Research goal

Nowadays, these methods are still used when designing photolithographic machines. Although it is not yet reported that a photolithographic machine failed, because of dynamic coupling, it will become important very soon. Furthermore, these design methods might be conservative, such that a machine can be designed much cheaper or a better performance can be achieved.

Since it is very time consuming to build a model of a building for each machine, a better technique has to be developed. Based on the problem of the dynamic coupling, the

following research question is defined:

Investigate the dynamic behaviour of factory floors and propose a method to properly predict the dynamic coupling between the machine and the floor it is placed on.

When the response of the machine to the vibrations of the floor is calculated, the floor is assumed rigid. When a better dynamic description of the floors is found, it can be used to improve this calculation. Therefore the second research goal is defined:

Develop a method to predict the new vibration level of the floor, based on the dynamic response and the free vibration level

In this goal, the *new* vibration level, is the vibration level of the floor with the machine installed.

For both these goals, it should be noted that it is very likely that the developed methods will increase the amount of work during the design phase. It should therefore be kept in mind when observing the results, if the improvements compensate for the extra work.

1.2 Thesis outline

This thesis is divided in a theoretical part and an experimental part. The theoretical part describes all the theory and some background that will be used for this thesis. After that, the theory will be experimentally validated with a simple test case. Finally some conclusions will be drawn and how these techniques can be applied on real cases

Theoretical

The scope of the theoretical part of this thesis is graphically shown in figure 1.1. The two green boxes are the main components for the coupling. The first part is the application, which in this case is sensitive machinery. The second part is the floor.

Machine dynamics The first chapter in this part will show some more detail about the applications for this thesis. The basic coupling technique as used nowadays will be shown and how this influences the dynamic response on these machines.

Floor dynamics Before a better coupling technique is proposed, some more detail about floor dynamics are given, such that the reader will have slightly better overview of what to expect from a floor. First, the general details will be discussed about the basic floor types and construction methods. After that the typical excitations will be discussed. The third part of this chapter will discuss the methods to quantify the vibration levels of the floor. Next the modelling techniques will be discussed shortly. This chapter will conclude with a section about experimental methods to measure the response of the floor.

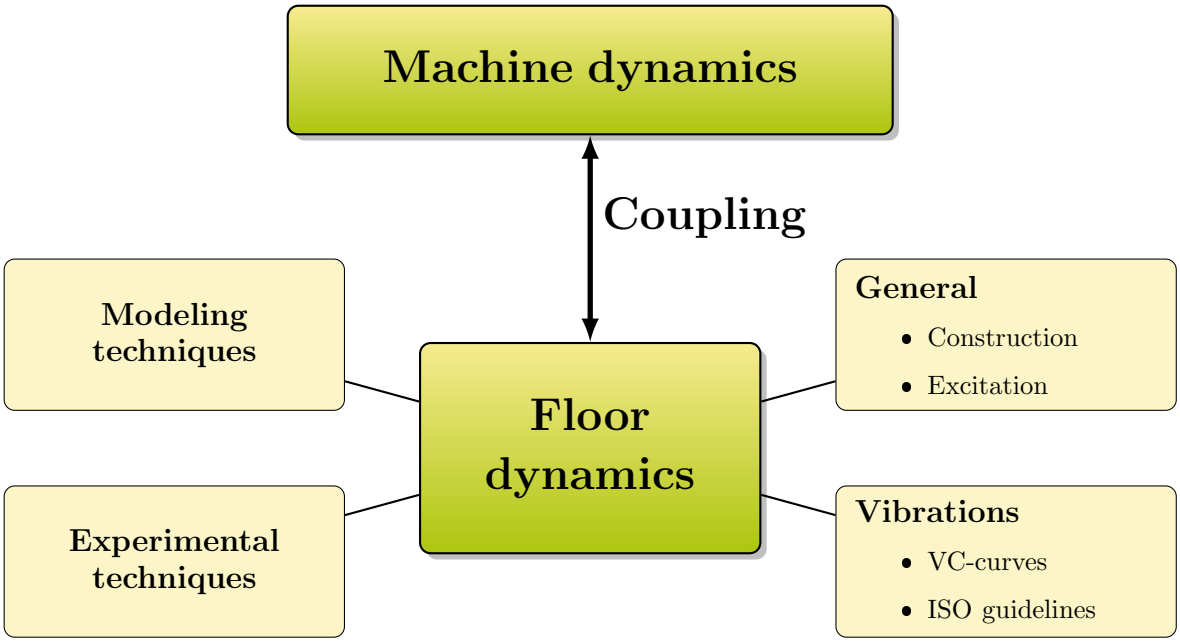

Figure 1.1: Graphical overview of thesis

Coupling Chapter 4 will discuss how the dynamic charerisation of the floor can be used to predict the coupled response. For this coupling dynamic substructuring will be used. Since the coupling will only be done in the frequency domain, this chapter discusses the theory behind Frequency Based Substructuring (FBS) and the experimental issues one might encounter by applying this technique. At the end of this chapter it will be shown how this technique can be used to predict the coupled response.

This technique has mostly been used to calculate the coupled dynamic response when the uncoupled response is known. However it is also possible to predict the vibration level of the floor when coupled if only the uncoupled vibrations are known. This is called *Ground Vibration Transmission* and will be discussed in chapter 5.

Experimental

To validate these techniques a test case has to be set up. This test case will be introduced in chapter 6. The coupling procedure to validate the proposed techniques is explained in chapter 7.

The most important component for the coupling is the response of the floor. The measurement and the settings will be discussed in chapter 8.

When this is all done, the coupled response can be measured and compared to the response as predicted with the FBS method. Also the ground vibration transmission will be validated. These results are shown in chapter 9.

Comparison and conclusion

The last part of this thesis contains the comparison with the existing techniques and conclusions on the improvement of this technique will be done. Also some recommandations will be given on how to apply this method and for further improvements on this method.

Part I

Theory

Chapter 2

Application

This chapter will give a short introduction about the essential parts of a photo lithographic machine. This will then be converted to an equivalent system which will be used to design a test case. The influence of the floor it is placed on, as calculated with the currently used methods, will also be shown on this system.

A schematic representation of the typical application is shown in figure 2.1.

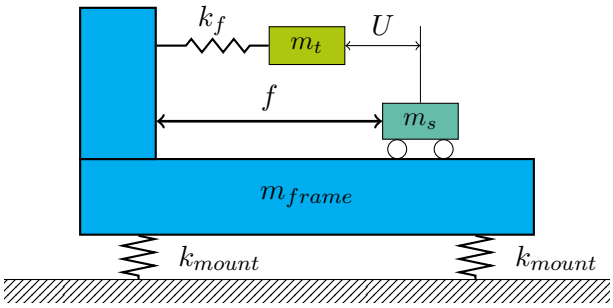

Figure 2.1: Typical sensitive machinery

In this figure the mass m_s represents the stage. The position is of this stage is controlled by a force that acts between the stage and the frame. The mass m_t represents a tool that is mounted to the frame with a certain frame stiffness k_f. This stiffness is typically as low as possible.

The distance U is the input for the controller that controls the force f. The error between this distance and a set reference actually determines the accuracy of this machine. When the controller accelerates or decelerates the stage, it applies a reaction force to the frame. Because this force is typically like a step function, it contains a lot of different frequencies. This force will probably excite the internal modes of the machine. When this force excites the eigenfrequency of the tool, the accuracy will be reduced. Furthermore, the vibrations of the floor will also excite the internal modes of the machine which will further decrease the accuracy.

The goal is to design such machine within the given specifications (accuracy, productivity, cost, etc). During the design process, the eigenfrequencies of this system can easily be

calculated and a proper controller can be designed such that the specifications are met. However when the machine is placed on the floor, the internal dynamics will change. It is therefore important to judge early in the design stage whether this coupling will adversely affect the achievable accuracy.

2.1 Basic model

To construct a basic model, the machine as shown in figure 2.1 is rotated to a vertical model. This is done, such that the main coupling effect will be in the translational movement, instead of the rotational. The basic model is shown in figure 2.4.

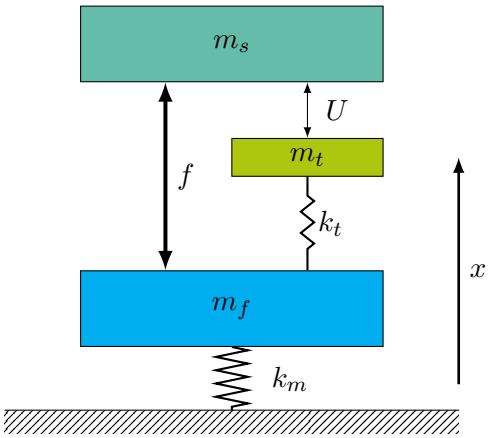

Figure 2.2: Simple model

In this figure the mass m_f represents the frame and mass m_t the tool. The mass m_s represents the stage and is *floating in space*. The position of the stage x_s is controlled by the force f and because this mass feels no damping or stiffness, the position is only dependent of the force f. Therefore, the error in U is only caused by the oscillations of m_t, so the mass m_s will be omitted and only the transfer function from the force acting on the frame to the displacement x_t is observed here.

The dynamic equation for this system is

$$\left(-\omega^2 \begin{bmatrix} m_f & 0 \\ 0 & m_t \end{bmatrix} + \begin{bmatrix} k_m + k_t & -k_t \\ -k_t & k_t \end{bmatrix}\right) \boldsymbol{x} = \begin{bmatrix} f \\ 0 \end{bmatrix} \tag{2.1}$$

In figure 2.2 no dampers are shown, but limit the amplitude at a resonance frequency, 1% damping is introduced for each isolated single DOF system. The response is evaluated with $m_f = 1500$ kg and $m_t = 100$ kg. The mounting stiffness $k_m = 15 \cdot 10^6$ N/m and $k_t = 50 \cdot 10^3$ N/m. The resulting magnitude plot is shown in figure 2.4.

2.2 Floor stiffness

A basic method, which is currently used, is to represent the floor with a simple spring. This is shown in figure 2.3.

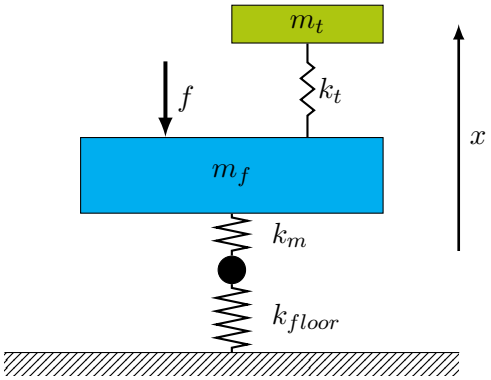

Figure 2.3: Simple model with floor stiffness

For this model, the mounting stiffness k_m and the floor stiffness k_{floor} can be substituted with an equivalent stiffness, given by

$$k_{equivalent} = \frac{k_m \cdot k_{floor}}{k_m + k_{floor}} \tag{2.2}$$

Typically the stiffness of a floor is around 10^8 $^{\mathrm{N}}/_{\mathrm{m}}$, so the equivalent stiffness is dominated by the floor stiffness. Modelling the floor like this, will result in a frequency shift of the second eigenfrequency. Because the equivalent stiffness is slightly less than the mounting stiffness, the second eigenfrequency will also be less.

In figure 2.4 the response for the fixed model, together with the response of the model with the additional floor stiffness is shown.

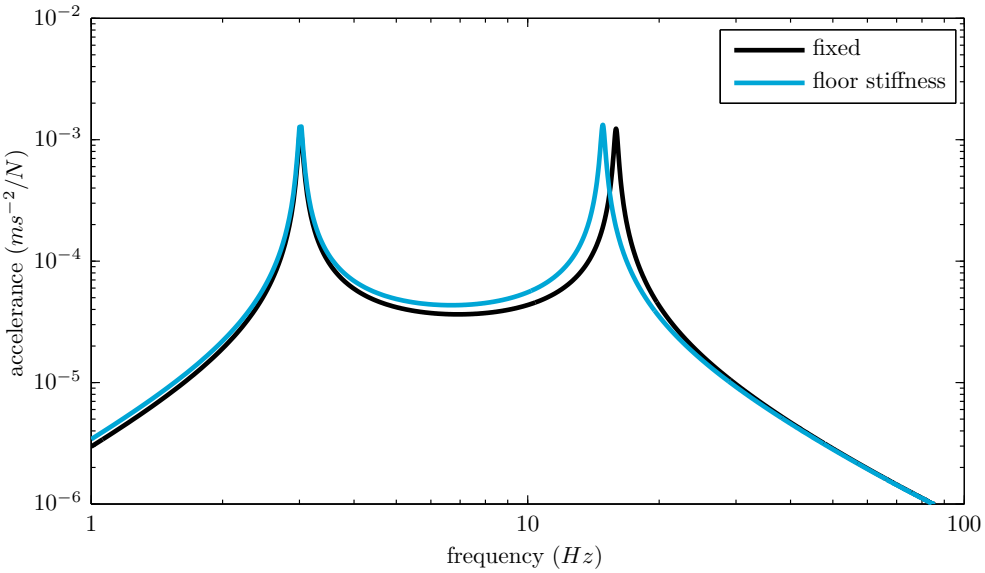

Figure 2.4: Response of x_t to f for fixed model and added floor stiffness

From this figure it is easy to see that the location of the second pole has shifted slightly. It should also be noted that for low frequencies, the stiffness is indeed slightly less. The

amplitude of the second mode has also changed, but not much conclusions should be drawn from this figure, because this might also depend on the frequency resolution at which equation 2.1 is evaluated.

From this simple model it is already clear that the dynamics of the floor are important for the accuracy of the tooling. Floor dynamics will be observed in the following chapter.

Chapter 3

Floor Dynamics

In the previous chapter it is assumed that a floor behaves like a spring. This is probably a very crude approximation. This chapter will discuss some general information about the characteristics of floors based on a literature review.

To estimate the behaviour of a floor, the technique of modal superposition is commonly used and advocated by several design codes, for instance by the Concrete Center [1] and by the Steel Construction Institute [2] (SCI). This technique, together with other more primitive techniques and Finite Element Analysis will be discussed in section 3.4.

Before a model can be made, the structure itself has to be observed. The two basic construction types are discussed in section 3.1. The excitation sources of a floor will be discussed in section 3.2.

This chapter will conclude with a section about measurement techniques.

3.1 Construction of floors

Basically there are two types of floor construction [3].

- **Slab on grade**: The floor slab is built directly on the soil subgrade. Slab on grade floors perform generally well in response to internal vibrations and are often used for factories. The performance is however only as good as the ambient conditions. To overcome this problem, some solution are presented to isolate the building from the ambient conditions [4], but these are all impractical. To properly analyse such a construction type, a good soil model is needed, as well as the properties of the soil.
- **Suspended slabs**: The floor slab is supported by a grid of columns. Suspended floors are much easier to excite than slab on grade floors, therefore these type of floors perform worse to internal vibrations. These floors are very frequently used, because a slab on grade can only be build on the first floor.

  For the suspended construction there are several options for the type of slab. The most ordinary is just a flat slab of concrete on concrete columns. For this type of

slab, both the stiffness and the weight depend on the thickness, so this type of slab is not ideal when the frequency response needs to be improved.

For sensitive laboratories and microelectronic fabrication plants, the waffle style slab is most commonly used. A cross-section of such slab looks like a row of T segments. These slabs are stiffer than flat slabs with the same weight. Some examples of waffle floors can be found in [3] and [5]. From these references it follows that these slabs can have a thickness up to 1 m and span a distance up to 7.32 m.

Although the floors carrying sensitive equipment are traditionally constructed using reinforced concrete, many new hospital buildings are made with some *office style* construction techniques. These are lightweight, composite methods, containing a steel framing with a concrete slab, such as the Corus' SlimDek floors [6]. There was a concern that due to the reduction in mass, this type of floors would not meet the stringent criteria. However it is shown in several publications that this type of construction can be successfully applied in hospitals. These floors can span a distance up to 9 m.

It is also possible to construct the floor entirely of steel. Although it is possible to meet very high vibration criteria, quite large truss structures are needed, as found by Amick et al. [3].

3.2 Excitation sources

The most severe source of excitation for floors is usually due to people walking on the floor [2]. There are other sources of excitation, but these are mainly depended on the machinery that is used.

3.2.1 Pedestrian excitation

A lot of research about walking forces is done in the field of biomechanics. For instance Kerr and Bishop [7] characterised a single footfall force and found that it typically depends on the walking speed.

Beside the walking speed, the footfall force also depends on the stride length, pace rate and the persons weight. Bertram and Ruina [8] did some research on the influence of different parameters on the walking force and came up with relations between the walking speed and the pacing frequency. Kerr [9] found it necessary to normalise the force with respect to the persons weight, height en pace rate, but mostly the force is given as a function of the pacing frequency and normalised by the weight.

A reliable statistical description of normal walking frequencies was given by Matsumoto et al. [10], who investigated a group of 505 persons. They found that the frequencies followed a normal distribution with a mean pacing rate of 2.0 Hz and standard diviation of 0.173 Hz. Kerr and Bishop [7] found a mean pacing frequency of 1.9 Hz for a group of 40 people.

When it is assumed that these force is perfectly periodic and identical for both feet, it can be used to construct a continues time signal. During walking there are some instances

when both feet are on the ground, resulting in an overlapping between the left and right feet. This can cause a higher total peak force. While during running there are periods when both feet are off the ground, causing the total force to be zero.

Generally a single footfall excitation force can be represented in time by a Fourier series

$$F_p(t) = G + \sum_{n=1}^{N} G\alpha_n \sin(2\pi n f_p t - \phi_n) \tag{3.1}$$

where G is the person's weight in Newton, α_n the Fourier coefficient of the nth harmonic, f_n is the activity rate in Hertz, n the order number of the harmonic, ϕ_n the phase shift of the nth harmonic. From the representation in equation 3.1, it is clear that a footfall force can easily be represented in the frequency domain.

Based on this formula, many researchers have tried to quantify the Fourier coefficients α_n, as well as the number of harmonics needed to properly reconstruct the time signal by this series. Kerr [9] showed that with 5 harmonics the Fourier series was very similar to the original force and with 10 harmonics it was practically indistinguishable by eye. Most researchers however quantified only up to the first four harmonics. Some used constant coefficients, while others propose coefficients as a function of the activity frequency. Zivanovic et al. [11, Table 1] produced a nice overview of the coefficients found by different researchers.

Some researchers also investigated the Fourier coefficients for groups [11] and found that the average coefficients for the second, third and fourth harmonic are less for groups then a single person.

It is commonly agreed that a footfall force contains most of its energy below 10 Hz. This boundary is the origin of the classification *High Frequency Floor* (HFF). If the first natural frequency of a floor is above 10 Hz, this is called an HFF. These floors are typically used in hospitals, laboratories and factories.

If the first eigenfrequency of the floor is below 8 Hz, this floor is called a *Low Frequency Floor* (LFF). These floors are typically found in offices and bridges. When the first eignfrequency is between 8 and 10 Hz, there is no such classification, so the calculations of the response should depend on its application. However it is found that the first eigenfrequency is either between 2 to 5 Hz for LFF or above 10 Hz for HFF.

One relatively new technique is to represent a footfall by an impulse. This method originates in the fact that an LFF shows a resonant response to the low frequency content of a footfall excitation and an impulsive response to the high frequency content. So for an HFF, the response to a footfall excitation is always impulsive.

The most common version of this method is also known as *Arup's effective impulse* and is proposed by Willford et al. [12]. He found that a footfall force can be represented by

$$I_{eff} = 54\frac{f_p^{1.43}}{f_n^{1.3}} \tag{3.2}$$

where f_p is the pacing frequency and f_n is the frequency of the mode under consideration. The coefficients are determined by feeding measured footfall forces into an SDOF oscillators in a range of frequencies. By taking the resulting peak velocity as the impulse for that floor/pacing frequency combination he found the best fit relationship. The SCI used a different version of the impulse method.

3.2.2 Other excitation sources

Beside pedestrian excitation, there is also mechanical excitation. This excitation is caused by the installed machinery.

The generated force and its characteristics should follow from the specification as given by the manufacturer or should follow from a model. Because this strongly depends on the case, nothing can be said about this excitation in general.

As a last excitation source there is also a random excitation. These excitations are for instance caused by wind blowing against the building, by turbulence in the piping system, a highway that is located nearby or by an earth quake.

3.3 Vibration criteria

As found in [13] the original design criteria for floors were determined by an Ultimate Limit State (ULS). This gives a boundary for the static deflection, such that the finishes would not crack. When the floor vibrations became more important, the problem was still limited to perception by humans. Although humans are not the topic of this thesis, a short overview is given in section 3.3.1. More information about the perception of vibrations by humans can be found in [14] and [11].

Since the guides for the human perception of vibrations are not suitable as criteria for sensitive machinery, Bolt Barenek and Newman Inc. attempted to create a generic set of Vibration Criteria for sensitive machinery [15]. These are commonly known as the VC-curves and will be discussed in more detail in section 3.3.2. These criteria are the most commonly known criteria, but it has a few drawbacks, therefore there are also some other criteria proposed, but these are not as generic as the VC-curves. These will be discussed in section 3.3.3.

3.3.1 Humans

The reaction of humans to vibrations is a very complex issue, having in mind that humans are *the greatest variables with which anyone may deal.* It is found that not only different people react differently to the same vibration conditions, but also an individual exposed to the same vibrations on different days will likely react differently [11].

Probably one of the earliest work was by Reiher and Meister [16]. They investigated the effect of harmonic vibrations on ten people having different postures (laying, sitting, standing) on a test platform driven by different amplitudes, frequencies and direction of vibrations. As a result they classified the human perception into six categories and as a function of vibration amplitude and frequency.

These classification have evolved over the years and resulted in a lot of different international standards. For instance in the United Kingdom the standard is defined in BS 6472. In this standard an isoline for the smallest accelerations a human can perceive is given.

Based on this definition, a response factor is defined. This is a multiplication factor of the isoline and gives an indication of the vibrations a human perceives. This response factor

is calculated by summing the accelerations for each harmonic of the footfall excitation. The response factor for office floors range from 2 to 6, while for hospitals the response factor is between 0.25 and 0.60 [2].

For LFF the response is calculated as an harmonic response. Mostly this is directly given as an acceleration. For an HFF the response is calculated as an impulse response. This is typically a velocity. To compare these situations, the isoline can simply be divided by $2\pi f$ to obtain the velocity isoline.

3.3.2 BBN VC-curves

During the 1970's Bolt, Barenek and Newman (BBN) started working on the problem of excessive vibrations of floors for sensitive machinery. Back then it was not clear how to represent the vibration acceptance criteria. Based on data from facilities before and after vibration problems were solved, BBN created sensitivity curves which were published in 1992 [15]. These are shown in figure 3.1 and also in table 3.1. In table 3.1 the typical applications and general accuracy are also given for each criterion [1].

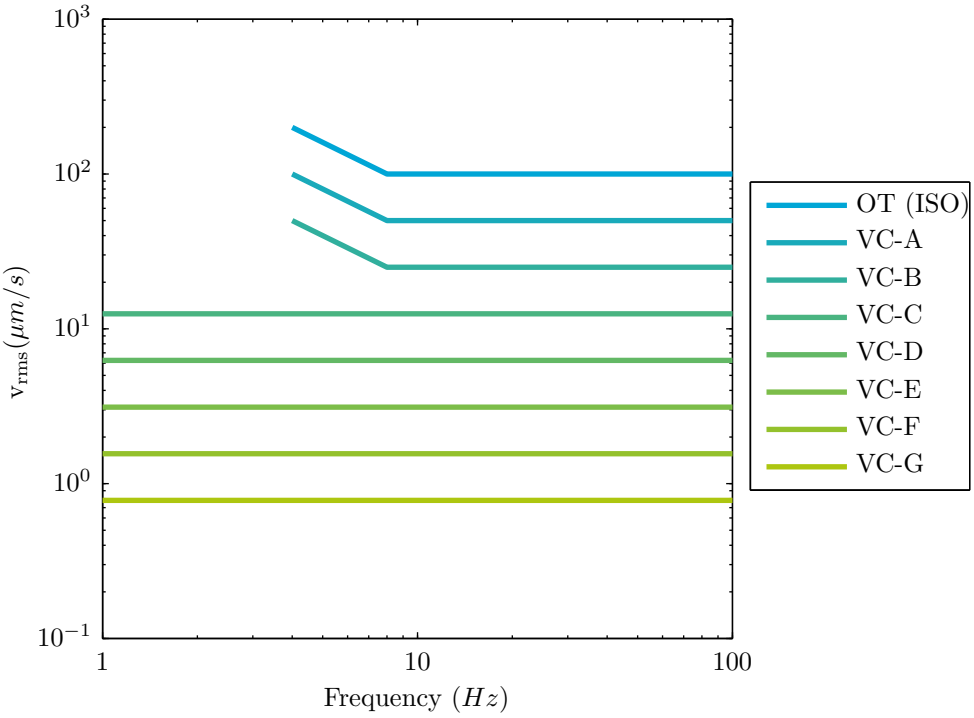

Figure 3.1: Generic vibration criteria

The vibration criteria as given in figure 3.1 are already the updated versions from 2005 [17]. The initial VC-curves all had the same shape and VC-F and VC-G did not exist in 1992. Note that the least stringent curve is not defined by BBN, but is the vibration criterion as defined by ISO for an operating theatre. This is also the same as the isoline for human perception (section 3.3.1), but now in velocity instead of acceleration.

To quantify the vibration level of a floor, the RMS velocity should be below a specified line. The criteria F and G are not listed in table 3.1, because they are only for evaluation purposes. The ambient vibration level of the earth is almost VC-E, so it is very difficult to reach the criteria below this.

For these criteria a few things should be noted.

- BBN found that velocity criteria appear constant for a class of machine with respect to frequency. These criteria are also focussed on photographic processes, so the quality is determined by the blurring. This is defined as the distance travelled during exposure, which is related to the velocity. If one wants to have accelerations or displacements, it is only one integration or differentiation step.

- These criteria are defined in a one-third octave frequency band. There are multiple reasons for that.

  1. The first reason was the availability of measurement equipment. At the time of the early studies, an FFT analyser was not commonly available, but one-third octave band *real-time* analysers were. However this reasoning is obsolete by now. Nowadays a one-third octave frequency spectrum is calculated as a post processing step.
  2. From a conservative view of damping, it follows that increased damping values widens the resonance peak. Therefore it will be excited by a range of frequencies around its natural frequency. The relation between the damping and the with of the peak is given by [13, 15]

     $$\zeta = \frac{x}{2\omega_r}$$

     where x is the half power (-3dB) width of the resonance peak and ω_r is the natural frequency. From this equation it is easy to see that the bandwidth is proportional to the natural frequency for constant damping.
  3. When the vibration of a floor is evaluated with a narrow bandwidth, typically a lot of tonal information is found for the high frequencies. Given the fact that most real-life vibration environments are dominated by broadband energy much more than by discrete (tonal) energy that is concentrated at one or several frequencies, it makes more sense to use a broadband representation of the vibrations.

- The VC curves are also defined as the root mean square (RMS) of the velocity. This will average out any unusual peak from a time history. The RMS value is defined as

  $$v_{RMS} = \sqrt{\frac{1}{T}\int_0^T v(t)^2\,dt} \tag{3.3}$$

  Based on this definition it is clear that the RMS velocity highly depends on the time T for decaying and non-stationary signals. According to Brownjohn and Pavic [18], values as low as 1 second are appropriate.

Criterion	Max. v_{rms} level ($\mu m/s$)	Detail size (μm)	General use
Workshop (ISO2631)	800	NA	Distinctly perceptible vibration. Appropriate to workshops and non-sensitive areas.
Office (ISO2631)	400	NA	Perceptible vibration. Appropriate to offices and non-sensitive areas.
Residential day (ISO2631)	200	75	Barely perceptible vibration. Appropriate to sleep areas in most instances. Probably adequate for computer equipment, probe test equipment and low-power (20×) microscopes.
Operating theatre (ISO2631)	100	25	Threshold of perception. Suitable for intensive sleep areas. Suitable in most instances for microscopes to 100× and for other equipment of low sensitivity.
VC-A	50	8	Adequate in most instances for optical microscopes to 100×, microbalances, optical balances, proximity and projection aligners, etc.
VC-B	25	3	An appropriate standard for optical microscopes to 1000×, inspection and lithography to 3 micron line widths.
VC-C	12.5	1	A good standard for most lithography and inspection equipment to 1 micron detail size.
VC-D	6.25	0.3	Suitable in most instances for the most demanding equipment including electron microscopes and E-beam systems, operating in the limits of their capability.
VC-E	3.12	0.1	A difficult criterion to achieve in most instances. Assumed to be adequate for the most demanding of sensitive systems including long path, laser-based, small target systems and other systems requiring extraordinary dynamic stability.

Table 3.1: Generic vibration criteria

- It is agreed by most that the tools are sensitive to certain frequencies due to internal resonance. At these specific resonant frequencies the relative movements of the internal will be the greatest, therefore the sensitive machinery will have different sensitivity at different frequencies. That is why a frequency spectrum is used instead of a time history signal for this vibration criteria.

In the early form, all the VC criteria were defined in a frequency range between 4 and 100 Hz. This was mainly because most tool manufactures did not impose a vibration criteria below 5 Hz. The upper bound is chosen, because there is significant evidence that frequencies above 100 Hz rarely causes problems [19]. Based on the same experience the criteria are less stringent below 8 Hz, because there is usually no chance of resonance below this frequency, so the criteria can be less stringent.

Due to the technological improvement in the microelectronic industry, the criteria from VC-C and below are now flat and the frequency range starts at 1 Hz. This is caused by the increasing use of pneumatic springs inside the tools. So it is suggested by Gordon [19] that the flat criteria be used if there are air springs used.

The main disadvantage of this vibration criteria is the use of the RMS velocity. Because the method averages out the peaks, which can cause disruption of the tool operation due to large but short transients.

The American Society of Heating, Refrigerating and Air-Conditioning Engineers (ASHRAE) uses the same vibration criteria, but with different notation.

3.3.3 Other criteria

Ahlin's equivalent peak velocity spectrum Another vibration criteria is developed by Ahlin [20]. Because most vibration criteria are defined for a sinusoidal excitation, sensitive equipment might still fail due to shocks.

The method of Ahlin is based on the idea of equivalence. For an SDOF oscillator it calculates the equivalent sinusoidal excitation such that the maximum displacement for both the transient and the sinusoidal vibrations are equal. This SDOF oscillator is basically a filter, so a *response equivalent peak velocity spectrum* for any vibration can be calculated by feeding this signal into a number of parallel filters, just like it is done in the one-third octave analysers.

The advantages of this method are clear. It works for every type of vibration, it is more accurate and it still works with the readily available vibration criteria as defined by manufacturers. It also does not average out the peaks. The drawbacks are also pretty clear. While the one-third octave analysers are readily available, there is no analyser that does this type of filtering directly. This method is also not as generic as the BBN-curves.

Receptance criteria Traditionally, photolithography tools were known as *steppers*, the tool stopped and was at rest during the exposure. The newest tools are known as *scanners*, they do the exposure on the fly, increasing production, but not allowing the tool to be at rest before the exposure. The floor must be stiff enough to resist the force of

the scanner as it is moving; as such some tool manufacturers specify receptance criteria. This defines how much the floor will displace with respect to force.

It has been seen that where a floor has passed the VC criteria, it can then fail the receptance criteria supplied from the manufacturer. These criteria are likely to become more significant in the future [13].

NIST There are also some other criteria. For instance the *National Institute of Standards and Technology* (NIST) criteria. There are only two of these defined, NIST-A and NIST-A1. NIST-A is almost equal to VC-E, but for frequencies below 20 Hz it is ever more stringent. NIST-A1 is generally a better than ambient criteria [17].

Medearis Medearis [13] also proposed a vibration criteria. He argues that the production costs are too high, due to the fact that velocity is used for the BBN criteria. He suggests a peak to peak displacement method combined with the static stiffness of the floor in the time domain. Displacement is used because a time history of velocity can be biased by high frequency components. To argue for displacement, he uses an example of damage due to excessive stress and, therefore, displacement. This method makes no sense as vibration problems are highly frequency dependent and are due to relative movements, not stresses. Spectra can also be converted between the three metrics [13].

3.4 Modelling techniques

To estimate the response, a couple of techniques are available. The most basic techniques are found in section 3.4.1, which are based on simplified formulas and empirically determined constants. These methods typically give a maximum velocity for one of the eigenfrequencies of the floor caused by walking excitation. A better description of a floor is given by its modal properties. There are also some guidelines developed to estimate these properties which will be given in section 3.4.2. Because computational power has become less expensive, Finite Element Analysis (FEA) has become more popular. This technique will be discussed in more detail in section 3.4.3.

3.4.1 Empirical methods

***kf*-method** In 1979 Ungar and White [21] proposed a very simply method for predicting the floor response. This method is based on measurement data of real footfall forces. Ungar and White used an SDOF oscillator and loaded it with the footfall force. Based on the maximum deflection of this oscillator, they found that the velocity for a harmonic response of the first eigenfrequency can be approximated by

$$v_{max} \approx \frac{\pi F_{peak}}{t_0^2 k f_n} \tag{3.4}$$

where F_{peak} is the peak force, k the static stiffness in the middle of a bay and M is the *participating mass*. This method is slightly altered by Amick et al. [3]. They approximate

the velocity by

$$v_{max} \approx \frac{C_w}{kf_n} \tag{3.5}$$

where C_w is an empirical constant based on the walkers weight and speed and should follow from the derivation as given by Ungar and White [21]. Amick et al. [3] also adopted this method to predict the response of the floor for mechanical excitation. The velocity is then predicted with

$$v_{max} \approx \frac{C_m}{k} \tag{3.6}$$

where C_m is empirical and should follow from statistical studies. This is off course a rather crude approximation.

Initially only the slab was considered with the kf-method. Amick et al. [3] showed a relation between the stiffness of the slab and the stiffness of the supporting columns. It is found that when the ratio $k_{slab}/k_{support}$ is less than 0.5, the error introduced by assuming rigid supports is only slight. When it exceeds 0.5, support stiffness must be considered. When the stiffnesses are equal, the error is a factor of 2. It should be noted that k_s should include both the column and footing stiffness.

Arup's effective impulse When the footfall is described by the impulse given in equation 3.2, the peak velocity of a single mode is given by

$$v_{max(i,j)} = \mu_i \mu_j \frac{I_{eff}}{M} \tag{3.7}$$

where μ_i and μ_j are the modeshape deflections of the response and the force point respectively. M is the modal mass of the mode under consideration.

The total response is then calculated by summing the contributions for different modes. To obtain the response directly in the one-third octave band, the summation should only be performed over the modes inside each frequency band. To obtain a proper time function from this method, the summation should at least be done over all the modes with a frequency up to twice the fundamental frequency.

Slab on grade Amick et al. [3] provides a little bit of information about slab on grade floors. Although the response of this type of floor cannot be easily predicted, the point stiffness is equal to

$$k = 8\sqrt{SD} \tag{3.8}$$

where S is the subgrade modulus and D is the plate rigidity. Commonly the plate rigidity is given by

$$D = \frac{Eh^3}{12(1-\nu^2)} \tag{3.9}$$

whereas the stiffness of a regular foundation can be simplified by

$$k = SA \tag{3.10}$$

where A is the area of the foundation. These values can then be used for the kf-method.

Some other methods for slab on grade floors are given by Chowdhury and Dasgupta [22]. These methods are typically based on equivalent spring models. The most common method is known as *Winkler springs*. Another method is used by for instance Ahn et al. [23] and Haifeng et al. [24]. For this method, the soil is modelled with an *elastic half-space* with a rigid massless foundation on top. With this technique, the dynamic properties of the soil can be estimated, but it is not used very often. According to Chowdhury and Dasgupta, this method can also be used in a Finite Element Analysis, when infinite finite elements are used.

3.4.2 Lumped Parameter

A very popular and easy way is to assume that a floor behaves like an SDOF oscillator. This is especially true for suspended type floors. The frequency response of an SDOF oscillator is shown in figure 3.2.

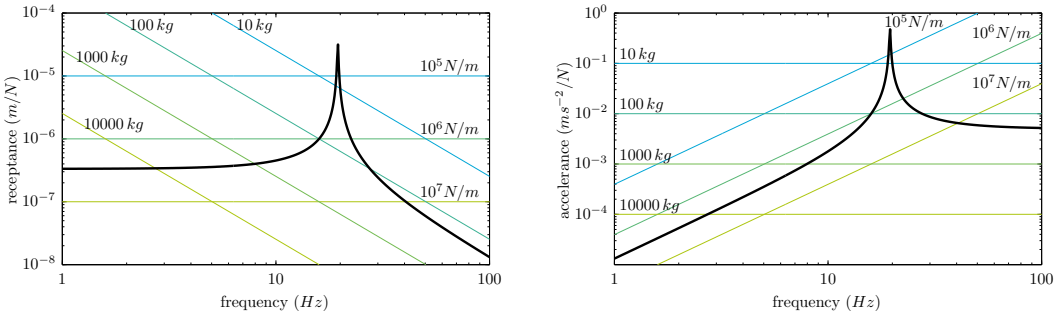

Figure 3.2: SDOF response

The response in both figures is equal, but it is measured in different quantities. The accelerance is obtained by multiplying the receptance by $-\omega^2$ and vice versa. This example shows that for low frequencies the stiffness is dominant and the higher frequency range is dominated by the mass.

These responses are generally characterised by its modal parameters. The natural frequency, together with the modal mass determines the stiffness. The modal mass is the mass that participates in the first modeshape. The modal damping determines the amplitude at a resonance frequency. Each of these elements will be discussed shortly with some methods to estimate the values.

Natural frequency

From the previous sections it has become clear that it is necessary to properly estimate the natural frequency. Not only is it the basis for the qualification of a floor, it is also important to predict the response.

- The most simple method is to assume the floor behaves like a beam. When the

equivalent mass and stiffness is known, the eigenfrequency is given by

$$f_n = \frac{K}{2\pi}\sqrt{\frac{EI}{mL^4}} \tag{3.11}$$

where L is the span of the floor and m is mass per unit length. K is a constant that is defined by the support of the beam and the mode number.

- To improve this method, a floor is assumed to behave like an isotropic plate. When this plate is simply supported, the fundamental eigenfrequency is given by

$$f_n = \frac{\lambda^2}{2\pi L^2}\sqrt{\frac{Eh^3}{12m(1-\nu^2)}} \tag{3.12}$$

where λ is the ratio between the length and the width of the plate. L is again the span of the floor and m is now the mass per unit area.

- When the midpoint stiffness and the mass is known, the fundamental frequency can be easily approximated by assuming a simple mass spring model. The eigenfrequency is then given by

$$f_n = \frac{1}{2\pi}\sqrt{\frac{k}{m}} \tag{3.13}$$

The mass and stiffness distribution is not always available. The eigenfrequency can also be approximated by making use of the static deflection. The static deflection is given by

$$\Delta = \frac{mg}{k} \tag{3.14}$$

When the static deflection is substituted in equation 3.13, the fundamental frequency is given by

$$f_n = \frac{1}{2\pi}\sqrt{\frac{g}{\Delta}} \approx \frac{18}{\sqrt{\Delta}} \tag{3.15}$$

This method is also known as the *self-weight deflection method*. The accuracy of this method depends on the similarity between the static deflection and the modeshape. It can be shown that this method makes an error of 11% for a beam and 22% for a plate. Due to this error, some people have tried to improve it by choosing a different constant [13].

- Another commonly used way to estimate the fundamental eigenfrequency, is by using *Dunkerly*'s formula. This is

$$\frac{1}{f_n^2} \approx \frac{1}{f_1^2} + \frac{1}{f_2^2} + \cdots \frac{1}{f_k^2} \tag{3.16}$$

where f_k are the frequencies of the different components, such as the beams and the slab.

Modal mass

Since a lot of methods that estimates the floor vibration are based on an SDOF oscillator, the mass of the floor that is participating in each mode has to be known.

Modal mass is obtained by summing physical mass contributions to total mass, scaled by the mode shape values. For a given modeshape and a mass defined as a function of position, the modal mass is defined by

$$M_n = \iint \phi_n^T(x,y) m(x,y) \phi_n(x,y) \mathrm{d}x\mathrm{d}y \tag{3.17}$$

where ϕ is the shape of the mode. Since the amplitude of the mode is not defined, any modal mass can be obtained. For obtaining the response of a floor, the commonly the modeshape is normalised such that the largest amplitude of a mode shape is equal to one. When the mass is equally distributed, this gives a modal mass of 0.5M for a beam and 0.25M for a plate, for the first eigenmode.

As stated earlier, this is a little different when the mass distribution is not known. Some design guides propose a method to approximate the modal mass by assuming a effective width and length. For instance, according to the SCI [2] design guide, the modal mass can be approximated by

$$M_n = mSL \tag{3.18}$$

where m is the mass per unit area and S and L are the effective length and width. They provide a table with different values for different construction methods.

According to Middleton and Brownjohn [13], the modal mass is the most important parameter for floors with a high fundamental frequency (above 20Hz).

Damping

The last modal parameter needed is the damping. Although damping is not that important for an HFF when only footfall excitations are observed, because a resonance response is not likely to occur. However the damping will play a part in reducing the RMS values of velocity, due to the decay during the averaging period. Furthermore, the when dynamic coupling occurs between the floor and the machine, the damping in the floor will dissipate energy from the machine.

Generally there are three types of damping, viscous, coulomb and hysteretic. Generally a structure is assumed to behave as if the damping is viscous.

Some attempts have been made to calculate the damping, but these methods are mostly impractical for design use or case specific. Damping can be obtained from measurements, but then the result is only a value such that the model fits the measurement, so they have a limited physical meaning.

Generally the design guides just propose a table with general damping values. A nice overview for different damping values is given in the design guide by The Concrete Center [1]. They state that an empty steel structure has a damping between 0.8% and 1.5%. Bare reinforced concrete floors typically have damping values between 1% and 2%. For a fully fitted floor, the damping is typically between 2% and 4.5%. The SCI [2] provides a similar table.

3.4.3 Finite Element Analysis

Although the FEA is relatively new in floor dynamics, both the SCI and the Concrete Centre provides some guidance on how to build a finite element model. Although it is generally more work to build a proper finite element model then to perform some basic hand calculations, there are also some advantages.

The current FEA are still based on the beam and shell models, so a Finite Element Model is build with beam and shell elements. The advantage is in the freedom to create any geometry and to use different connections between the shells and the plates. Typically the connections are pinned, but sometimes they are also fixed, which is only useful if the used beam element has a rotational stiffness.

It was also found by the Concrete Center that the stiffness of a floor not only depends on the columns it rests on, but also on the columns that supports the floor above. So if only a single floor is of interest, the columns for the second floor should also be incorporated, but the other ends of the beam can simply be fixed.

The connection between the slab and column can either be a point connection, such that the rotations are free, or a clamped connection. It depends on the construction methods used for the actual building what a better approximation is. There is however no consistency between different design guides about this connection.

3.5 Measurement techniques

To perform dynamic testing on a building floor is a bit harder then normal structural dynamic tests. Because of the size of the structure, a lot of energy is needed to provide a proper excitation, resulting in a poor signal to noise ratio. However some techniques to improve FRF data have been proposed by Gur et al. [25]. Furthermore, the testing has to be done *in-situ*, because it is normally not possible to remove the floor from a building and measure it separately. There are however some techniques that have been successfully used to test civil structures.

3.5.1 Operation Modal Analysis

One way to obtain some modal parameters of a floor is to use Operational Modal Analysis (OMA). This is also known as Output Only Analysis or Ambient Modal Analysis.

This technique measures the acceleration at several points. The relationship between the input $x(t)$ and the output $y(t)$ is given by

$$G_{yy}(i\omega) = H(i\omega)G_{xx}H^H(i\omega) \tag{3.19}$$

where $G_{xx}(i\omega)$ is the input power spectral density, which is a constant because it is assumed to be white noise. $G_{yy}(i\omega)$ is the output power spectral density and $H(i\omega)$ is the FRF. The ^{H} denotes the Hermitian transpose.

It is clear that this FRF is very sensitive to the noise level, which is generally unknown. From this FRF the eigenfrequency and the deflection shape can be obtained. This is not

the real modeshape, because the modal mass is not defined. Furthermore the input must be completely random. When there is any correlation between the input signals, it will be visible in the FRF as an resonance peak.

To properly scale the obtained FRF, there are several options. One method was discussed by Reynders et al. [26] and it uses both unknown and known input forces. With the known input, the obtained FRF can be scaled to obtain a proper FRF. This is known as OMAX.

Another option is add a known mass to the structure. Because of the change caused by the mass, the modal properties of the structure can be estimated.

3.5.2 Modal testing with an excitation force

When the excitation is known, the real FRF can be estimated directly. Basically there are two options to apply an excitation force, impulse or shaker excitation. Reynolds and Pavic [27] published a paper where they compare both methods and their preference.

Impact excitation

A very simple method to excite a structure is to hit it with a hammer. This can either be an instrumented with a force sensor, which is preferred, but it is also possible to use a sledge hammer with an accelerometer. When the mass of the head is known, the force can be calculated from the accelerations.

The advantage of this excitation is that it is generally fast, easy to set up and cheap. The disadvantages are also obvious. The biggest disadvantage is that a floor typically has a lot damping, so the response will be short. This affects the frequency resolution. Furthermore the impact is done by an operator who is present at the surface of the floor. Generally it is assumed that the mass of the operator can be neglected, but has to be as steady as possible after the impact and the excitation should be equal for every hit.

The biggest disadvantage is that with impact excitation, one has not much control over the frequency content of the impact. As shown in section 3.4.2, more energy is needed for low frequencies, therefore the impact point should be as soft as possible. For instrumented hammers, different tips are available. When sledge hammers are used, a rubber mat can be used at the location of impact. This will typically cause an input spectrum which is flat up to 200 Hz.

Shaker excitation

A more complex but more advanced method is to excite the structure with a shaker. These shakers have a large mass, which can be excited vertically. This can be placed on a floor free or fixed. When the shaker is used free, reaction masses can be added to increase the force limit.

With a shaker all the problems in the previous paragraph are solved. The excitation can be controlled for every frequency, so for instance the input spectrum can be equal to the inverse of the expected response. Furthermore the measurement block can be much

longer, so the frequency resolution can be improved. Also the impact is equal for every impact and the operators do not need to move during a measurement.

To further improve the shaker excitation method, multiple shakers can be used [2]. This changes the floor from a SIMO to a MIMO system. The advantage is that the excitation energy can be distributed more evenly over the floor area.

The disadvantages are also obvious. Using shaker excitation is not as fast, cheap and easy to set up and cheap as an impact excitation, but the quality of the measurements is much better.

Chapter 4

Coupling

As found in the previous chapter, a floor is better characterised with a mass, spring and damper than with only a spring. The model in figure 2.3 can therefore be updated by adding a mass and a damper. The coupled model is shown in figure 4.1.

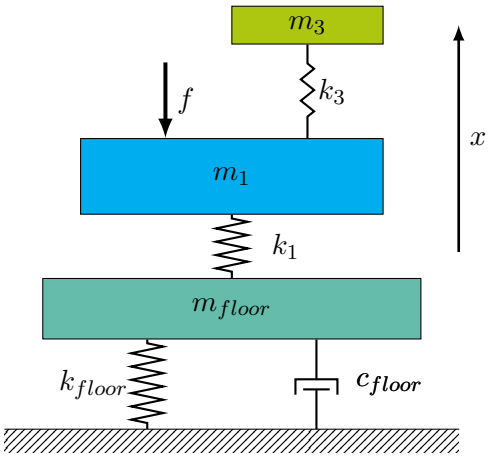

Figure 4.1: Test case with 1DOF floor with damping

The stiffness of the the floor is still 10^8 $^{\mathrm{N}}/_{\mathrm{m}}$, but the mass of the floor is set to 10 tonne and the damping is set to 5 %. The response of this model, together with the response of the models in chapter 2 is shown in figure 4.2.

From this figure it is found that for frequencies well below the second eigenfrequency of the machine or the eigenfrequency of the floor, the response is pretty well estimated when only the floor stiffness is taken into account. Around the second eigenfrequency things have changed dramatically. Both uncoupled frequencies were around 15 Hz.

For this model, an SDOF oscillator needs to be fitted on floor measurements. This is quite cumbersome to do for real floors and still does not solve the problem for multiple mounts, or other than translational modeshapes. To improve on this method, dynamic substructuring will be used. Dynamic substructuring has become very popular during

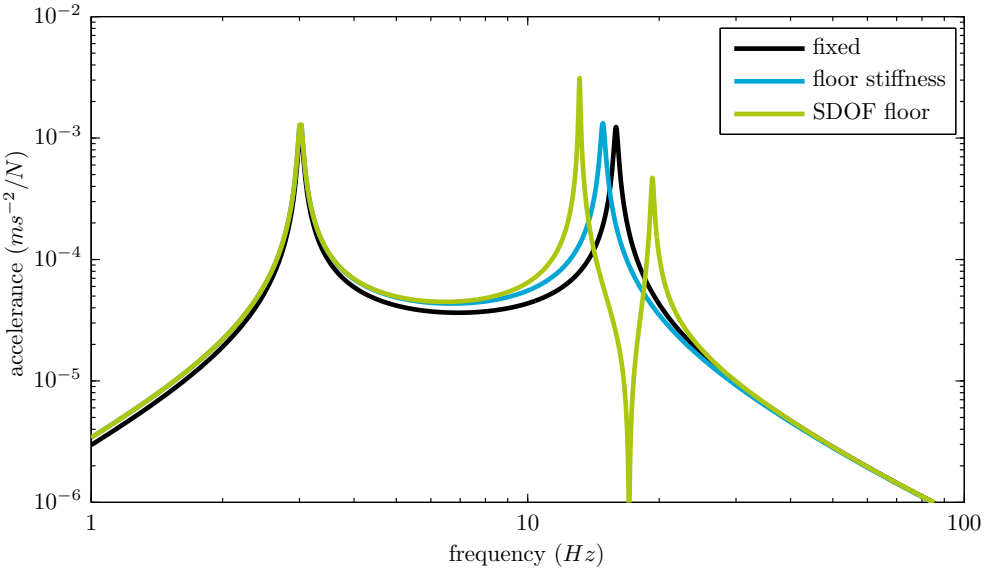

Figure 4.2: Magnitude plot for simple models

the recent years. For this technique a large structure is divided in several substructures which can be analysed separately and coupled. This technique has a lot of advantages.

- When a structure consists of several identical parts, this part can be analysed separately and then used as a *superelement* to analyse the total structure. For instance the blades of a wind turbine.
- If some components are very difficult to model correctly, it is better to measure them. These measurements can then be coupled to the total structure, for which a model exists. For instance the interior of a car.
- Substructures can be easily exchanged between different groups and companies. For instance in space engineering, where one company makes a satellite and another the launcher, the model of the satellite can be easily coupled to the launcher. A big advantage is that this is safe for both companies, because they only have to share a set of matrices that are condensed on the interface DOF, they are not revealing any secrets.
- For more computational efficiency, this technique also allows for a lot of model reduction techniques to be implemented successfully. For instance with the methods as proposed by Craig and Bampton or Guyan.

To represent a substructure there are two options, to represent it in the time domain or in the frequency domain. The time domain can be split in the physical domain and the modal domain. A very good overview of how to couple the substructures in the different domains is given by de Klerk et al. [30]. For this thesis only the coupling in the frequency domain will be used. In section 4.1 Frequency Based Substructuring will be explained, based on this overview.

To apply this techniques in an experimental setting, some other strategies might be needed. These will be discussed in section 4.2.

4.1 Frequency Based Substructuring

Consider a system as being described by its dynamic stiffness[1] $\boldsymbol{Z}$, which is defined as

$$\boldsymbol{Z}(j\omega) \triangleq -\omega^2\boldsymbol{M} + j\omega\boldsymbol{C} + \boldsymbol{K} \tag{4.1}$$

where the mass, damping and stiffness matrix can be obtained from the mechanical and geometrical properties of the system. The dynamic stiffness can also be obtained by inverting the dynamic flexibility, which can be easily measured. The equations of motion for a substructure s may then be written as

$$\boldsymbol{Z}^{(s)}(j\omega)\boldsymbol{u}^{(s)}(j\omega) = \boldsymbol{f}^{(s)}(j\omega) + \boldsymbol{g}^{(s)}(j\omega) \tag{4.2}$$

where $\boldsymbol{f}^{(s)}(j\omega)$ are the external applied forces and $\boldsymbol{g}^{(s)}(j\omega)$ are the forces from the neighbouring substructures. The explicit frequency dependency will be omitted for the remainder of this thesis.

For a number of substructures these equations can be rewritten in a block-diagonal format as

$$\boldsymbol{Z}\boldsymbol{u} = \boldsymbol{f} + \boldsymbol{g} \tag{4.3}$$

where this $\boldsymbol{Z}$ matrix has the different matrices of the substructures on its diagonal and the displacement and force vectors are column vectors with respectively the DOF for the different substructures and the forces acting on the different substructures.

In the displacement vector $\boldsymbol{u}$ all the interface DOF appear twice, because they are defined for every substructure. To ensure that the substructures are coupled, the compatibility condition is introduced. This is defined as

$$\boldsymbol{B}\boldsymbol{u} = \boldsymbol{0} \tag{4.4}$$

where $\boldsymbol{B}$ is a signed Boolean matrix which ensures that the distance between the coupled DOF is zero. Of course this is only that easy when the interface has a conforming mesh on both substructures. If this is not the case, $\boldsymbol{B}$ is no longer a signed Boolean matrix, but equation 4.4 still holds.

Beside compatibility, the interface forces on each substructure needs to be in equilibrium. The equilibrium condition is expressed as

$$\boldsymbol{L}^T\boldsymbol{g} = \boldsymbol{0} \tag{4.5}$$

where $\boldsymbol{L}$ is the Boolean matrix localizing the interface DOF of the substructure in the global dual set of DOF. This condition assures that the sum of the forces on each interface DOF is zero.

[1] There is little consistency in the terminology, but for this thesis the definitions as given by Ewins [31] are used. See appendix 11.2.3 for the definitions

So the total set of equations is given by

$$\begin{aligned} \boldsymbol{Zu} &= \boldsymbol{f} + \boldsymbol{g} \\ \boldsymbol{Bu} &= \boldsymbol{0} \\ \boldsymbol{L}^T\boldsymbol{g} &= \boldsymbol{0} \end{aligned} \tag{4.6}$$

This equation describes the coupling between any number of substructures with any number of arbitrary couplings. From this set of equations the coupled system can be obtained in either a primal or a dual way.

4.1.1 Primal formulation

In the primal formulation, a unique set of interface DOF is defined and the interface forces are eliminated as unknowns using the interface equilibrium. Mathematically this is given by

$$\boldsymbol{u} = \boldsymbol{Lq} \tag{4.7}$$

where $\boldsymbol{q}$ is the unique set of interface DOF and L is matrix defined by equation 4.5. Because of the definition of $\boldsymbol{q}$ it is obvious that the compatibility condition is satisfied for all $\boldsymbol{q}$, which is

$$\boldsymbol{Bu} = \boldsymbol{BLq} = \boldsymbol{0} \quad \forall\, \boldsymbol{q} \tag{4.8}$$

Actually, $\boldsymbol{L}$ represents the null space of $\boldsymbol{B}$ and vice versa. Because the compatibility condition is automatically satisfied, the total system is now given by

$$\begin{aligned} \boldsymbol{ZLu} &= \boldsymbol{f} + \boldsymbol{g} \\ \boldsymbol{L}^T\boldsymbol{g} &= \boldsymbol{0} \end{aligned} \tag{4.9}$$

Premultiplication of the first set by $\boldsymbol{L}^T$ and quoting that $\boldsymbol{L}^T\boldsymbol{g}$ equals zero, the primal assembled system is given by

$$\tilde{\boldsymbol{Z}}\boldsymbol{q} = \tilde{\boldsymbol{f}} \tag{4.10}$$

where the primally assembled dynamic stiffness and forcing amplitudes are given by

$$\begin{aligned} \tilde{\boldsymbol{Z}} &\triangleq \boldsymbol{L}^T\boldsymbol{ZL} \\ \tilde{\boldsymbol{f}} &\triangleq \boldsymbol{L}^T\boldsymbol{f} \end{aligned} \tag{4.11}$$

4.1.2 Dual formulation

In a dual formulation, all the boundary DOF are still present in the equation. To obtain the dual assembly, the equilibrium condition is satisfied a priori. This is obtained by choosing the interface forces in the form

$$\boldsymbol{g} = -\boldsymbol{B}^T\boldsymbol{\lambda} \tag{4.12}$$

where $\boldsymbol{\lambda}$ are Lagrange multipliers, corresponding to the interface forces.

By choosing the interface forces in this form, they act in opposite directions for any pair of dual interface DOF, due to the way the Boolean matrix $\boldsymbol{B}$ is constructed. The equilibrium condition is then given by

$$\boldsymbol{L}^T\boldsymbol{g} = -\boldsymbol{L}^T\boldsymbol{B}^T\boldsymbol{\lambda} = \boldsymbol{0} \tag{4.13}$$

Because $\boldsymbol{L}^T$ is the null space of $\boldsymbol{B}^T$, the equilibrium condition is always satisfied. So now the dual assembled system is given by

$$\begin{aligned} \boldsymbol{Z}\boldsymbol{u} + \boldsymbol{B}^T\boldsymbol{\lambda} &= \boldsymbol{f} \\ \boldsymbol{B}\boldsymbol{u} &= \boldsymbol{0} \end{aligned} \tag{4.14}$$

In matrix notation this is

$$\begin{bmatrix} \boldsymbol{Z} & \boldsymbol{B}^T \\ \boldsymbol{B} & \boldsymbol{0} \end{bmatrix} \begin{bmatrix} \boldsymbol{u} \\ \boldsymbol{\lambda} \end{bmatrix} = \begin{bmatrix} \boldsymbol{f} \\ \boldsymbol{0} \end{bmatrix} \tag{4.15}$$

Although the number of equations is not decreased, this method is still very popular. With this method the interface forces are also obtained and can be used to judge the quality of the coupling. This method is also the basis of a family of parallel solvers, known as dual Shur complement solvers. These solvers can for instance solve large problems more efficient on dual core processors.

Note that the formulation of equation 4.15 needs the dynamic stiffness $\boldsymbol{Z}$, where in experimental dynamics mostly the receptance matrix $\boldsymbol{Y}$ is obtained. This is defined as the inverse of the dynamic stiffness matrix. How to cope with this will be discussed in more detail in the next section.

4.2 Experimental frequency based substructuring

The coupling procedures as described in section 4.1 are both exact and equal for analytical models. In the experimental world, it is a bit different. In the physical domain, the coupling is equal to assembling the system matrices. These are impossible to obtain from an experiment, so this is never done in experimental substructuring. Generally the experimental substructuring is done either in the modal domain or in the frequency domain. When a modal fit is done on measurement data of all the substructures, it is equal to use the modes directly for the coupling, or to use the resynthesized FRFs. It is however much easier to incorporate the residuals when resynthesized FRFs are used. Because it is expected that it is not easy to perform a modal fit on a measured floor, the experimental substructuring will be done in the frequency domain. The problems one might encounter will be discussed in more detail in this section.

As stated in section 4.1, the coupling in the frequency domain is done with the dynamic stiffness matrix $\boldsymbol{Z}$. In general the dynamic flexibility (or receptance) matrix $\boldsymbol{Y}$ is measured, which is the inverse of the dynamic stiffness.

Consider the following two subsystems as given by their measured receptance matrices

$$Y^A = \begin{bmatrix} \boldsymbol{Y}_{ii}^A & \boldsymbol{Y}_{ic}^A \\ \boldsymbol{Y}_{ci}^A & \boldsymbol{Y}_{cc}^A \end{bmatrix} \qquad Y^B = \begin{bmatrix} \boldsymbol{Y}_{ii}^B & \boldsymbol{Y}_{ic}^B \\ \boldsymbol{Y}_{ci}^B & \boldsymbol{Y}_{cc}^B \end{bmatrix} \tag{4.16}$$

where the superscipt denotes the substructure and the subscript either the internal DOF or the coupling DOF.

Classically the coupling is done in a primal way, which results in [32]

$$\boldsymbol{q} = \tilde{\boldsymbol{Z}}^{-1}\boldsymbol{f} \tag{4.17}$$

where the assembled stiffness matrix is then defined as

$$\tilde{\boldsymbol{Z}} = \begin{bmatrix} \begin{bmatrix} \boldsymbol{Y}_{ii}^{A} & \boldsymbol{Y}_{ic}^{A} \\ \boldsymbol{Y}_{ci}^{A} & \boldsymbol{Y}_{cc}^{A} \end{bmatrix}^{-1} & \boldsymbol{0} \\ \boldsymbol{0} & \boldsymbol{0} \end{bmatrix} + \begin{bmatrix} \boldsymbol{0} & \boldsymbol{0} \\ \boldsymbol{0} & \begin{bmatrix} \boldsymbol{Y}_{cc}^{B} & \boldsymbol{Y}_{ci}^{B} \\ \boldsymbol{Y}_{ic}^{B} & \boldsymbol{Y}_{ii}^{B} \end{bmatrix}^{-1} \end{bmatrix} \tag{4.18}$$

From this definition it is clear that for two substructures already three inversions are needed. This is computationally inefficient and prone to severe error amplification. This method is also very sensitive to round off errors when the matrix is bad conditioned. This method is sometimes called *Impedance Coupling*.

In 1988, Jetmundsen et al. [33] reformulated the coupling to reduce the number of matrix inversions and calculated the coupled receptance matrix directly with

$$\tilde{\boldsymbol{Y}} = \begin{bmatrix} \boldsymbol{Y}_{ii}^{A} & \boldsymbol{Y}_{ic}^{A} & \boldsymbol{0} \\ \boldsymbol{Y}_{ci}^{A} & \boldsymbol{Y}_{cc}^{A} & \boldsymbol{Y}_{ic}^{B} \\ \boldsymbol{0} & \boldsymbol{Y}_{ci}^{B} & \boldsymbol{Y}_{ii}^{B} \end{bmatrix} - \begin{pmatrix} \boldsymbol{Y}_{ic}^{A} \\ \boldsymbol{Y}_{cc}^{A} \\ \boldsymbol{Y}_{ci}^{B} \end{pmatrix} \left(\boldsymbol{Y}_{cc}^{A} + \boldsymbol{Y}_{cc}^{B}\right)^{-1} \begin{pmatrix} \boldsymbol{Y}_{ic}^{A} \\ \boldsymbol{Y}_{cc}^{A} \\ \boldsymbol{Y}_{ci}^{B} \end{pmatrix}^{T} \tag{4.19}$$

It is clear that this formulation reduces the number of inversions from three to one. Furthermore the size of the matrix that needs to be inverted is now only defined by the number coupling DOF. This method can be generalized to couple any number of substructures. The only downside of this method is that a Boolean matrix is needed for every substructure and one global Boolean matrix. This method is generally known as *admittance coupling*.

In 2006 de Klerk et al. [34] formulated the FBS method with Lagrange Multipliers. When the first set of equation 4.15 is solved for $\boldsymbol{u}$, the following equation is obtained

$$\boldsymbol{u} = \boldsymbol{Y}(\boldsymbol{f} - \boldsymbol{B}^{T}\boldsymbol{\lambda}) \tag{4.20}$$

where $\boldsymbol{Y}$ is the block diagonal matrix with the receptance matrices of the different substructures. Substituting this equation into the second part and solving for $\boldsymbol{\lambda}$ results in

$$\boldsymbol{\lambda} = (\boldsymbol{B}\boldsymbol{Y}\boldsymbol{B}^{T})^{-1}\boldsymbol{B}\boldsymbol{Y}\boldsymbol{f} \tag{4.21}$$

When substituting equation 4.21 into equation 4.20, the following equation is obtained

$$\boldsymbol{u} = \boldsymbol{Y}\boldsymbol{f} - \boldsymbol{Y}\boldsymbol{B}^{T}(\boldsymbol{B}\boldsymbol{Y}\boldsymbol{B}^{T})^{-1}\boldsymbol{B}\boldsymbol{Y}\boldsymbol{f} \tag{4.22}$$

It is shown by de Klerk et al. [34] that this method is equal to the method as defined by Jetmundsen et al. [33]. From a computational point it is also equivalent, because there is still only one inversion needed of the same size. This method is called the *Lagrange Multiplier Frequency Based Substructuring* (LM FBS). This method however is much easier to apply, because only one Boolean matrix is needed and the receptance matrices of the substructures do not need to be partitioned.

4.2.1 Difficulties with experimental FBS

Because it is not possible to measure all the properties of a subsystem properly, there are some errors made in the coupling. Next the main difficulties will be discussed, as well as the solutions proposed in literature [30].

Truncation errors

A problem in experimental measurements is the modal truncation. Because the frequency range of the measurements is limited, not al the modal degrees of freedom, describing the substructures dynamics, are obtained from the measurements.

When all the modes are known (in theory there are infinite modes), the receptance is given by

$$\boldsymbol{Y}(j\omega) = \sum_{r=1}^{N} \frac{A_r}{\omega_r^2 - \omega^2} \tag{4.23}$$

From experiments only the modes m_1 to m_2 are obtained. When only these modes are used to represent the receptance, the substructure will behave more stiffly.

One way to compensate for this is called *residual flexibility* [31]. For the lower frequencies a residual mass M^R is defined and for the higher frequencies a residual stiffness is defined. These residuals are an approximation of the unmeasured modes. So now the receptance can be approximated by

$$\boldsymbol{Y}(j\omega) \cong -\frac{1}{\omega^2 M^R} + \sum_{r=m_1}^{m_2} \frac{A_r}{\omega^2 - \omega_r^2} + \frac{1}{K^R} \tag{4.24}$$

This should be taken into account when performing the coupling of modal substructures or when a modal identification is performed on the measurements to improve the quality of the FRFs for a frequency based substructuring. When the measured FRF data is used, the residuals are included naturally.

Rotational degrees of freedom

Because from measurements normally only translation data is obtained. When the interface is very flexible, rotational deformations are also important. For instance when one of the substructures is made of rubber and the interface area is small.

Basically there are two options to obtain the rotational information. The rotation can be measured directly, or the rotational data can be obtained from translations of the neighbouring DOF. When it is assumed that the surface has only local rigid body modes, the rotational information can be obtained from a minimum of six coupling DOF at three nodes [35]. This will only give good results up to frequencies where local deformation between the interface nodes starts to take place.

For the application in this thesis, it is expected that local rotations will not be a problem, since a floor will be quite stiff and the frequency region of interest is low. Global rotations will be important, but these will be measured automatically.

Continuity of the interface

For every application, the substructure interface is continuous in reality. Measurements describe the interface only on a discrete number of points. The region between the measured points can be reconstructed by assuming that the interface is rigid as a simple solution. A more complex way is to use finite element models to expand the measured DOF statically to the neighbouring DOFs.

Rigid body modes

Because the displacement of a structure is always a combination of rigid body modes and flexible modes, it is necessary to include the rigid body modes in the substructure. For frequency based substructuring the rigid body modes are obtained naturally. However, it should be taken into account when setting up the experiment.

Dynamics of joints

For dynamic substructuring, the coupling is most of the times ensured with equation 4.4. This is a very stiff compatibility condition which does not allow for coupling deformation. Another way is model the joints with linear flexibility [36].

Experimental errors

When dynamic substructuring is used with experimental data, the measurement errors will affect the coupled response. For instance Rixen [37] and Nicgorski and Avitabile [38] did some research on how measurement inaccuracies will pollute the assembled response.

For both the admittance coupling and the Lagrange Multiplier FBS, the interface flexibility $\boldsymbol{BYB}^T$ needs to be inverted. Because of this operation, small measurement errors can be significantly amplified. To quantify the error caused by this inversion, the condition number of the interface flexibility can be monitored.

The experimental data is obtained with a finite accuracy, because of multiple reasons. These are mainly caused by the physical limitations of the sensor, the test set-up or the finite accuracy of the digital acquisition system.

The case when a driving point can not be measured directly and therefore an approximation is used, was investigated by Nicgorski and Avitabile [38]. This is for instance the case when the impact location could not be in the same place as the accelerometer. For their test case it made almost no difference. This difference depends on the interface rigidity, which can be quantified by using for instance the technique as described in [35] or by checking the sign of the imaginary part of the FRF.

Another issue with FBS is the reciprocity of the measured FRF. This can for instance be violated with inaccurate sensor placement or alignment. Anti-resonances are very sensitive to the sensor location and the input location, but they determine a significant part the FRF.

When not all the desired data can be obtained from a single measurement, the modal basis for each experiment could change due to mass or stiffness loading from sensors or shakers. This might result in different poles for different FRFs or perturbed modeshapes. Rixen [37] investigated these two situations and showed that these errors can cause spurious peaks in the assembled receptance matrix.

Of course measurement noise is also a problem for the accuracy of the assembled matrix. Both Rixen [37] and Nicgorski and Avitabile [38] simulated some cases where the FRF of the substructure was polluted with noise. They both find that the noise was amplified in the assembled receptance matrix, especially for low frequencies. This also changed the amplitude of the resonances and the modeshapes. When the test object can not be measured free, for instance a floor, the measurement will also be polluted with mechanical vibrations that are present in the structure.

Also care should be taken to set up a test case. Especially for lightly damped structures, the suspension can have a large influence in the measured response.

To solve these problems, a lot of effort is spent on filtration techniques, using for instance singular value decomposition [39] or a modal parameter estimation. To perform a modal fit on the experimental data is very popular. This method solves a lot of problems, for instance the same poles are used for the every FRF, but only at the average frequency. Multiplicative noise is still contained in the fit, as well as the mass and stiffness loading. As stated before, care must be taken to accurately estimate the residuals, when performing the modal fit.

4.3 Coupled machine response

Reconsider the application as described in chapter 2. The receptance matrix is given by

$$\begin{bmatrix} \boldsymbol{u}_i^m \\ \boldsymbol{u}_o^m \\ \boldsymbol{u}_c^m \end{bmatrix} = \begin{bmatrix} \boldsymbol{Y}_{ii}^m & \boldsymbol{Y}_{io}^m & \boldsymbol{Y}_{ic}^m \\ \boldsymbol{Y}_{oi}^m & \boldsymbol{Y}_{oo}^m & \boldsymbol{Y}_{oc}^m \\ \boldsymbol{Y}_{ci}^m & \boldsymbol{Y}_{co}^m & \boldsymbol{Y}_{cc}^m \end{bmatrix} \begin{bmatrix} \boldsymbol{f}_i^m \\ \boldsymbol{f}_o^m \\ \boldsymbol{f}_c^m + \boldsymbol{g}_c^m \end{bmatrix} \tag{4.25}$$

where the subscripts i,o and c indicates the input, output and coupling DOF. The superscript m indicates that these entries are related to the machine, where superscript f will indicate that it is related to the floor. $\boldsymbol{f}$ are the externally applied forces and $\boldsymbol{g}$ is the force needed to couple this machine to the floor.

For this coupling, the compatibility and force equilibrium are given by

$$\begin{aligned} \boldsymbol{I}\boldsymbol{u}_c^m - \boldsymbol{I}\boldsymbol{u}_c^f &= \boldsymbol{0} \\ \boldsymbol{I}\boldsymbol{g}_c^m = -\boldsymbol{I}\boldsymbol{g}_c^f &= \boldsymbol{I}\boldsymbol{\lambda} \end{aligned}$$

where $\boldsymbol{I}$ is an identity matrix of the size of the coupling DOF. Substituting equation 4.25 into the compatibility condition and solving for $\boldsymbol{\lambda}$ yields

$$\left(\boldsymbol{Y}_{cc}^m + \boldsymbol{Y}_{cc}^f\right)\boldsymbol{\lambda} = -\begin{bmatrix} \boldsymbol{Y}_{ci}^m & \boldsymbol{Y}_{co}^m & \boldsymbol{Y}_{cc}^m \end{bmatrix} \begin{bmatrix} \boldsymbol{f}_i^m \\ \boldsymbol{f}_o^m \\ \boldsymbol{f}_c^m \end{bmatrix} - \begin{bmatrix} \boldsymbol{Y}_{ci}^f & \boldsymbol{Y}_{co}^f & \boldsymbol{Y}_{cc}^f \end{bmatrix} \begin{bmatrix} \boldsymbol{f}_i^f \\ \boldsymbol{f}_o^f \\ \boldsymbol{f}_c^f \end{bmatrix}$$

For this application, the response to a force somewhere in the building is not computed directly. To predict the disturbance from the forces inside a building, the technique as described in chapter 5 will be used. For this technique, it is not necessary to know the forces exactly, so the force vector $\boldsymbol{f}^f$ will be set to zero. Using the equilibrium condition, this result can be substituted into equation 4.25. The coupled response is then given by

$$\begin{bmatrix} \boldsymbol{u}_i^m \\ \boldsymbol{u}_o^m \\ \boldsymbol{u}_c^m \end{bmatrix} = \boldsymbol{Y}^m \boldsymbol{f}^m - \boldsymbol{Y}^m \begin{bmatrix} \boldsymbol{0} \\ \boldsymbol{0} \\ \boldsymbol{I} \end{bmatrix} \left(\boldsymbol{Y}_{cc}^m + \boldsymbol{Y}_{cc}^f \right)^{-1} \begin{bmatrix} \boldsymbol{Y}_{ci}^m & \boldsymbol{Y}_{co}^m & \boldsymbol{Y}_{cc}^m \end{bmatrix} \begin{bmatrix} \boldsymbol{f}_i^m \\ \boldsymbol{f}_o^m \\ \boldsymbol{f}_c^m \end{bmatrix} \tag{4.26}$$

From this equation, it follows that to predict the coupled response with FBS, the full matrix as shown in equation 4.25 is needed for the machine as if it is floating free. For the floor only the interface flexibility is needed.

Chapter 5

Ground vibration transmission

In section 4.3 it was described how the coupled response of the machine on the floor can be predicted, if the interface flexibility is known. Because the internal forces in the floor are generally not known, they were neglected. Because it is practically almost impossible to know all the forces that are of importance and to measure the transmissibility to the interface, another method had to be used which is known as *Tranfer Path Analysis* (TPA).

TPA was used by de Klerk and Rixen [40] to analyse the propagation of the forces inside the differential to the noise inside the car. For them it was not possible to measure the forces directly, so they used an equivalent system. It turned out that they had to fix the interface of the differential and measure the interface forces. When these forces are then applied on the interface of the assembled system, a system that is equivalent for what concerns the car body to the original problem is obtained.

This method, as well as a mathematical proof, is explained in more detail in appendix 11.2.3. This method depends on the fact that it should be possible to fix the interface. This is impossible for buildings, so an analogues method should be derived based on free interface data. This is done in section 5.1, which is based on a note by prof. D.J. Rixen. In section 5.2 it shown how this method can be used to predict the new vibration level of a floor.

5.1 Free interface

Observe a system that consists of two substructures A and B. The dynamics for both substructures are given by its dynamic flexibility as in

$$\begin{bmatrix} \boldsymbol{Y}_{ii}^A & \boldsymbol{Y}_{ic}^A \\ \boldsymbol{Y}_{ci}^A & \boldsymbol{Y}_{cc}^A \end{bmatrix} \begin{bmatrix} \boldsymbol{f}_i^A \\ \boldsymbol{f}_c^A \end{bmatrix} = \begin{bmatrix} \boldsymbol{u}_i^A \\ \boldsymbol{u}_c^A \end{bmatrix} \qquad \begin{bmatrix} \boldsymbol{Y}_{cc}^B & \boldsymbol{Y}_{ci}^B \\ \boldsymbol{Y}_{ic}^B & \boldsymbol{Y}_{ii}^B \end{bmatrix} \begin{bmatrix} \boldsymbol{f}_c^B \\ \boldsymbol{f}_i^B \end{bmatrix} = \begin{bmatrix} \boldsymbol{u}_c^B \\ \boldsymbol{u}_i^B \end{bmatrix} \tag{5.1}$$

The subscript $_i$ denotes the *internal* DOF[1] and the subscript $_c$ denotes the *coupling* DOF.

[1] Not to be confused with *interface* DOF

When substructure A and B are assembled on the interface, the compatibility and equilibrium condition are given by

$$\begin{aligned} \boldsymbol{f}_c^A + \boldsymbol{f}_c^B &= \boldsymbol{0} \\ \boldsymbol{u}_c^A - \boldsymbol{u}_c^B &= \boldsymbol{0} \end{aligned} \tag{5.2}$$

Like in chapter 4, the Lagrange multiplier $\boldsymbol{\lambda}$ is used to satisfy the interface force equilibrium. This is defined as

$$\boldsymbol{\lambda} = \boldsymbol{f}_c^A = -\boldsymbol{f}_c^B \tag{5.3}$$

When equation 5.1 is substituted in equation 5.2, the primally assembled flexibility matrix is found. The total dynamics are then given by

$$\begin{bmatrix} \boldsymbol{Y}_{ii}^A & \boldsymbol{Y}_{ic}^A & \boldsymbol{0} \\ \boldsymbol{Y}_{ci}^A & \boldsymbol{Y}_{cc}^A + \boldsymbol{Y}_{cc}^B & -\boldsymbol{Y}_{ci}^B \\ \boldsymbol{0} & -\boldsymbol{Y}_{ic}^B & \boldsymbol{Y}_{ii}^B \end{bmatrix} \begin{bmatrix} \boldsymbol{f}_i^A \\ \boldsymbol{\lambda} \\ \boldsymbol{f}_i^B \end{bmatrix} = \begin{bmatrix} \boldsymbol{u}_i^A \\ \boldsymbol{0} \\ \boldsymbol{u}_i^B \end{bmatrix} \tag{5.4}$$

Note the similarity between this system and the primal assembled system in equation 1.

5.1.1 Force excitation

Next suppose that an unknown force $\bar{\boldsymbol{f}}_i^A$ is acting on the internal DOF of substructure A. It turns out that this system is then equivalent regarding substructure B to a system with no internal force on substructure A and a gap between the interface of the different substructures. This is shown in figure 5.1.

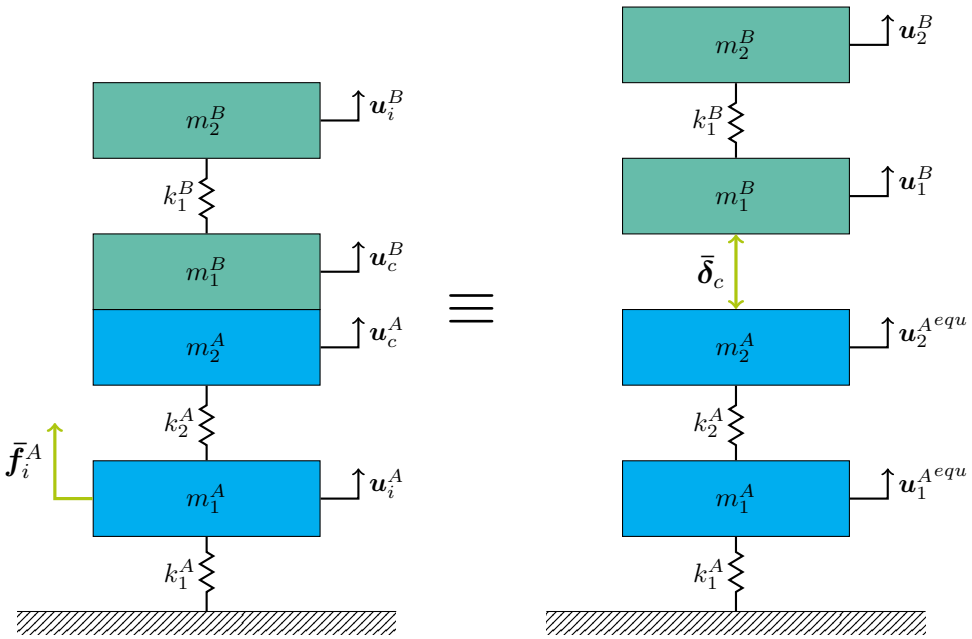

Figure 5.1: Equivalent interface gap, imposed force

The interface gap $\bar{\boldsymbol{\delta}}_c$ is equal to minus the free vibrations of substructure A caused by the force $\bar{\boldsymbol{f}}_i^A$. This can be proved in the following way. The total dynamics are given by

$$\begin{bmatrix} \boldsymbol{Y}_{ii}^A & \boldsymbol{Y}_{ic}^A & 0 \\ \boldsymbol{Y}_{ci}^A & \boldsymbol{Y}_{cc}^A + \boldsymbol{Y}_{cc}^B & -\boldsymbol{Y}_{ci}^B \\ 0 & -\boldsymbol{Y}_{ic}^B & \boldsymbol{Y}_{ii}^B \end{bmatrix} \begin{bmatrix} \bar{\boldsymbol{f}}_i^A \\ \boldsymbol{\lambda} \\ \boldsymbol{0} \end{bmatrix} = \begin{bmatrix} \boldsymbol{u}_i^A \\ \boldsymbol{0} \\ \boldsymbol{u}_i^B \end{bmatrix} \tag{5.5}$$

When the internal DOF of substructure A is eliminated, the following equation is obtained.

$$\begin{bmatrix} \boldsymbol{Y}_{cc}^A + \boldsymbol{Y}_{cc}^B & -\boldsymbol{Y}_{ci}^B \\ -\boldsymbol{Y}_{ic}^B & \boldsymbol{Y}_{ii}^B \end{bmatrix} \begin{bmatrix} \boldsymbol{\lambda} \\ \boldsymbol{0} \end{bmatrix} = \begin{bmatrix} -\boldsymbol{Y}_{ci}^A \bar{\boldsymbol{f}}_i^A \\ \boldsymbol{u}_i^B \end{bmatrix} \tag{5.6}$$

When only substructure A is observed, with the same force applied and the interface DOF is free, the dynamics are given by

$$\begin{bmatrix} \boldsymbol{Y}_{ii}^A & \boldsymbol{Y}_{ic}^A \\ \boldsymbol{Y}_{ci}^A & \boldsymbol{Y}_{cc}^A \end{bmatrix} \begin{bmatrix} \bar{\boldsymbol{f}}_i^A \\ \boldsymbol{0} \end{bmatrix} = \begin{bmatrix} \boldsymbol{u}_i^A \\ \boldsymbol{u}_c^A \end{bmatrix} \tag{5.7}$$

From this equation it is easily found that the free vibrations of the interface are equal to

$$\boldsymbol{u}_c^A = \boldsymbol{Y}_{ci}^A \bar{\boldsymbol{f}}_i^A = -\bar{\boldsymbol{\delta}}_c \tag{5.8}$$

Now reconsider the compatibility condition (5.2) and note that the distance between $\boldsymbol{u}_c^A$ and $\boldsymbol{u}_c^B$ is now no longer zero, but there is an interface gap, such that the compatibility is now defined as

$$\boldsymbol{u}_c^A - \boldsymbol{u}_c^B = \bar{\boldsymbol{\delta}}_c \tag{5.9}$$

With this compatibility condition the total dynamics of the equivalent system are given by

$$\begin{bmatrix} \boldsymbol{Y}_{ii}^A & \boldsymbol{Y}_{ic}^A & 0 \\ \boldsymbol{Y}_{ci}^A & \boldsymbol{Y}_{cc}^A + \boldsymbol{Y}_{cc}^B & -\boldsymbol{Y}_{ci}^B \\ 0 & -\boldsymbol{Y}_{ic}^B & \boldsymbol{Y}_{ii}^B \end{bmatrix} \begin{bmatrix} \boldsymbol{0} \\ \boldsymbol{\lambda} \\ \boldsymbol{0} \end{bmatrix} = \begin{bmatrix} \boldsymbol{u}_i^{A^{equi}} \\ \bar{\boldsymbol{\delta}}_c \\ \boldsymbol{u}_i^{B^{equi}} \end{bmatrix} \tag{5.10}$$

From this equation also the internal DOF of substructure A if eliminated, which results in the following equation

$$\begin{bmatrix} \boldsymbol{Y}_{cc}^A + \boldsymbol{Y}_{cc}^B & -\boldsymbol{Y}_{ci}^B \\ -\boldsymbol{Y}_{ic}^B & \boldsymbol{Y}_{ii}^B \end{bmatrix} \begin{bmatrix} \boldsymbol{\lambda} \\ \boldsymbol{0} \end{bmatrix} = \begin{bmatrix} \bar{\boldsymbol{\delta}}_c \\ \boldsymbol{u}_i^{B^{equi}} \end{bmatrix} \tag{5.11}$$

Equation 5.11 together with the definition in equation 5.8 is equal to equation 5.6. This proves that the equivalent DOF $\boldsymbol{u}_i^{B^{equi}}$ from equation 5.10 is equal to the original DOF $\boldsymbol{u}_i^B$ from equation 5.5, so both systems in figure 5.1 indeed equivalent for what concerns substructure B.

5.1.2 Imposed displacement

The perturbation might not always be caused by an internal force, it can also be caused by an imposed displacement. Suppose that there is an unknown displacement $\bar{\boldsymbol{u}}_i^A$ imposed on the internal DOF of substructure A. It turns out that this system is then equivalent to

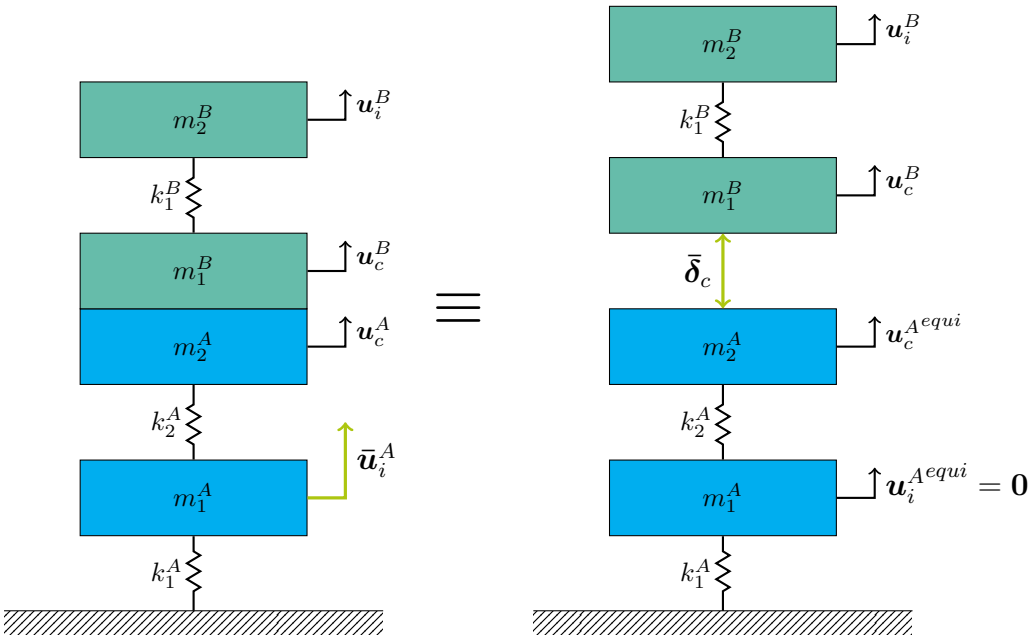

Figure 5.2: Equivalent interface gap, imposed displacement

a system with the internal DOF in substructure A fixed and a gap between the interface of the different substructures. This is shown in figure 5.2

The interface gap $\bar{\boldsymbol{\delta}}_c$ is equal to minus the free vibrations of substructure A caused by the displacement $\bar{\boldsymbol{u}}_i^A$. This can be proved in the following way. The total dynamics are now given by

$$\begin{bmatrix} \boldsymbol{Y}_{ii}^A & \boldsymbol{Y}_{ic}^A & 0 \\ \boldsymbol{Y}_{ci}^A & \boldsymbol{Y}_{cc}^A + \boldsymbol{Y}_{cc}^B & -\boldsymbol{Y}_{ci}^B \\ 0 & -\boldsymbol{Y}_{ic}^B & \boldsymbol{Y}_{ii}^B \end{bmatrix} \begin{bmatrix} \boldsymbol{f}_i^A \\ \boldsymbol{\lambda} \\ \mathbf{0} \end{bmatrix} = \begin{bmatrix} \bar{\boldsymbol{u}}_i^A \\ \mathbf{0} \\ \boldsymbol{u}_i^B \end{bmatrix} \tag{5.12}$$

Next the internal force $\boldsymbol{f}_i^A$ is eliminated from this equation. For the first line of equation 5.12 it follows that

$$\boldsymbol{f}_i^A = \boldsymbol{Y}_{ii}^{A^{-1}} \left(\bar{\boldsymbol{u}}_i^A - \boldsymbol{Y}_{ic}^A \boldsymbol{\lambda} \right)$$

When this is substituted into the second line, the following equation is obtained

$$\begin{bmatrix} \boldsymbol{Y}_{cc}^A + \boldsymbol{Y}_{cc}^B - \boldsymbol{Y}_{ci}^A \boldsymbol{Y}_{ii}^{A^{-1}} \boldsymbol{Y}_{ic}^A & -\boldsymbol{Y}_{ci}^B \\ -\boldsymbol{Y}_{ic}^B & \boldsymbol{Y}_{ii}^B \end{bmatrix} \begin{bmatrix} \boldsymbol{\lambda} \\ \mathbf{0} \end{bmatrix} = \begin{bmatrix} -\boldsymbol{Y}_{ci}^A \boldsymbol{Y}_{ii}^{A^{-1}} \bar{\boldsymbol{u}}_i^A \\ \boldsymbol{u}_i^B \end{bmatrix} \tag{5.13}$$

Note that the interface flexibility from equation 5.13 differs from the interface flexibility in the case where a force is applied (5.6). Actually the interface flexibility from substructure A is the interface flexibility for the case when the internal DOF of substructure A is fixed.

Again substructure A is separated from the system and the same displacement is imposed on the internal DOF and the interface DOF is now free.

$$\begin{bmatrix} \boldsymbol{Y}_{ii}^A & \boldsymbol{Y}_{ic}^A \\ \boldsymbol{Y}_{ci}^A & \boldsymbol{Y}_{cc}^A \end{bmatrix} \begin{bmatrix} \boldsymbol{f}_i^A \\ \mathbf{0} \end{bmatrix} = \begin{bmatrix} \bar{\boldsymbol{u}}_i^A \\ \boldsymbol{u}_c^A \end{bmatrix} \tag{5.14}$$

From this equation it is easily found that the free vibrations of the interface are equal to

$$\boldsymbol{u}_c^A = \boldsymbol{Y}_{ci}^A \boldsymbol{Y}_{ii}^{A^{-1}} \bar{\boldsymbol{u}}_i^A = -\bar{\boldsymbol{\delta}}_c \tag{5.15}$$

When this interface gap is substituted into equation 5.10 and it is made sure that interface flexibility of substructure A is for the case when the internal DOF of substructure A is fixed, the equivalent DOF $\boldsymbol{u}_i^{B^{equi}}$ is equal to the original DOF $\boldsymbol{u}_i^B$ from equation 5.12.

Although it appears that there is a little difficulty to obtain the interface flexibility of substructure A with the points fixed where a displacement is imposed, but if the disturbance originates from an imposed displacement, this is obtained for free. Consider the system in figure 5.2, the imposed displacement does not care about the stiffness k_1^A, so from the interface of substructure A only the stiffness k_2^A will be measured. This illustrates also the efficiency of this method, because whether the disturbance originates from a force or a displacement, the method is exactly the same.

5.1.3 Dynamic stiffness

Although this method is now formulated with dynamic flexibility, it is also possible to use the dynamic stiffness if desired. As in equation 4.6, the set of equations is given by

$$\begin{aligned} \boldsymbol{Z}\boldsymbol{u} + \boldsymbol{B}^T\boldsymbol{\lambda} &= \boldsymbol{f} \\ \boldsymbol{B}\boldsymbol{u} &= \boldsymbol{0} \end{aligned} \tag{5.16}$$

where $\boldsymbol{Z}$ is the block diagonal matrix containing the dynamic stiffness matrices of the substructures. From equation 5.10 it follows that the applied forces are zero. From the definition of the interface gap, the second equation in 5.16 is equal to $\bar{\boldsymbol{\delta}}_c$.

For the system as illustrated in figure 5.1, the full dual formulation is

$$\begin{bmatrix} \boldsymbol{Z}_{ii}^A & \boldsymbol{Z}_{ic}^A & \boldsymbol{0} & \boldsymbol{0} & \boldsymbol{0} \\ \boldsymbol{Z}_{ci}^A & \boldsymbol{Z}_{cc}^A & \boldsymbol{0} & \boldsymbol{0} & \boldsymbol{I} \\ \boldsymbol{0} & \boldsymbol{0} & \boldsymbol{Z}_{cc}^B & \boldsymbol{Z}_{ci}^B & -\boldsymbol{I} \\ \boldsymbol{0} & \boldsymbol{0} & \boldsymbol{Z}_{ic}^B & \boldsymbol{Z}_{ii}^B & \boldsymbol{0} \\ \boldsymbol{0} & \boldsymbol{I} & -\boldsymbol{I} & \boldsymbol{0} & \boldsymbol{0} \end{bmatrix} \begin{bmatrix} \boldsymbol{u}_i^{A^{equi}} \\ \boldsymbol{u}_c^{A^{equi}} \\ \boldsymbol{u}_c^B \\ \boldsymbol{u}_i^B \\ \boldsymbol{\lambda} \end{bmatrix} = \begin{bmatrix} \boldsymbol{0} \\ \boldsymbol{0} \\ \boldsymbol{0} \\ \boldsymbol{0} \\ \bar{\boldsymbol{\delta}}_c \end{bmatrix} \tag{5.17}$$

The system in 5.16 can also be primally assembled with the following definition of $\boldsymbol{u}_c$

$$\boldsymbol{u}_c^{A^{equi}} = \boldsymbol{u}_c + \bar{\boldsymbol{\delta}}_c \qquad\qquad \boldsymbol{u}_c^B = \boldsymbol{u}_c$$

so that

$$\begin{bmatrix} \boldsymbol{Z}_{ii}^A & \boldsymbol{Z}_{ic}^A & \boldsymbol{0} \\ \boldsymbol{Z}_{ci}^A & \boldsymbol{Z}_{cc}^A + \boldsymbol{Z}_{cc}^B & \boldsymbol{Z}_{ci}^B \\ \boldsymbol{0} & \boldsymbol{Z}_{ic}^B & \boldsymbol{Z}_{ii}^B \end{bmatrix} \begin{bmatrix} \boldsymbol{u}_i^{A^{equi}} \\ \boldsymbol{u}_c \\ \boldsymbol{u}_i^B \end{bmatrix} = \begin{bmatrix} -\boldsymbol{Z}_{ic}^A \bar{\boldsymbol{\delta}}_c \\ -\boldsymbol{Z}_{cc}^A \bar{\boldsymbol{\delta}}_c \\ \boldsymbol{0} \end{bmatrix} \tag{5.18}$$

At first glance, it seems a bit difficult to eliminate $\boldsymbol{u}_i^{A^{equi}}$ from equation 5.18, but this definition is equally powerful as for the dynamic flexibility. When the perturbation is caused by an imposed displacement, the equivalent DOF $\boldsymbol{u}_i^{A^{equi}}$ is then equal to zero and the last two lines of equation 5.18 can easily be solved.

If the perturbation originates from a force, $\boldsymbol{u}_i^{A^{equi}}$ needs to be eliminated from equation 5.18. The second line is then

$$\left(\boldsymbol{Z}_{cc}^{A} - \boldsymbol{Z}_{ci}^{A}\boldsymbol{Z}_{ii}^{A^{-1}}\boldsymbol{Z}_{ic}^{A}\right)\left(\boldsymbol{u}_c + \bar{\boldsymbol{\delta}}_c\right) + \boldsymbol{Z}_{cc}^{B}\boldsymbol{u}_c + \boldsymbol{Z}_{ci}^{B}\boldsymbol{u}_i^{B} = \boldsymbol{0}$$

where the first term contains the interface stiffness of substructure A and the internal stiffness, condensed on the interface of substructure A. This is also the stiffness one would measure at the interface, if the perturbations are caused by an imposed force.

5.2 Mount vibrations

For the application of this thesis, the free interface method will be used, so again the equation of motion of the machine are given by equation 4.25. When this is substituted in equation 5.10, the following equation is obtained.

$$\begin{bmatrix} \boldsymbol{Y}_{ii}^{m} & \boldsymbol{Y}_{io}^{m} & -\boldsymbol{Y}_{ic}^{m} & \boldsymbol{0} \\ \boldsymbol{Y}_{oi}^{m} & \boldsymbol{Y}_{oo}^{m} & -\boldsymbol{Y}_{oc}^{m} & \boldsymbol{0} \\ -\boldsymbol{Y}_{ci}^{m} & -\boldsymbol{Y}_{co}^{m} & \boldsymbol{Y}_{cc}^{m} + \boldsymbol{Y}_{cc}^{f} & \boldsymbol{Y}_{ci}^{f} \\ \boldsymbol{0} & \boldsymbol{0} & \boldsymbol{Y}_{ci}^{f} & \boldsymbol{Y}_{ii}^{f} \end{bmatrix} \begin{bmatrix} \boldsymbol{0} \\ \boldsymbol{0} \\ \boldsymbol{\lambda} \\ \boldsymbol{0} \end{bmatrix} = \begin{bmatrix} \boldsymbol{u}_i^{m} \\ \boldsymbol{u}_o^{m} \\ \bar{\boldsymbol{\delta}}_c \\ \boldsymbol{u}_i^{f^{equi}} \end{bmatrix} \tag{5.19}$$

From this equation the interface force $\boldsymbol{\lambda}$ can be solved.

$$\boldsymbol{\lambda} = \left(\boldsymbol{Y}_{cc}^{m} + \boldsymbol{Y}_{cc}^{f}\right)^{-1}\bar{\boldsymbol{\delta}}_c \tag{5.20}$$

The interface force is by definition minus the force acting on the coupling DOF of the machine. When the interface force is known, the internal displacement $\boldsymbol{u}_i^m$ and $\boldsymbol{u}_o^m$ are easily found. The new vibration level of the floor is found by computing

$$\begin{aligned} \boldsymbol{u}_c^{f} &= \boldsymbol{Y}_{cc}^{f}\boldsymbol{\lambda} + \bar{\boldsymbol{\delta}}_c \\ \boldsymbol{u}_c^{m} &= -\boldsymbol{Y}_{cc}^{m}\boldsymbol{\lambda} \end{aligned}$$

which of course should give the same result.

When these equations are compared to the equation is section 4.3, it should be noted that all the ingredients for this method are already measured or calculated for the FBS method, except the free vibrations. These can be very easily measured or a vibration criterion can be used.

Part II

Validation

Chapter 6

Test case

To see whether the theory as explained in the previous sections will also work in practice, an experiment will be performed. First a test case needs to be constructed that should represent the system as described in chapter 2.

6.1 Test case construction

The test case will consists of a large mass which represents the frame. The mass is suspended from the floor with four springs, instead of one. On top of this mass is a smaller mass, which should represent the tool. This mass is placed on top of the larger mass with three air mounts.

For the frame, a block of granite is selected, which measures approximately 1.2 by 1.2 by 0.3 m. With a density between 2700 and 2900 $^{kg}/_{m^3}$, this stone will have a mass of approximately 1200 kg. For the tool a smaller granite stone is selected. This stone measures approximately 0.8 by 0.5 by 0.1 m, so this stone has a mass of 110 kg.

To mount the frame on the floor, compression springs are needed. The first eigenfrequency of the floor which is used for this validation is around 13 Hz. To make sure that there will be some coupling visible, the suspension of the frame should also be around 13 Hz. From a simple model it is found that more coupling effects are visible if the eigenfrequency is higher than 13 Hz, than if the eigenfrequency is below 13 Hz, so 15 Hz is selected. The total mounting stiffness is given by

$$K_{mount} = (\omega \cdot 2\pi)^2 m = 11 \cdot 10^6 \, {}^{N}/_{m} \tag{6.1}$$

To create this stiffness, disc springs are used. Disc springs are conical shells that are available in a variety diameters and thicknesses and can be stacked if needed to obtain a certain stiffness or displacement. Typically a disc spring will carry a large load with a small deflection, so these are ideal for this application.

By DIN 2093 three types of disc springs are specified, series A, B and C. This specification is mostly given by the fraction $\frac{h_0}{t}$, where h_0 is the maximum deflection of the spring and

t is the thickness. For series A, this fraction is approximately 0.4, for series B 0.7 and for series C this is 1.3.

The characteristic of the series A springs is assumed to be almost linear, whereas the characteristic of the series B and C is degressive, so the stiffness decreases with the deflection. Although a series A is favourable, especially when one tries to do frequency based substructuring, these are also very stiff and allow only very small deflections because of the low fraction.

To obtain the desired stiffness, a single 71 mm outside diameter series C disc spring is used. This spring has a thickness of 2 mm and allows a maximum deflection of 2.60 mm. Because only one spring per mount is used, no guidance is needed. This way, there is only friction between the spring and the two adjacent surfaces. Because this is a series C spring, it has a highly degressive spring rate. The characteristic is shown in figure 6.1, together with a cubic fit as made with the *Basic fitting toolbox* of MATLAB.

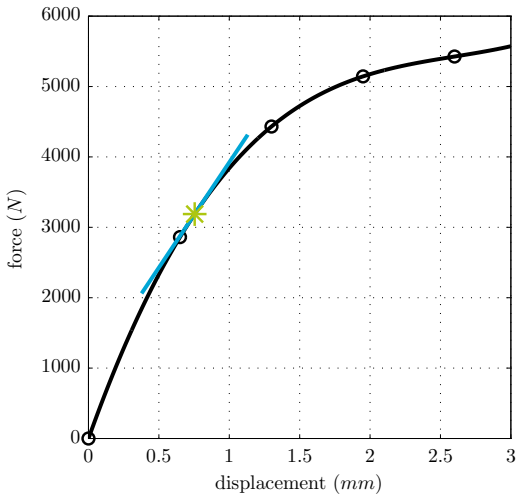

Figure 6.1: Characteristic of Series C disc spring

The cubic fit is given by

$$F(x) = 261x^3 - 2035x^2 + 5614x + 0.029 \tag{6.2}$$

which is very easy to differentiate with respect of x to obtain the stiffness as function of x. Because the dynamic deflection is very small, the linearised stiffness can be obtained around the static equilibrium position. The static deflection is 0.7542 mm, so the linearised stiffness at equilibrium is $2.9910^{6N}/_{m}$. The static deflection and the linearised stiffness are also shown in figure 6.1. Because the springs are not linear, it is important that the static deflection is equal for each of the four springs, to conserve the symmetry of the setup.

To align the disc springs properly with respect to each other and the frame, mounts are constructed. The detailed technical drawings are shown in appendix 11.2.3. These mounts consists of an aluminium stand with a steel base on top. Between the stand and the base,

shim rings can be used to make sure that all the mounting points are level before the stone is placed on it. The purpose of the stand is to create some space underneath, so it is much easier to place the stone on the springs. There are also steel bars made, which are used to connect the stands with each other. These bars also improves the repeatability of the setup.

On top of these steel base, a pocket is made in which the disc spring is placed. This is used as a guide for the disc spring and it also provides a safety stop, such that the disc spring will never be fully compressed. The disc spring inside the pocket of the base is shown in figure 6.2a. The black ring is the disc spring.

Since the contact region is only a line, high stresses are expected. To protect the stone from deep scratches, discs of hardened steel are placed on top of the disc springs. These are the actual mounting points for the frame, so it is made sure that these are level by adjusting the number of shim rings.

The four springs are placed on the four corners of the frame. So there should be one translation mode and two rocking modes, with approximately the same eigenfrequency. The setup without the frame is shown in figure 6.2b.

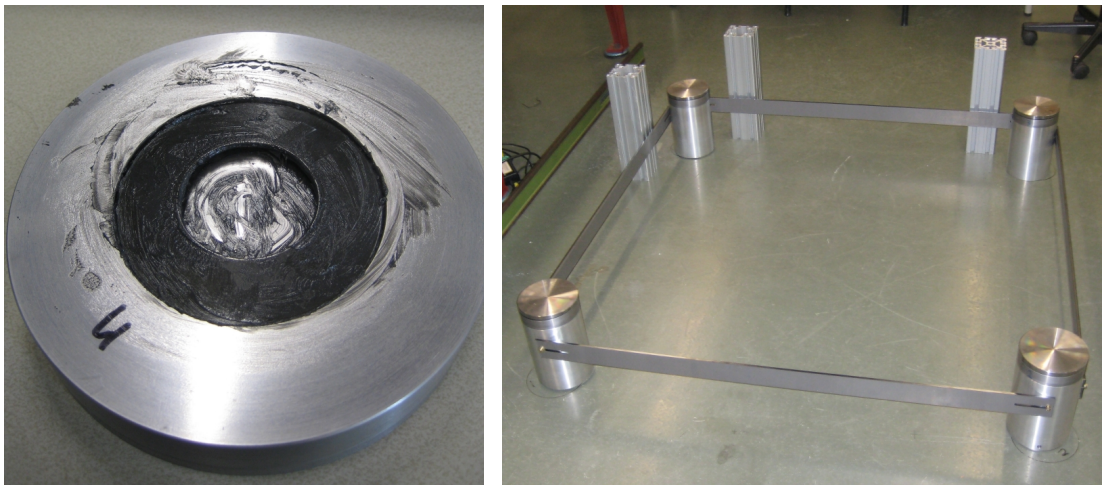

(a) Disc spring in base (b) Stands

Figure 6.2: Construction details

For the suspension of the tool, air mounts were used that were readily available. The used air mounts are from NewPort, type SLM-3A. These air mounts have a frequency between 3 and 4.5 Hz for a load between 34 and 136 kg per mount. In our case, the frequency of the translation mode should then be 4.5 Hz. The center of the stiffness should then be equal to the center of gravity. For this to happen, the air mounts need to placed near the center of gravity. When this is done, the frequencies of the rocking modes are also very close to the translational frequency. Therefore, two of the air mounts are placed on the corners of one long edge, while the other is placed in the middle of the opposite edge. This way, the rotational stiffness is enlarged, but the downside is that there is no pure translational mode. This has now become a combination of a translation and a rotation.

When the test case was built for the first time, the pressure in the air mounts was set such

that the tool was level. This pressure is not altered during the measurements. Because all the measurements were done within a month, the change in pressure is neglected, so the stiffness of the air mounts is assumed constant during the measurements.

A schematic top view of the test case, together with the measurement locations and the axis of the coordinate system is shown in figure 6.3.

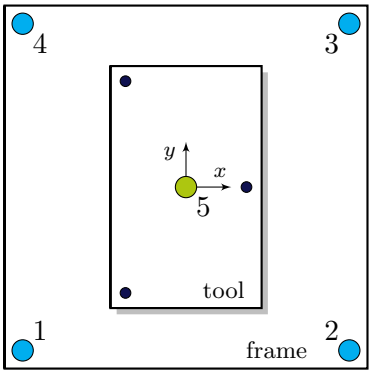

Figure 6.3: Top view of test case with measurement grid

In this figure the blue dots indicate the locations of the disc springs which are also equal to the measurement points on the frame. The smaller dark blue points indicate the locations of the air mounts and the green dot is the measurement point on the tool. This point also defines the center of the coordinate system which is used for the projection in chapter 7.

The constructed test case is shown in figure 6.4 and 6.5.

6.2 Test case model

For some reference calculations, a simple model is made. This model only contains the frame. The tool can be incorporated with the same method, but then each air mount needs to be identified, because it cannot be assumed that these are all equal.

For this model, the frame is assumed rigid, so it only has three DOF, one translation in the z-direction and two rotations around the x- and y-axis. The mass and stiffness matrices are obtained using the elastic and potential energy. The damping matrix follows from a Rayleigh dissipation function.

It is also assumed that the mass distribution is uniform, such that the moment of inertia is given by

$$I_f = \frac{1}{12} m_f l^2$$

where m_f is the mass of the frame and l is the width of the frame. The fixed model is shown in figure 6.6.

The general DOF are defined as

$$\boldsymbol{q}_f = \begin{bmatrix} u_{fz} & u_{f\theta_x} & u_{f\theta_y} \end{bmatrix}^T \tag{6.3}$$

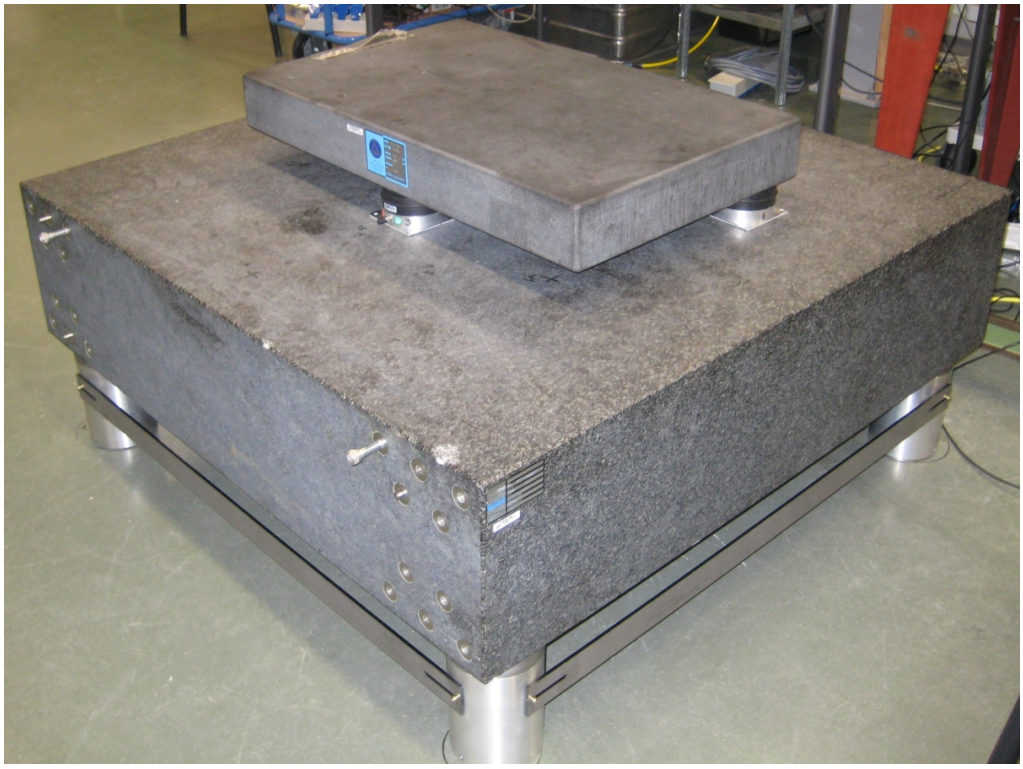

Figure 6.4: Constructed test case

The kinetic energy is given by

$$\mathcal{T} = \frac{1}{2}\dot{\boldsymbol{q}}_f^T \begin{bmatrix} m^f & 0 & 0 \\ 0 & I_f & 0 \\ 0 & 0 & I_f \end{bmatrix} \dot{\boldsymbol{q}}_f \tag{6.4}$$

For the potential energy, the general DOF are expanded to translations on the frame, above the spring. With these relations, the potential energy is given by

$$\mathcal{V} = \frac{1}{2}k \sum_i^4 \left(\begin{bmatrix} 1 & dy_i & -dx_i \end{bmatrix} \boldsymbol{q}_f \right)^2 \tag{6.5}$$

where dx_i is the distance in x-direction from the center of the test case to point i. The Rayleigh dissipation function is similar to the potential energy and given by

$$\mathcal{F} = \frac{1}{2}c \sum_i^4 \left(\begin{bmatrix} 1 & dy_i & -dx_i \end{bmatrix} \dot{\boldsymbol{q}}_f \right)^2 \tag{6.6}$$

The mass damping and stiffness matrix are then found with

$$\begin{aligned} \boldsymbol{M} &= \frac{\partial^2 \mathcal{T}}{\partial \dot{\boldsymbol{q}} \partial \dot{\boldsymbol{q}}} \\ \boldsymbol{C} &= \frac{\partial^2 \mathcal{F}}{\partial \dot{\boldsymbol{q}} \partial \dot{\boldsymbol{q}}} \\ \boldsymbol{K} &= \frac{\partial^2 \mathcal{V}}{\partial \boldsymbol{q} \partial \boldsymbol{q}} \end{aligned} \tag{6.7}$$

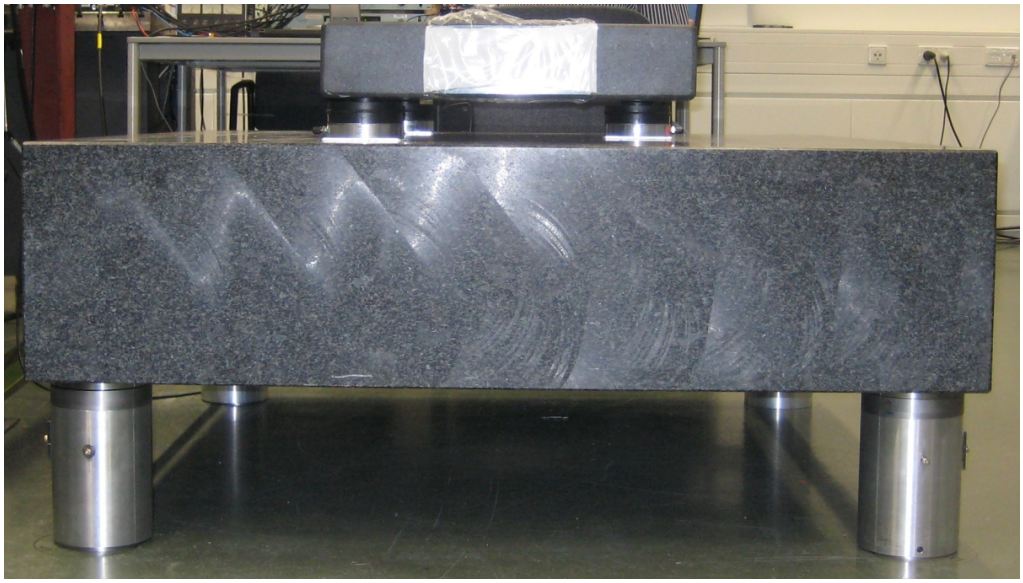

Figure 6.5: Constructed test case, side view

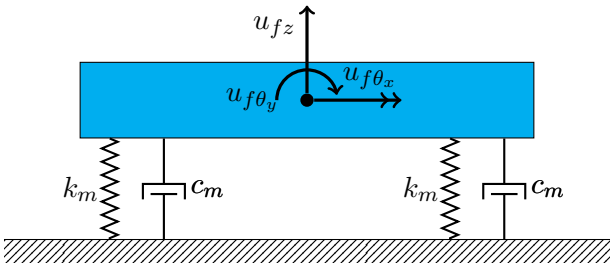

Figure 6.6: Test case model fixed

To obtain a free model, three additional DOF for the mounts are added to this description, as shown in figure 6.7.

These additional DOF are defined as

$$\boldsymbol{q}_m = \begin{bmatrix} u_{mz} & u_{m\theta_x} & u_{m\theta_y} \end{bmatrix}^T \tag{6.8}$$

The mass m_m of the mount is treated as a point mass at (dx_i, dy_i), so the inertia properties can be easily calculated and added to the kinetic energy. The stiffness and damping is now differential, so the potential energy is given by

$$\mathcal{V} = \frac{1}{2} k \sum_i^4 \left(\begin{bmatrix} 1 & dy_i & -dx_i \end{bmatrix} (\boldsymbol{q}_f - \boldsymbol{q}_m) \right)^2 \tag{6.9}$$

where i is the index in the measurement grid. The Rayleigh dissipation is similar and the free mass, damping and stiffness matrices can also be found with equation 6.7.

The values for m_f, m_m, c and k will be defined in chapter 7.

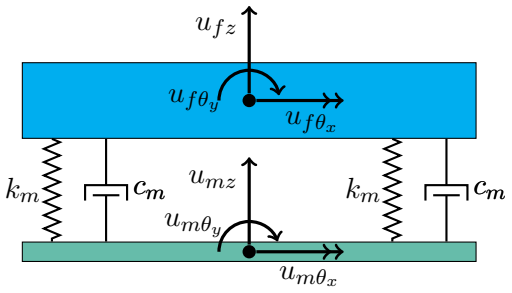

Figure 6.7: Test case model free

Chapter 7

Experimental validation

The theory as proposed in the first part of this thesis, will be validated with an experiment. Due to the nature of the test case, this validation is not straightforward. A number of post-processing steps need to be done, which are visualised in a flowchart as shown in figure 7.1.

In this figure, the datasets are shown with trapezium shaped blocks, the rectangular blocks are the processes and the diamond shaped blocks are decisions. The bold arrows indicate the normal verification process. The normal arrows are additional steps that will be used to visualise and originate the error in the final result.

In the big green box in the middle, the actual coupling as described in chapter 4 is performed. For this, the response of the floor and the free response of the test case is needed. The floor measurement will be obtained as described in chapter 8.

To obtain the free response of the test case, the translation at the corner points of the large mass and the translations in the middle of the smaller mass are measured, when the test case was on a very stiff floor. Because the frame is assumed to be rigid in the frequency region of interest, the large mass has only three DOF. To compensate for this and to make the inversions much more numerically stable, the four measured translation will be projected on a node in the middle, which has three DOF, one translation and two rotations. The procedure used for this will be explained in section 7.1. The procedure to obtain the free response from a fixed measurement will be explained in section 7.2.

The coupling is performed with only 3DOF, one translation and two rotations. Physically there are four translation DOF to be coupled, but for the same reasoning as for the frame, the fourth modeshape is not likely to be present in the measurements. So, for numerical stability, the coupling is only done with three DOF. The technique is however successfully used with four DOF coupling, so in this example there is no problem, but that might not always be the case.

The result of the coupling will be compared with a validation measurement. This measurement is the same as the fixed test case measurement, but now the test case is placed on the floor of interest. Because the validation measurement also has five DOF, while the result of the coupling has only four, another projection is needed.

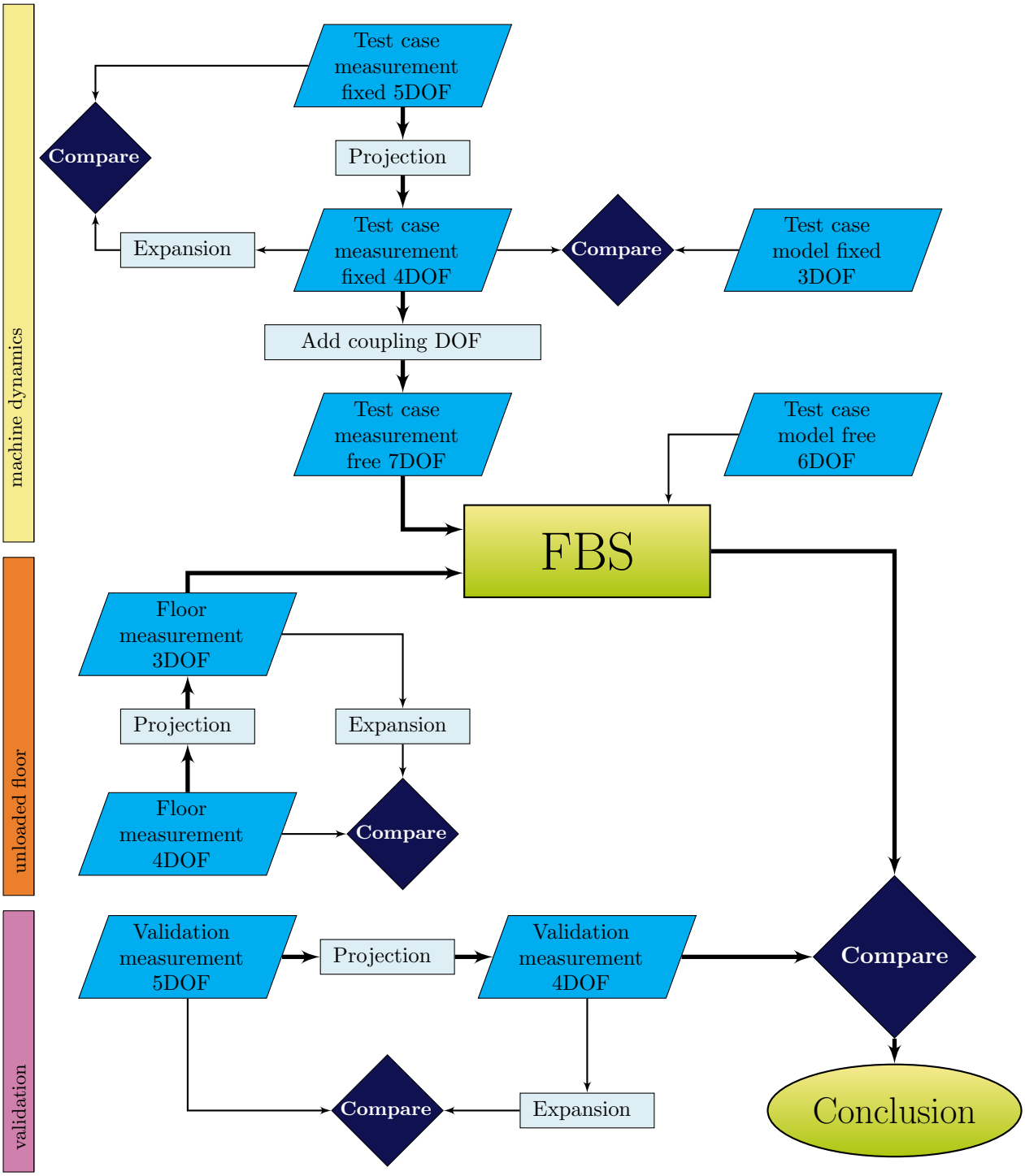

Figure 7.1: Flowchart experimental verification

With the projection process, a rigid motion is obtained for every frequency point with a least square method. Because a least square solution of measurements is almost never exact, a residual motion is wasted. To quantify the residual motion, the projected solution is expanded to obtain the rigid motion in the original DOF. This can be compared with

the original measurement to quantify the residual motion. The expansion is also explained in section 7.1.

There are also two models used for verification. These models are only of the frame, so the fourth DOF for the tool is not modelled. The model was already described in chapter 6.

7.1 Projection and expansion

The projection and expansion procedure used here is proposed by de Klerk et al. [35]. They called it the Equivalent Multi Point Connection (EMPC) and used it to describe the interface of a substructure with only one node with six DOF, while three translations on three nodes were measured.

Suppose that the full dynamics are given by

$$\boldsymbol{u}^f = \boldsymbol{Y}\boldsymbol{f}^f \tag{7.1}$$

and that the projection is defined by

$$\boldsymbol{u}^f = \boldsymbol{R}\boldsymbol{u}^{pr} + \boldsymbol{\mu} \tag{7.2}$$

where $\boldsymbol{u}^f$ are the DOF that are projected on a general set $\boldsymbol{u}^{pr}$ and $\boldsymbol{\mu}$ is the residual motion. Generally the number of DOF in $\boldsymbol{u}^{pr}$ is less than in $\boldsymbol{u}^f$, otherwise $\boldsymbol{\mu}$ would be zero. The matrix $\boldsymbol{R}$ is the reduction basis, which can for instance contain all the rigid body modes. Because the residual motion is perpendicular to the space spanned by $\boldsymbol{R}$, it follows that $\boldsymbol{R}^T\boldsymbol{\mu} = \boldsymbol{0}$. Premultiplication of equation 7.2 with $\boldsymbol{R}^T$ and solving for $\boldsymbol{u}^{pr}$ results in

$$\boldsymbol{u}^{pr} = (\boldsymbol{R}^T\boldsymbol{R})^{-1}\boldsymbol{R}^T\boldsymbol{u}^f \tag{7.3}$$

The procedure can also be used on the forces. The projection of the forces is defined as

$$\boldsymbol{f}^f = \boldsymbol{R}\boldsymbol{f}^{pr} + \boldsymbol{\gamma} \tag{7.4}$$

where $\boldsymbol{\gamma}$ are the residual forces and $\boldsymbol{f}^{pr}$ are only the combination of that can excite the shapes in $\boldsymbol{R}$. Following the same reasoning as before it is found that

$$\boldsymbol{f}^{pr} = (\boldsymbol{R}^T\boldsymbol{R})^{-1}\boldsymbol{R}^T\boldsymbol{f}^f \tag{7.5}$$

Substituting equation 7.1 and the last two equations in equation 7.3 results in

$$\boldsymbol{u}^{pr} = (\boldsymbol{R}^T\boldsymbol{R})^{-1}\boldsymbol{R}^T\boldsymbol{Y}\boldsymbol{R}(\boldsymbol{R}^T\boldsymbol{R})^{-1}\boldsymbol{R}^T\boldsymbol{f}^f \tag{7.6}$$

which can be rewritten as

$$\boldsymbol{u}^{pr} = \boldsymbol{T}\boldsymbol{Y}\boldsymbol{T}^T\boldsymbol{R}^T\boldsymbol{f}^f \tag{7.7}$$

where

$$\boldsymbol{T} = (\boldsymbol{R}^T\boldsymbol{R})^{-1}\boldsymbol{R}^T$$

For the test case used in this thesis, the four translations at the corners will be projected to one translation and two rotations in the middle. The translation of the tool remain

unaltered. The transformation matrix contains three rigid body modes for the frame and a 1 for tool, so the transformation is given by

$$\begin{bmatrix} u^f_{1z} \\ u^f_{2z} \\ u^f_{3z} \\ u^f_{4z} \\ u^t_{5z} \end{bmatrix} = \begin{bmatrix} 1 & dy_1 & -dx_1 & 0 \\ 1 & dy_2 & -dx_2 & 0 \\ 1 & dy_3 & -dx_3 & 0 \\ 1 & dy_4 & -dx_4 & 0 \\ 0 & 0 & 0 & 1 \end{bmatrix} \begin{bmatrix} u^f_z \\ u^f_{\theta^x} \\ u^f_{\theta_y} \\ u^t_z \end{bmatrix} \tag{7.8}$$

When $\boldsymbol{u}^{pr}$ from equation 7.6 is again premultiplied with $\boldsymbol{R}$, the original DOF are obtained. In figure 7.1 this is the process called expansion. Since in $\boldsymbol{u}^{pr}$ there are only rigid motions present, these expanded motions are also rigid.

When equation 7.3 is substituted in equation 7.1, the residual motion $\boldsymbol{\mu}$ can be solved. This will provide a good basis to quantify the quality of the projection. The change in FRFs can for instance be quantified with PAC numbers. PAC stands for Projection Assurance Criterion and is the similar to the Frequency Response Assurance Criterion (FRAC). The difference is that the values are only scaled by the original FRF. The PAC number is defined by

$$PAC_r = \frac{\left| \{\boldsymbol{RTY}\}^H_r \{\boldsymbol{Y}\}_r \right|}{\{\boldsymbol{Y}\}^H_r \{\boldsymbol{Y}\}_r} \tag{7.9}$$

where r defines the entry of the response matrix.

A regular FRAC number would also be scaled by the projected FRF, such that the values are always between zero and one. Therefore, if the amplitude of the projected FRF has changed, but the shape is still equal, the FRAC number would be one. The PAC number can be any positive value, where a value between zero and one indicates that the amplitude has decreased and value above one indicates that the amplitude has increased.

For general MAC values, it is assumed that a value above 0.9 is acceptable, so for this PAC number a value between 0.95 and 1.05 is acceptable.

Another check is to use the rigidity check as proposed by de Klerk et al. [35]. This computes the norm of the projected deformations scaled by the norm of the original deformations. This is done for each frequency point and with this check each column of the $\boldsymbol{Y}$ matrix can be evaluated. Because for this check, a graph is needed for every column, the PAC number is much easier to visualise.

7.2 Add DOF

As explained earlier, the free response of the test case is required for the FBS method. Normally one would suspend the object under test with very soft springs, for instance air mounts and excite each coupling DOF separately, so a SIMO system is obtained. Another option is to use a shaker with an impedance sensor on each coupling DOF simultaneously. By ensuring that all four inputs are uncorrelated, the full model description can be obtained by averaging the cross correlations or via the method as proposed by Dobrowiecki

et al. [41]. Although there were shakers available that could handle this weight and already had a force sensor built in, it turned out that the stiffness of this shaker will distort the measured response. Afterwards a dynamic model of the shaker need to be subtracted form the measurements.

For this thesis, the response of the test case is measured while the test case is supposed to be fixed and the coupling DOF are added computationally. The theory behind this and the practical problems will be discussed next.

7.2.1 Theory

Suppose a simple damped SDOF oscillator that is fixed at end. The dynamic flexibility is given by

$$\boldsymbol{Y}^{fixed} = \frac{1}{-\omega^2 m_1 + i\omega c + k} \tag{7.10}$$

which can be easily measured. Now the fixed interface will be freed and a mass will be added to the second DOF. The dynamic flexibility is then given by

$$\boldsymbol{Y}^{free} = \begin{bmatrix} \boldsymbol{Y}^{fixed^{-1}} & \boldsymbol{Z}_{ic} \\ \boldsymbol{Z}_{ci} & \boldsymbol{Z}_{cc} \end{bmatrix}^{-1} \tag{7.11}$$

At the first DOF the stiffness is simply the inverse of the measured flexibility. For the second DOF the stiffness is almost the same as for the first DOF, but with a different mass, so

$$\boldsymbol{Z}_{cc} = -\omega^2 m_2 + i\omega c + k$$

To define the coupling between these two DOF, the off diagonals $\boldsymbol{Z}_{ic}$ and $\boldsymbol{Z}_{ci}$ need to be defined, where $\boldsymbol{Z}_{ci}$ is equal to $\boldsymbol{Z}_{ic}^T$ by definition. In the measurement of $\boldsymbol{Y}^{fixed}$ the damping and stiffness is measured for an absolute displacement of the first DOF. Now that this system has become a two DOF system, the mass is only dependent on the absolute displacement. The damping and stiffness is dependent on both displacements. When both displacements are equal, the absolute damping and stiffness that is in the measurement of $\boldsymbol{Y}^{fixed}$ need to be subtracted by the off-diagonal, so the off-diagonal terms are given by

$$\boldsymbol{Z}_{ic} = -i\omega c - k$$

It is very easy to verify that when the dynamic stiffness is set up for a two DOF system directly, the same results are obtained.

7.2.2 Experimental difficulties

As already shown, this method works perfectly if the off-diagonal terms are estimated properly. If there is an error in this estimation, negative damping or a negative stiffness can occur for some deflection shapes. This is illustrated in figure 7.2.

In this figure, k_f and c_f represent the stiffness and damping that is measured in the fixed case. If in this case the mass m_1 moves upward, it feels the fixed damping and stiffness.

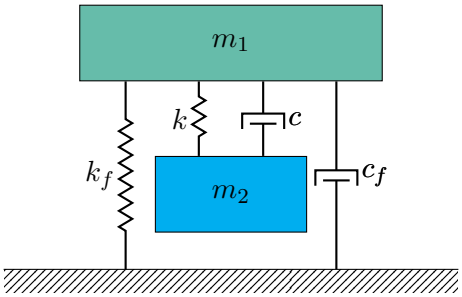

Figure 7.2: Visualisation of apparent stiffness and damping

However if the mass m_2 has the same displacement, the force caused by the stiffness k_f should be cancelled by the force caused by k and the same holds for the damping. Mathematically this is defined as

$$\boldsymbol{f} = k_f u_1 - k u_2 + c_f \dot{u}_1 - c \dot{u}_2$$

which is basically the first line of equation 7.11. From this it is pretty clear that if k differs from k_f, this will show as an artificial stiffness, which can even be negative if the estimated stiffness is larger than the fixed stiffness. Because stiffness can be very accurately estimated, this will not be too much of a problem.

However, the same holds for the damping, which proves to be a much bigger problem. In the previous section, this damping is assumed to be viscous, but for the real test case, this will probably only hold for a very small frequency band. Off course more complicated models can be set up, using for instance Maxwell models, but this is very time consuming and still only an approximation. From the definition of the dynamic stiffness it follows that the imaginary part of the measured stiffness is equal to the damping. So when $\text{Im}\left(\boldsymbol{Y}^{free^{-1}}\right)$ is substituted for ωc in the off diagonal terms, there will be no artificial damping. There might still be artificial stiffness.

From a simple model of the test case it followed that the total stiffness of all four mounts can be obtained from a transmissibility measurement along an edge of the frame, for instance from point 1 to 2 or 4. In this response function only the first translation mode should be visible, because one rotation mode is excited which is not measured at the other two corners. So in the measurement all four springs should be activated almost equally. From this response a linearised stiffness is obtained, which is four times the stiffness of a single disc spring. This results in a stiffness of $2.65^{kN}/_{mm}$ for each spring.

As another simple check, the linearised stiffness of a driving point can also be computed. When a driving point is observed, both the translational mode and one rotational mode is measured. The linearised stiffness of the translation mode is still four times the stiffness of a single spring and the linearised stiffness of the rotational modes only twice the stiffness of a single disc spring. Adding those results in a linearised stiffness for a driving point of $\frac{4}{3}$ of the stiffness of a single spring. From this reasoning, also a stiffness of $2.65^{kN}/_{mm}$ is obtained for each spring.

Now that the actual stiffness of the disc springs is known, the mass and damping of the frame can be calculated from the modal constants of the first eigenfrequency of the frame. To extract the location of the first eigenfrequency of the frame from the measurements,

the Rational Fraction Polynomial (RFP) method [42, 43] is used. From this calculation it is again verified that the stiffness of each spring is $2.65^{kN}/_{mm}$. Furthermore, the modal damping is found to be $\zeta_1 = 12\%$ and the eigenfrequency is found to be $\omega_r = 93^{rad}/_{s}$. With this damping, the undamped eigenfrequency varies only slightly from the damped eigenfrequency, so this is neglected. Now that the stiffness and eigenfrequency is known, the weight of the frame is found to be $1150kg$. With this mass, the dampers are found to be $6.5^{Ns}/_{mm}$. To verify these values, the modal damping for each rocking mode can be computed. With these linear dampers, the modal damping is 19%, which is also found with the RFP method.

The weight of the mount is not really important, because these will be directly coupled to the floor, which has a much bigger mass. From CAD data it followed that the mounts below the spring weigh 8 kg.

Now, finally the free response of the test case can be computed by adding the three coupling DOF. The translational stiffness between the coupling DOF and the internal DOF of the testcase is given by

$$\boldsymbol{Z}_{icz} = -4k - i\text{Im}\left(\left(\boldsymbol{TYT}^T\right)^{-1}_{zf}\right)$$

For the two rotations the stiffness is given by

$$\boldsymbol{Z}_{ic\theta_x} = -4k \cdot dy^2 - i\text{Im}\left(\left(\boldsymbol{TYT}^T\right)^{-1}_{\theta_x f}\right)$$

which is the same for the other rotation.

Note that there is no direct stiffness between the coupling DOF and the translation DOF of the frame, so the matrix $\boldsymbol{Z}_{ic}$ should be complemented with a column of zeros.

The stiffness for the translational coupling DOF is given by

$$\boldsymbol{Z}_{ccz} = -\omega^2 4m_m + 4k + i\text{Im}\left(\left(\boldsymbol{TYT}^T\right)^{-1}_{zf}\right)$$

where m_m is the mass off the mount. The stiffness for the rotational coupling DOF is given by

$$\boldsymbol{Z}_{cc\theta_x} = -\omega^2 4m_m \cdot dy^2 + 4k \cdot dy^2 + i\text{Im}\left(\left(\boldsymbol{TYT}^T\right)^{-1}_{\theta_x f}\right)$$

Chapter 8

Floor measurement

To perform a receptance measurements on a floor is a little different than normal. A floor has typically a big mass and for the purpose of this thesis, also has a big stiffness, so a lot of energy is needed to excite it properly. Furthermore a floor will typically have a lot of damping, so that the response will decay quickly and coupling between different modes might occur. The last problem is that the testing has to be done *in-situ*, because it is impossible to remove the floor from a building and test it separately.

For the floors of interest, the same response as shown in section 3.4.2 is expected. It should also be noted that the acceleration level is very low for low frequencies, it is zero for $\omega = 0$, so ideally there should be more input energy below the first eigenfrequency of the floor. There are also no rigid body modes expected, because there is stiffness on every DOF.

8.1 Measurement settings

To be able to capture the floor response accurate enough, the data acquisition system needs to be set up properly. Based on experience by Pavic et al. [44], the following settings are chosen. To validate these settings, a time trace with 10 impacts is recorded. So when applicable, the same measurements are used for the rest of this section.

Frequency range and resolution

The frequency range of interest is low, so the measurement bandwidth can be as low as 200 Hz. Because the impact time is also quite short, there should be enough data points to capture the input accurate enough. The width of the impulse is approximately 10 ms. A bandwidth of 200 Hz corresponds to a sampling frequency of 512 Hz, so the input is captured by 5 data points, which should be sufficient.

Together with the bandwidth, the number of data points should be set. This number determines the length of the measurement block. Because the response is expected to decay quickly, a short block length should be sufficient.

The block length also determines the frequency resolution. The frequency resolution is given by

$$\Delta f = \frac{f_{sample}}{N_{data}} = \frac{1}{t_{block}} \tag{8.1}$$

Because the mode density is assumed to be high, a good frequency resolution is needed to capture enough details. Increasing the measurement time results in a better frequency resolution. However, after the response has been damped out, the signal only contains background noise.

In figure 8.1 a driving point measurement is shown for three different frequency settings. The black line has a block length of 2 seconds, the blue line has a block length of 4 s and the green line has a block length of 8 s. These results are obtained from the same measurements. The sample frequency is set to 512 Hz, the number of averages is 10 and there are no windows applied.

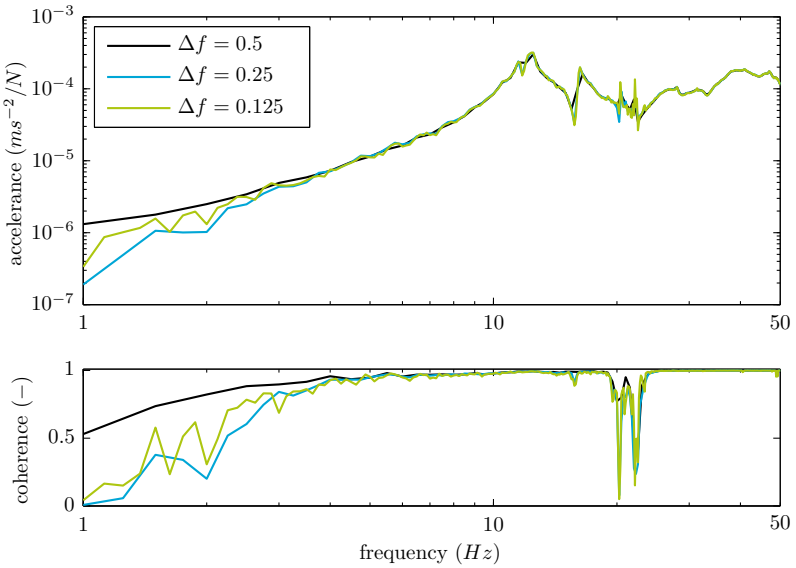

Figure 8.1: Different frequency resolutions

It should be noted that there are two harmonic disturbances present just above 20 Hz, which causes the sharp peaks and bad coherence around 20 Hz. This is probably caused by a pump or air ventilation somewhere in the building

Overall, all of these three settings are capable of reproducing the same results. However the results with a better frequency resolution, have sharper resonant peaks, but does not show any new information. Because the response decays very quick, after 4 seconds there is only background noise present in the measured signal. This explains the bad coherence around 20 Hz for the green line. For the blue line it is only slightly better, so the response is expected to only last for slightly longer than 2 seconds. However, there are two resonances visible around the first eigenfrequency, which is not captured by the black line, but the other two settings are pretty much equal. For this floor, a frequency resolution of 0.25 is needed. To compensate for the slightly worse coherence and not so

smooth accelerance of the measurement with the higher frequency resolution, windowing will be used.

Windowing

The next setting to choose is the windowing. The main reason to apply a window on a measurement block is to reduce signal leakage. Because of the large damping, this is not very likely to happen with floor measurements and judging the results in figure 8.1, leakage is not very likely to happen with this measurement.

As stated in the previous paragraph it might still be useful to apply a window. Because the response is pretty short, the data obtained in the first part of the measurement block contains more useful information than the data at the end of the block. So applying an exponential window reduces the background noise that is measured at the end of the measurement block, but should not alter the information at the beginning of the measurement block too much. However, an exponential window increases the measured damping. For this measurement, windowing is used to suppress the resonant peaks just above 20 Hz.

In Siglab it is possible to have a boxcar window (which is actually not a window) on all channels, or to apply a an exponential window on the response channels. However some care should be taken when using Siglab for this purpose.

1. The first problem is caused by the pre-trigger settings. Siglab applies the exponential window starting from the first point in the measurement block. This means that this window is less than 1 at the instance when the impact is applied. This results in a gain error in the measured FRF. This error is normally small, but for a low bandwidth measurement with a large measurement block, this error can be significant.

2. The next problem is caused by the AD converter. Even if the filtering of the response channel is set to AC, there is still a small constant signal present in the measured response. Without a window, this is no problem, because it will only result in peak at zero Hz. With an exponential window, this constant signal is now no longer constant. The frequency response of this constant is now equal to the Fourier transform of an exponential window, which is a $-20dB/decade$. Because the response is very low for low frequencies, this will result in a fake anti resonance, as if there are rigid body modes present. Because this part of the response is created by the window, which is the same for every measurement, the coherence is also very good.

When the post processing is not done with Siglab, these problems can be solved. For the gain problem, a block exponential window can be used. This is an exponential window which is shifted over time. The entries in front are filled with ones, so the decay now starts after the impact is applied. These windows are illustrated in figure 8.2, together with a part of the time trace.

The windows are slightly exaggerated for visibility reasons, but off course both windows start at 1. This figure also illustrates the origin of the gain problem.

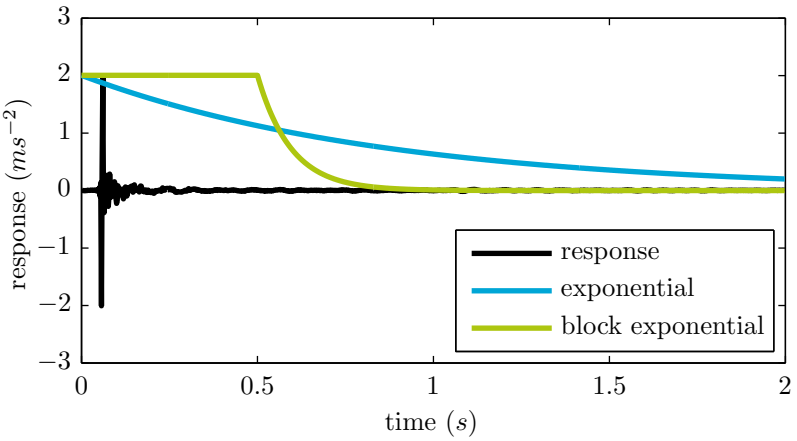

Figure 8.2: Different windows in the time domain

In figure 8.2 the block in the block exponential window is larger than the pre-trigger time. This is done such that the first part of the response is not affected by the window. In this example, the decay of the exponential window is such that at the end of the measurement block, the amplitude is 1%, whereas for the block exponential window the amplitude is only 0.01%. The block of the window is set to ⅛ of the measurement block. From figure 8.2 it shows already that for the block exponential window, the decay can be much steeper, which is preferred for this measurement. For a certain combination of the length of the block and a the decay of the exponential part an optimum can be found, such that most of the background noise is suppressed, while only a little bit of damping is added to the response.

To solve the problem caused by the constant contribution, a linear fit is subtracted from the time response. This is done with the `detrend` function in MATLAB. For a sequence of ten measurements an average constant of 0.003 is found, when the signal conditioner is set to $10V/g$.

The influence of this trend is illustrated in figure 8.3. In this figure the estimated response is shown for the same driving point as before. For the black line, an exponential window is directly applied to the obtained response, like Siglab will do. For the blue line, the `detrend` function is applied before the same exponential window.

For the the blue line, the coherence is bad below 2 Hz and it even becomes zero. This was also expected, because for low frequencies, the acceleration is very small and therefore the measured response only contains noise. Also, if the blue line is extrapolated for low frequencies, its response is more like the expectation. So the `detrend` function will be used for every measured output signal.

Now that the problem of the DC component is solved, the influence of the different windows can be evaluated in the frequency domain. In figure 8.4 the same driving point measurement as before is shown, but now with three different windowing options. The black line has a boxcar windown, the blue line has the exponential window applied and the green line has the box exponential window.

As expected, the response of the blue line is slightly below the other responses. The black line shows much sharper resonant peaks, but has the worst coherence around 20 Hz. Both

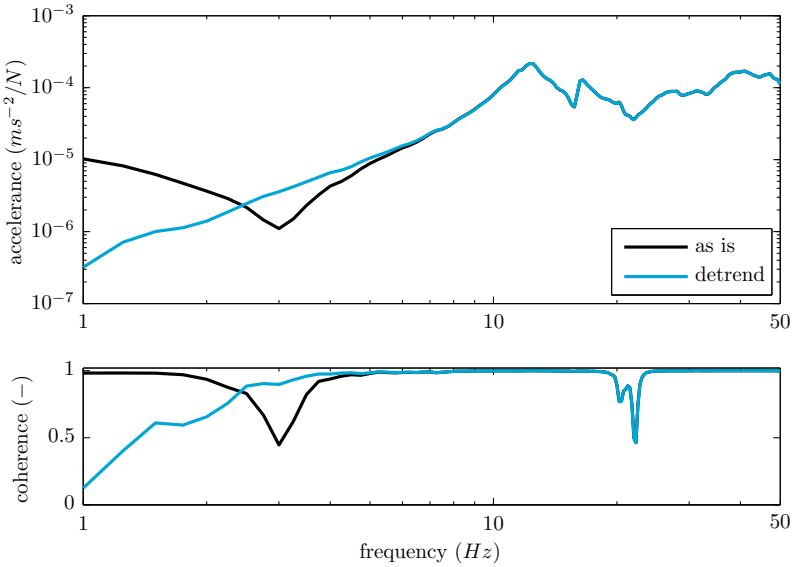

Figure 8.3: Artificial anti-resonance

the exponential and the block-exponential window suppress this background noise. The level for the block exponential is equal for the boxcar window. Except that the block exponential window smooths the first floor resonance, this window shows a much better response than the other two, so this window is used.

Because this is an impact measurement, the reference signal is only a short peak which is present at the beginning of the measurement block. So it might also be useful to apply a force window on the reference signal. This window is just a block that has a width of 20% of the full measurement block. This window eliminates any signal that the force sensor might pick up after the impact that should not be considered as input for the system. The impact hammer is held steady after the impact and it is found that the input spectrum was constant for the measurements in the frequency range of interest.

Number of averages

Another parameter to vary is the number of averages. Because the background noise is assumed to be completely random, increasing the number of averages, should result in a better coherence. In figure 8.5 the number of averages is changed for the same measurement results as before.

From this figure it is clear that the number of averages only changes the response around 20 Hz. Based on these results, it is sufficient to use 5 averages.

Dynamic range

The last setting is the range of the signals. This range determines the resolution of the response and should therefore be as low as possible. Initially the response contains a large

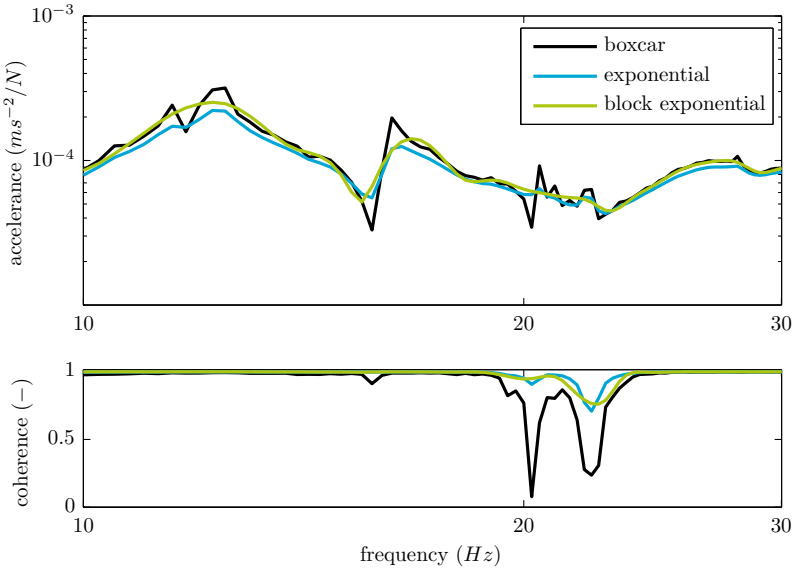

Figure 8.4: Different windowing settings

peak acceleration that can easily cause an overload when the range is set too low. When the range is set too high, the background noise will either be digitized as zero or a small and constant number, which might cause problems when calculating the coherence as found by Pavic et al. [44]. The solution is to reduce the range and excite the structure just below the range limit. However, for this measurements no problems were found with either the largest range or a slightly smaller range. It is observed that the initial acceleration of a driving point is much larger than other measurements, so the measurements might improve when changing the settings during the measurement. Because of the way the data is obtained, it is not easy to reject the frames with an overload, so the dynamic range of the data acquisition is set to 10 V. The amplifier settings on the signal conditioner can also be changed to provide sufficient input voltage.

8.2 Measurement set up

The measurement hardware is mainly selected on availability. Impact excitation is selected and the impact is applied with an instrumented hammer of 5.5 kg. With the soft tip, this will excite frequencies up to 200 Hz. The accelerometers to measure the response of the floor are charge transducer from Brüel & Kjær, type 4379. More details on the measurement set up can be found in appendix 11.2.3.

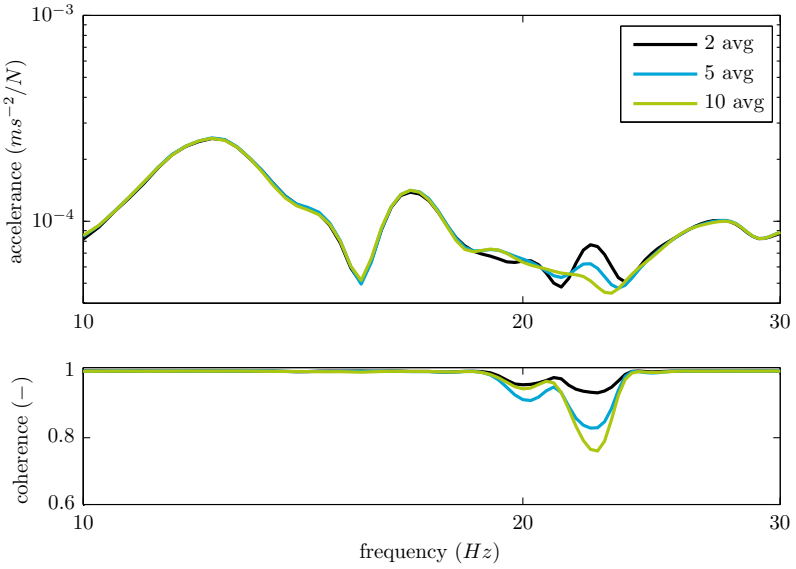

Figure 8.5: Increase number of averages

Chapter 9

Results

Now that the floor measurements are done, experimental verification as shown in figure 7.1 can be performed. This will result in a better approximation of the coupled response of a machine. Next, also the technique as outlined in chapter 5 will be validated.

9.1 Coupled response

To obtain a free description of the test case, first the test case will be measured on a much stiffer floor. For this measurement the same set up and post processing is used as for the floor measurements. At this point five translations are measured. Four translations at the corners of the frame and one in the middle of the tool. The first four translations are mapped into one translation and two rotations, so the 4 DOF test case measurement is obtained. The test case had to be built twice, first to measure the fixed response and a second time for the validation measurement. To check if the dynamics will not change between these two measurements, the repeatability is checked by rebuilding it three times on the stiff floor. The projected driving points for the translation are shown in figure 9.1.

In this figure, the top graph shows the accelerance for the three measurements. The bottom graph shows the imaginairy part of the dynamic stiffness. This is equal to the damper as measured for this system. The first build is without the tool, so the disc springs have a different static loading. Between the second and third build, the tool was positioned slightly different. Except for the added small antiresonance at 11 Hz for the second build, the accelerance is similar for each build. Unfortunately not as similar as hoped for, but the changes are small.

In the second graph, the damper values are shown. Between 12 and 18 Hz, these are similar for the second and third build. The values for the first build are slightly different, but this is probably caused by the different static deflection. It is also noted that between 18 and 19 Hz, this value becomes negative for each build. This is of course not possible for a passive system. This negative damper originates from the projection method. It is verified that the imaginary part of each driving point in the original DOF is always positive, but after the projection, the driving point for the translations is no longer always positive.

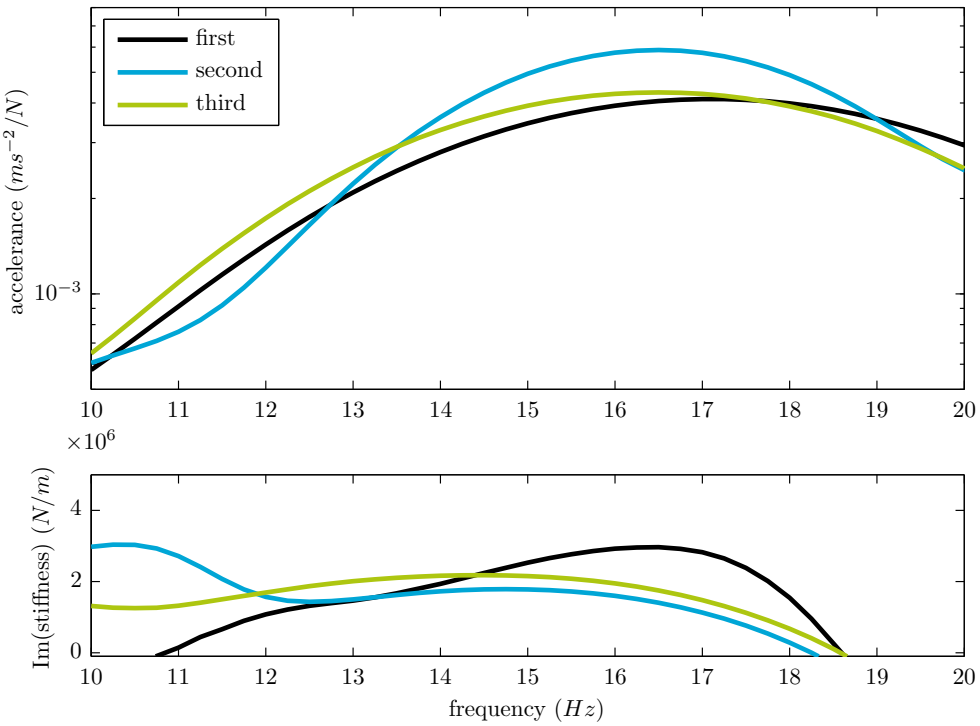

Figure 9.1: Repeatability test

Between 19 and 21 Hz it becomes negative, which translates to a negative damper. For the driving points, the impact location was next to the sensor, so the rotational modes are not excited as assumed by the projection. This does not matter for the translational mode.

For the data block *Test case fixed 5DOF* in figure 7.1 the third build is used. To account for the negative imaginary part of the stiffness, the value between 14 and 15 Hz is used for the complete frequency range. This will be denoted as the modified response. Basically the damping is assumed to be hysteretic. The damping is mainly caused by the friction between the disc spring and the base and top. It was tried to minimize this friction by smoothing the surface of the base or to lubricate the contact region, but neither of these shows any decrease in damping. Figure 9.2 shows the driving point measurement for the projected translation, together with the modified response and the same response for the model.

In this figure, the measured response show a very wide resonance peak. The modified response show a slightly different response around 18 Hz, which is caused by the change in damping. The shape of the resonance peaks shows why the problems as explained in section 7.2.2 might occur.

For high frequencies it looks like the mass is underestimated, but it is more likely that the difference is caused by measurement noise and the projection method used. The same holds for the stiffness for low frequencies. For the modified response, the damping is now fully hysteretic, so the stiffness is a little bit increased for the modified response. The

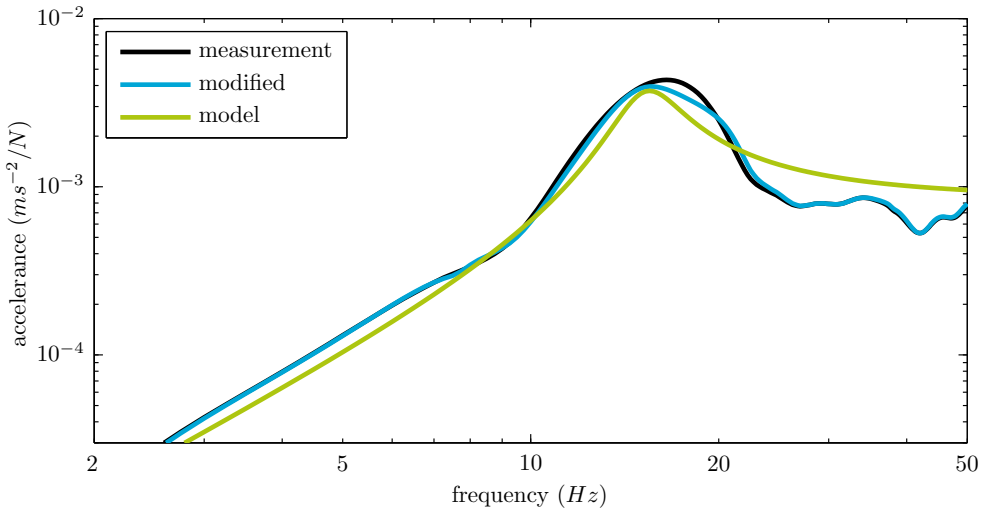

Figure 9.2: Fixed test case response, measured, modified and modelled

modified response will by used for the data block *Test case fixed 4DOF*.

To quantify the residual motion, the PAC numbers are calculated. Because these are defined as a summation over the frequency points, only the frequency points between 1 and 40 Hz are used to compute the PAC numbers. The values are shown in figure 9.3. In this figure the original measurements are on the horizontal axis and the expanded projections are on the vertical axis. The numbers correspond to the points on the test case. The size of the squares and the color represent the value of the PAC number. The scale is such that for values between 0.95 and 1.0, the square should turn from blue to green and for values between 1.0 and 1.05, the square should turn from green to orange. So as long as a square is not bright orange or blue, the PAC number is acceptable.

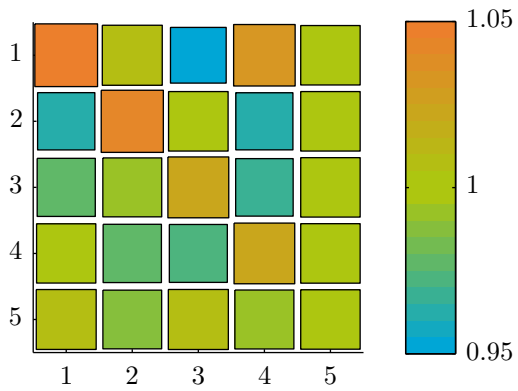

Figure 9.3: PAC numbers original measurement vs. expanded projection

From these numbers it follows that the residual motion, which is wasted by the projec-

tion, is very small. Generally the driving point measurements on the frame are slightly weakened, but most of the values are still acceptable. Two values in the first row are out of the range, but only slightly. More important is that the PAC numbers for the transmissibility measurements from the frame to the tool are very good, which are the most important entries for this validation.

When the coupling DOF are added to the test case, the actual FBS can be performed. The floor measurements will be used directly and the transmissibility from a force on the large mass to the translations of the second mass is shown in figure 9.4. In this figure, the black line is for the fixed case, the blue line is the result of the FBS method and the green line is the validation measurement.

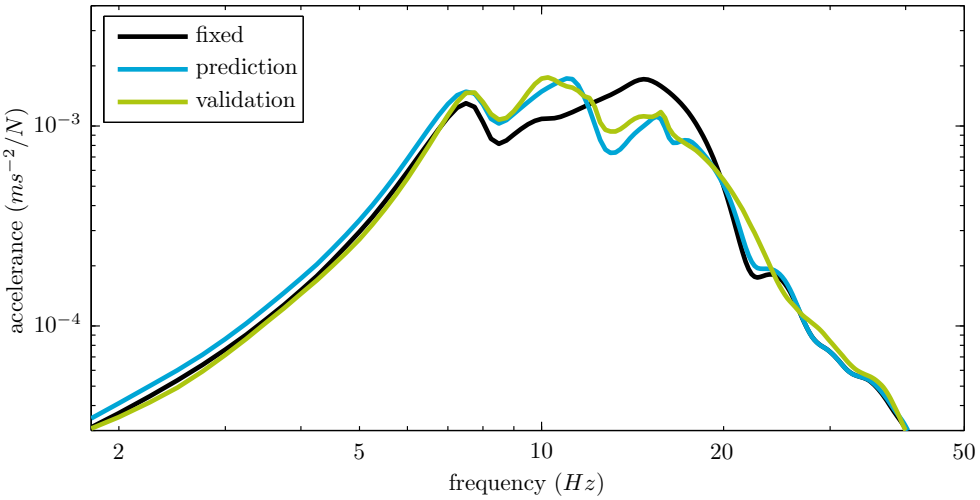

Figure 9.4: Fixed response, predicted coupled response, actual response

When the fixed measurement is compared to the coupled measurement, it is noted that the floor frequency is visible in this response, around 12 Hz. Because the level of this resonance is higher than the original level, this might cause problems for the accuracy if this was a real machine. The level of the first resonance of the frame however is less than for the fixed case. This is advantageous for the accuracy if this was a real machine.

When the predicted coupling is compared with the measured coupling, a few things are noted. First the two dominant eigenmodes of the machine at 7 and 15 Hz are predicted properly.

The floor mode at 12 Hz is slightly overestimated in the predicted response. Because for this mode, the error caused by the apparent stiffness is large, this will explain the overestimation.

The response between 12 and 15 Hz is slightly underestimated. It is not really clear what causes this underestimation. One explanation might be that the predicted response has a higher and sharper resonance peak for the floor mode, which is likely to be followed by a deeper anti resonance.

When the original projection would be used instead of the modified projection, another artificial resonance would be found at 18 Hz. This is caused by the fact that the damping

becomes zero for the projection. Also the amplitude of the floor mode would be larger, because there is less damping. Above 20 Hz the predicted response is equal to the fixed response, so no coupling is expected above this frequency. The validation measurement slightly differs from this response, but this is probably caused by the fact that the construction of the test case will be slightly different for both measurements.

For frequencies below 7 Hz, a little bit stiffness is lost for the predicted response. One explanation might be that there is some added noise in the sensors. Because both the test case and the floor is measured with the same sensors, this might add in the predicted response, especially when the measured signal is low. In figure 9.2 it was also found that the projected stiffness was less than the modelled stiffness, so this loss in stiffness could also result from the projection.

To quantify the residual motion in the projection of the validation measurement, the PAC numbers are computed. These numbers are shown in figure 9.5.

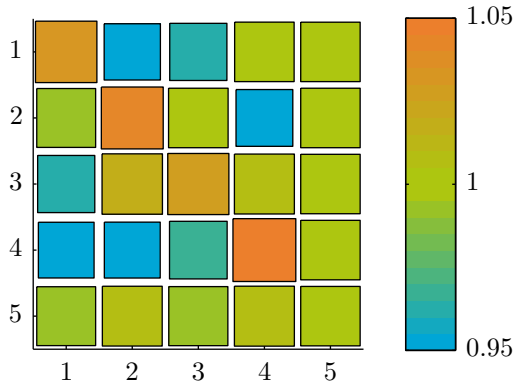

Figure 9.5: PAC numbers for validation measurement

Although the residual motion in the validation measurement is slightly larger, the same conclusions as for the PAC numbers of the fixed measurement can be drawn from this figure. The driving point measurements on the frame are less stiff, but the transmissibility from the frame to the tool is very good.

To further analyse the origin of the differences in figure 9.4, the coupling is performed with the 6DOF free model. Because the second mass is not modelled, a driving point for the translation of the frame is observed, as in figure 9.2. These coupling results are shown in figure 9.6.

In this figure the black line is the coupled response with a machine obtained from the fixed measurement, the blue line is the coupled response with a modelled machine and the green line is the response from the validation measurement. From this figure it should be noted that for the blue line, there is no loss in stiffness for the lower frequencies. Both machine descriptions are equally capable of reproducing the actual coupled response.

Figure 9.6 shows that FBS with the modelled test case estimates both the coupling with

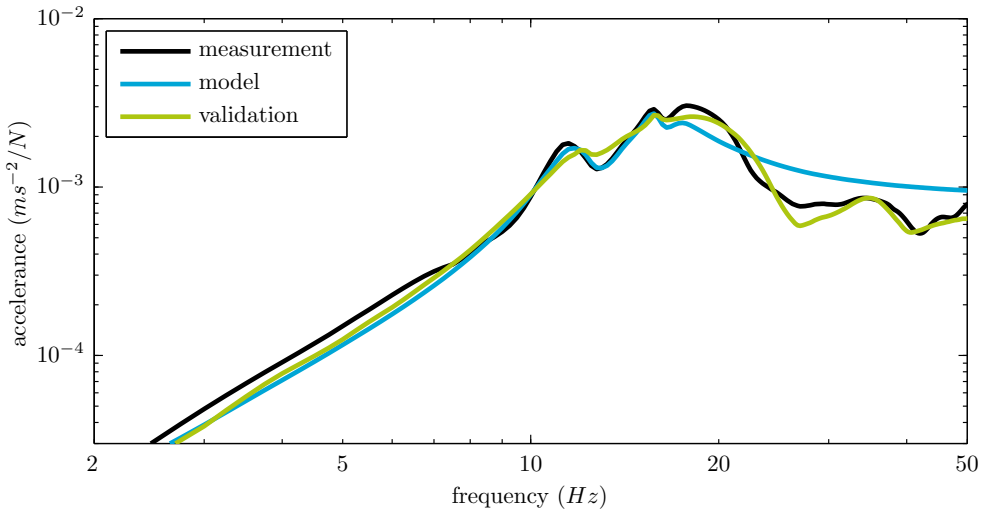

Figure 9.6: Predicted coupled response with measured and modelled test case and actual response

the floor at 12 Hz and the eigenmode of the frame at 15 Hz properly. Because the model is symmetric, there is no coupling between a force at the midpoint of the frame and the rotations of the frame. Therefore this model is not capable of reproducing the response around 18 Hz properly. A small peak is visible at 16 Hz, which is a second mode of the floor.

For low frequencies it is observed that the same difference is found between the model and the measurement. The model is closer to the validation measurement, which proves that the difference in of the stiffness in figure 9.4 is caused by the measured model description.

Around a resonance frequency, the stiffness and inertia terms of a response function are almost equal and should therefore cancel each other. Therefore the response around a resonance frequency is dominated by the damping, which is imaginary. To visualise the deflection shapes of the predicted response, the imaginary part of the accelerance can be observed. The real and imaginary parts are shown in figure 9.7.

In this figure the black line is the projected translation of the mount, which is equal to the translation of the floor. The blue line is the translation of the frame and the green line is the translation of the tool. The orange and purple lines are the validation measurements for either the frame and the tool.

From this figure it shows that the response of the frame is overestimated at the first eigenfrequency of the floor. Around 13 Hz the mounts and the frame should move upward, but the translation of the frame is exaggerated. This is caused by the phenomenon as described in section 7.2.2. The used disc springs are not linear, so around a resonance, the deformations are larger and therefore the spring is less stiff. So at these frequency the added stiffness is overestimated which results in an apparent stiffness which is less than the actual stiffness.

Overall it can be concluded from figure 9.7 that the imaginary part is mostly overestimated, while the real part is mostly underestimated. The validation response show a

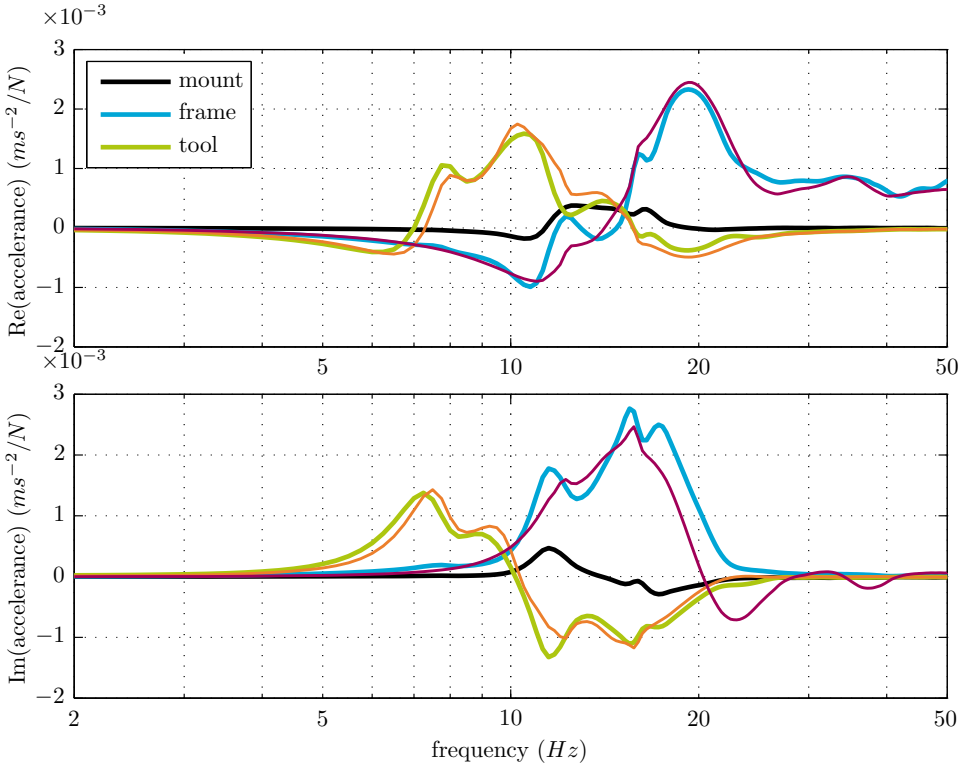

Figure 9.7: Real and imaginary part of predicted response, with validation measurement

more complex deflection shapes. This is also caused by the projection, as with the fixed measurement. The purple line in the second plot also crosses the frequency axis, which is physically not possible for a passive system.

9.2 Floor vibrations

To validate the technique as described in chapter 5, the floor vibrations are also measured, as explained in section 8.2. The sensors were positioned next to each mount. The frequency resolution should of course be equal to the frequency resolution of the other measurements, which is 0.25 Hz. The total measurement length is 1600 seconds, so 400 blocks can be made from this signal.

To provide sufficient and consistent vibrations a shaker with a small mass was placed near the test case. The excitation signal was a two tone at 12 and 16 Hz. This measurement was performed with and without the test case installed, while the shaker was in the same position and the excitation amplitude was equal.

The vibration levels are obtained at each physical coupling point, but these are not the actual coupling DOF as used in this method. To obtain the translational vibrations, the four measurements are averaged. This averaging is done for the complex frequency spectrum, so 400 complex spectra are obtained. These are used as the translational interface gap. This is also done for the validation measurement. The rotational interface gap is zero.

The results are shown in figure 9.8. In this figure the average spectrum of the 400 measurement blocks are shown.

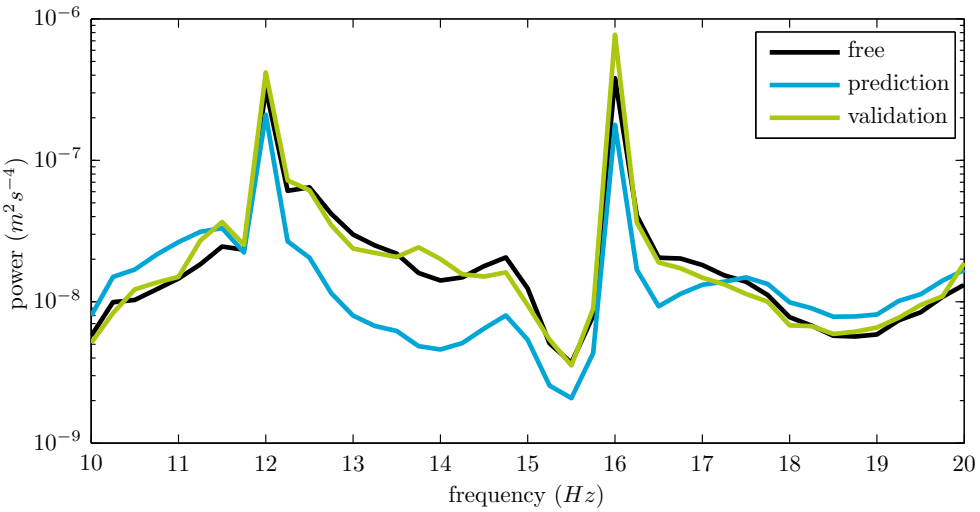

Figure 9.8: Power spectrum of floor vibrations with measured test case

In this figure the black line are the free vibrations. These are also used in equation 5.19 for $\bar{\boldsymbol{\delta}}_c$. The blue line are the vibrations when the interface force is applied on the coupling DOF of the floor and the green line are the vibrations of the floor with the test case on it.

From these measurements it shows that the vibration level of the floor should not really change, whether the test case is placed on the floor or not. The only difference is at the two excited frequencies, which are slightly amplified by the test case.

There is however a lot of difference predicted by this ground vibration transmission technique. As found in the previous section, the stiffness of the spring was slightly weakened around 12 Hz when the coupling DOF were added. This might cause the test case to behave more like a mass tuned damper, which causes the underestimation of the vibration at 12 Hz.

As another check, the vibration levels are again computed with the 6DOF free model of the test case. These results are shown in figure 9.9.

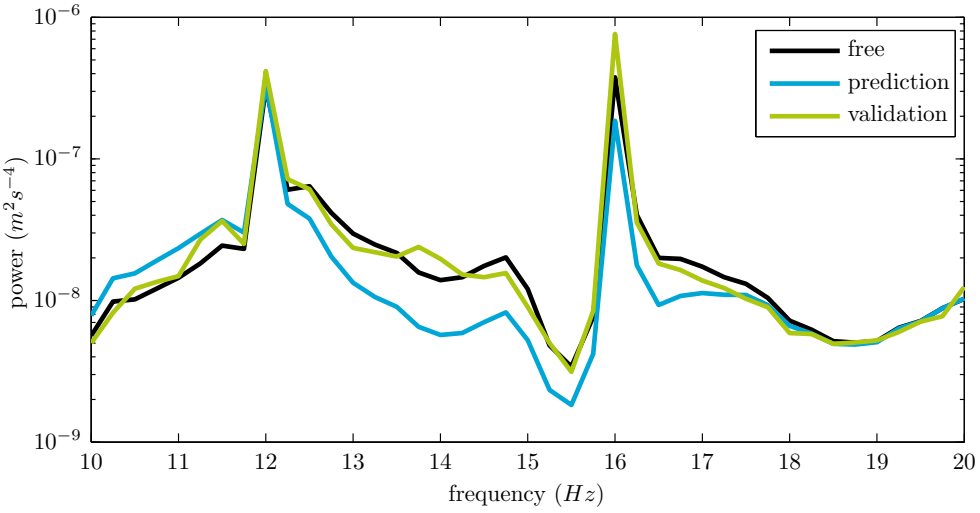

Figure 9.9: Power spectrum of floor vibrations with test case model

From figure 9.9 a few things should be noted. First, the predicted vibration level around 12 Hz has improved, the blue line is closer to the green line, than it was in figure 9.8. In figure 9.6 it was shown that the coupled response for the measured test case was different from the modelled test case around 16 Hz. In figure 9.9 however, the predicted vibration level at 16 Hz is for both cases almost equal.

Although the rotational vibrations are wasted, this is not the origin of this error. It was found that when the coupling is done with the four physical DOF, such that the measured vibrations can be used directly, the same result is obtained. Because the floor has a relatively high rotational stiffness, it is not likely to vibrate in rotations.

Part III

Comparison and Conclusion

Chapter 10

Comparison

Now that the techniques as proposed by this thesis are verified with an experimental test case, it interesting to see how these technique will improve the estimation over the current methods as used by Philips. For this comparison the same 6DOF test case model from chapter 6 will be used, but this time with an additional translation DOF for the tool. This model is shown in figure 10.1.

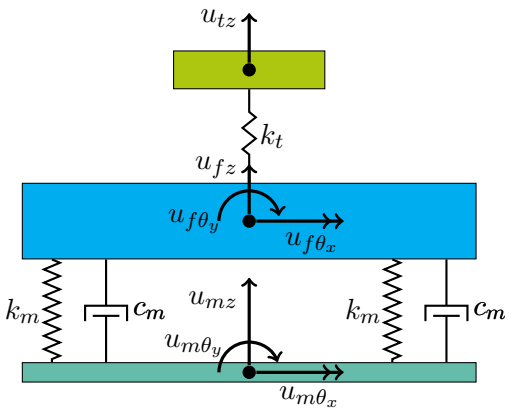

Figure 10.1: Model used for comparison

This comparison will be done for the coupled response in section 10.1 and for the vibration levels in section 10.2.

10.1 Coupled response

To predict the coupling of the machine with the floor, there are three alternatives suggested.

1. Only the floor stiffness is taken into account.
2. Only driving point measurements of the floor are used.

3. The interface of the floor is assumed rigid and can therefore be characterised with a single driving point measurement.

These will be discussed in this section and to the reference case. The coupling is always done with the FBS method, only the description of the interface of the floor is altered. The reference case will always be the coupling to the full measurements of the floor. This will be shown as *full coupling*.

10.1.1 Floor stiffness

To predict the coupled response for the machine, typically only the floor stiffness is taken into account. If this stiffness is not yet known, a value of 10^8 N/m is assumed, otherwise the stiffness is obtained from the measurements. This stiffness is then obtained by linearising measured response below the first eigenfrequency. For the floor under consideration, a linearised stiffness k_f of $7.7 \cdot 10^7$ N/m is found. The accelerance for the interface of the floor is now given by

$$\boldsymbol{Y}_{cc}^{f} = \boldsymbol{T} \begin{bmatrix} \frac{-\omega^2}{k_f} & \mathbf{0} & \mathbf{0} & \mathbf{0} \\ \mathbf{0} & \frac{-\omega^2}{k_f} & \mathbf{0} & \mathbf{0} \\ \mathbf{0} & \mathbf{0} & \frac{-\omega^2}{k_f} & \mathbf{0} \\ \mathbf{0} & \mathbf{0} & \mathbf{0} & \frac{-\omega^2}{k_f} \end{bmatrix} \boldsymbol{T}^T \tag{10.1}$$

where $\boldsymbol{T}$ is the transformation matrix to project four translations on one translation and two rotations (section 7.1). The response for the linearised stiffness, together with the fixed response and a full coupled response is shown in figure 10.2.

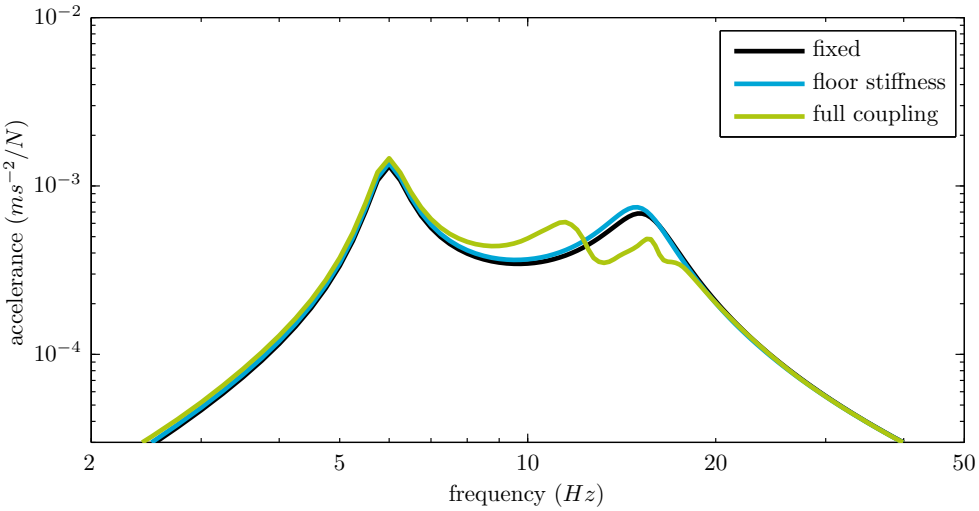

Figure 10.2: Comparison between floor stiffness and full coupling

This figure shows the same behaviour as already found in chapter 2. The response for the first eigenmode of the machine is equal to the fixed response and the frequency of the

second mode has shifted slightly. In the full coupling the eigenfrequency of the floor is visible and the second mode of the machine is damped, due to the mass of the floor.

10.1.2 Four driving points

The measurements to obtain the linearised floor stiffness are typically performed on each mounting location, but the transmissibility between mounting locations is almost never measured, due to time constraints. This is equal to when only the driving point measurements of the floor are used for the coupling. With this method, there is also a mass of the floor present in the coupling. So the accelerance for the interface of the floor is now given by

$$\boldsymbol{Y}_{cc}^{f} = \boldsymbol{T} \begin{bmatrix} \boldsymbol{Y}_{cc}^{1} & \boldsymbol{0} & \boldsymbol{0} & \boldsymbol{0} \\ \boldsymbol{0} & \boldsymbol{Y}_{cc}^{2} & \boldsymbol{0} & \boldsymbol{0} \\ \boldsymbol{0} & \boldsymbol{0} & \boldsymbol{Y}_{cc}^{3} & \boldsymbol{0} \\ \boldsymbol{0} & \boldsymbol{0} & \boldsymbol{0} & \boldsymbol{Y}_{cc}^{4} \end{bmatrix} \boldsymbol{T}^{T} \tag{10.2}$$

where $\boldsymbol{Y}_{cc}^{i}$ is the driving point measurement of the floor at location i. This response together with the fixed response and a full coupled response is shown in figure 10.3.

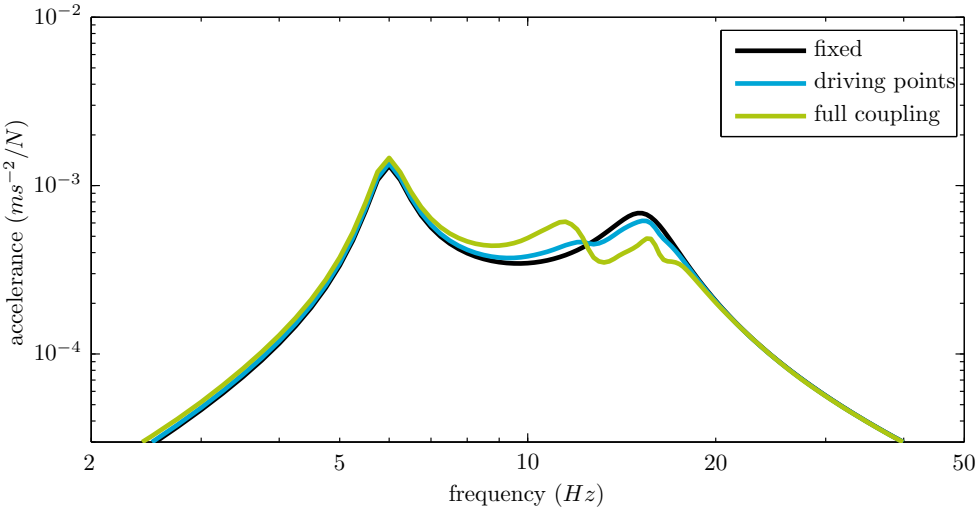

Figure 10.3: Comparison between only driving points and full coupling

When figure 10.3 is compared to figure 10.2, this method does not show much improvement. The eigenmode of the floor is visible, but the amplitude is very much underestimated. The amplitude for the second mode of the machine is damped slightly, but still overestimated. Generally, the stiffness of the floor is overestimated with this method, because the predicted response is very close to fixed response.

10.1.3 Single driving point

The machine has three coupling DOF, one translation and two rotations. The floor measurement in the original DOF are also translations and from previous results it is

found that the interface of the floor is very rigid. This means that for each point on this interface the same stiffness is found, so one measurement should be sufficient if only translations are observed. Next the translation coupling DOF is coupled to one of the original driving point measurements of the floor. The rotations are left free in this case, but these could also be fixed or coupled to a very stiff rotational spring if needed. The accelerance for the interface of the floor is now simply defined as

$$\boldsymbol{Y}_{cc}^{f} = \boldsymbol{Y}_{cc}^{i} \tag{10.3}$$

where $\boldsymbol{Y}_{cc}^{i}$ is one of the four driving point measurements of the floor. Note that now there is only one coupling DOF, so $\boldsymbol{B}$ is a single row vector. The result is shown in figure 10.4.

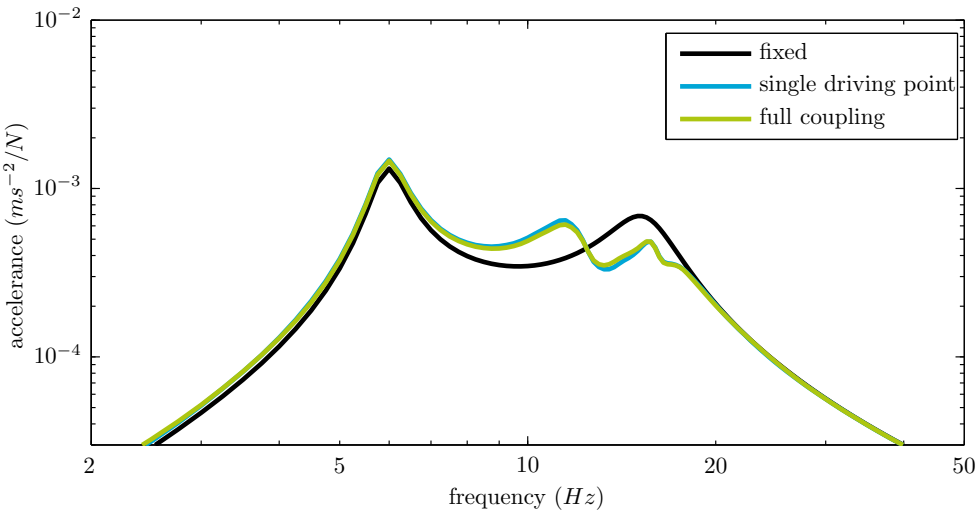

Figure 10.4: Comparison between single point coupling and full coupling

For this example it turns out that it is sufficient to use only one driving point. This is because this example is symmetric, so there is no coupling between the translation and the rotation. It is found however that if the location of one mount is changed slightly, the results are still very good. The stiffness of the floor is very well estimated with this method. Between 12 and 15 Hz, it slightly deviates from the full coupling. For the full coupling, the full floor measurements are used. After the projection, an averaged response for the floor is obtained, which will be slightly different from a single measurement.

10.2 Vibration levels

Currently, the vibration levels are directly imposed on the coupling DOF of the machine. This way, the floor is assumed rigid, which is a crude approximation as shown earlier. Although the results from section 9.2 were not really satisfying, it is still interesting to compute if the tool would see a different vibration level for both methods. The same model and floor measurement as used in the previous section are also used here. Furthermore, for the floor a flat power spectrum with an amplitude of $10^{-2}m^2s^{-4}$ is assumed for the translation, there are no rotational vibrations. In figure 10.5 the vibrations of the tool are shown when the vibrations are directly imposed on the coupling DOF together with the vibrations as obtained with the vibration transmission method.

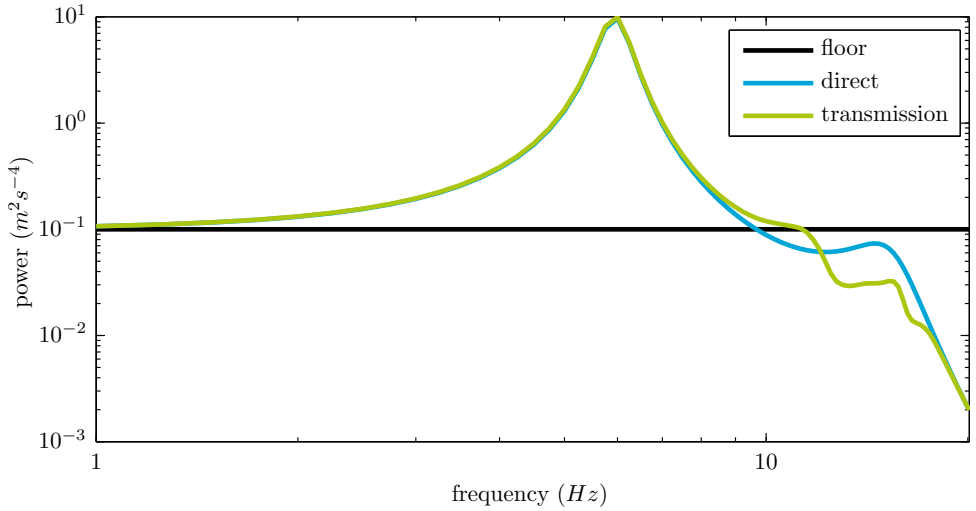

Figure 10.5: Comparison between direct imposed vibrations and vibration transmission method

In this figure, the vibrations around 6 Hz are strongly amplified. This is the eigenfrequency of the tool, so this was expected. Both methods show the same amplification, so floor stiffness has no influence on this frequency. In the previous section it was already found that the coupled response at these frequencies is close to the fixed response. Above 10 Hz, the methods show a different power spectrum. This is because there are more resonance frequencies present in the coupled response, which will either amplify or damp the vibrations. After 20 Hz, the vibrations for both methods are again equal, which also corresponds to the previously obtained results.

Chapter 11

Conclusions and recommendations

The objective of this thesis has been to better predict the coupled response of sensitive machinery, when the floor can not be assumed as rigid. To do such, the FBS method is proposed and validated on a test case. From this validation, a number of conclusions can be drawn. These are discussed in section 11.1. This chapter concludes with recommendations about how and when this technique should be applied. Also some recommendations about further research are presented.

11.1 Conclusions

The conclusions are divided in three parts. The first part focusses on floor measurements. Some conclusions on the quality and number of measurement points are drawn. Secondly, the proposed technique to predict the coupled response is validated. Together with the comparison of the existing techniques, some conclusions are given. For the third part, a new method to predict the vibration levels of the floor is proposed. This was also validated, which results in a number of conclusions.

11.1.1 Floor measurements

From chapter 8 it follows that it possible to obtain a quite good response of the floor with an impact excitation. However some care should be taken when selecting the post-processing settings. Because the dynamic response of the floor is low, the windowing might cause an artificial anti resonance, as shown in section 8.1.

Because of the large damping, only very short response signals are measured. This limits the frequency resolution. The only option to improve the resolution is to use a shaker. With a shaker, it is possible to have longer response signals and therefore a much better frequency resolution.

11.1.2 Coupling

From the results in section 9.1 it can be concluded that Frequency Based Substructuring can predict the coupled response of the machine on the floor accurately. The predicted response showed only slight deviations from the validation measurement, but these were mainly caused by the free description of the test case. It turned out that, although the test case was designed to be as simple as possible, it was very hard to obtain a proper dynamic description of this system. This will not be the case when a machine is still being designed, because then the free response can easily be calculated from the model.

In chapter 10 it was found that it is insufficient to only use the linearised stiffness of the floor. When this is done, a number of errors are made.

- The floor stiffness depends on the number of coupling points, because for each mount another spring is added to the total system.
- The rotational stiffness of the floor depends on the geometry of the machine, rather than on the floor. If the mounts are placed further apart in the model, a larger rotational stiffness is found for the floor.
- The participating mass is simply ignored. For the case treated in this thesis the eigenfrequency of the floor was within the frequency range of interest. Therefore another resonance appears in the coupled response. This is never found when only the floor stiffness is used.

From section 10.1 it is found that it is also insufficient to only use driving point measurements. Furthermore it follows from this comparison that increasing the number of mounting points for a machine does not increase the apparent floor stiffness. This is caused by the fact that the interface of the floor is generally very rigid.

11.1.3 Vibration levels

The proposed TPA method to predict the new vibration levels of the floor could not be validated based on the results shown in section 9.2. Theoretically this is a much better technique than to apply the floor vibrations directly on the mounts of the machine, because this technique also takes the floor dynamics into account.

From section 10.2 it followed that the vibration levels inside the machine for both methods are equal for frequencies where no coupling occurs between the floor and the machine.

11.2 Recommendations

11.2.1 When to use the FBS method

Although the results obtained with the FBS method are always more accurate than any other assumption, it is not always worth the effort. To provide a rough indication, a short analysis is done with a simple model. For this model the machine is assumed to be an

SDOF system, with a mounting stiffness k_m and an eigenfrequency ω_m^{fixed}. The floor is also assumed to be an SDOF oscillator, with a stiffness k_f and an eigenfrequency ω_f. In figure 11.1 the ratio $\frac{\omega_m^{coupled}}{\omega_m^{fixed}}$ is shown.

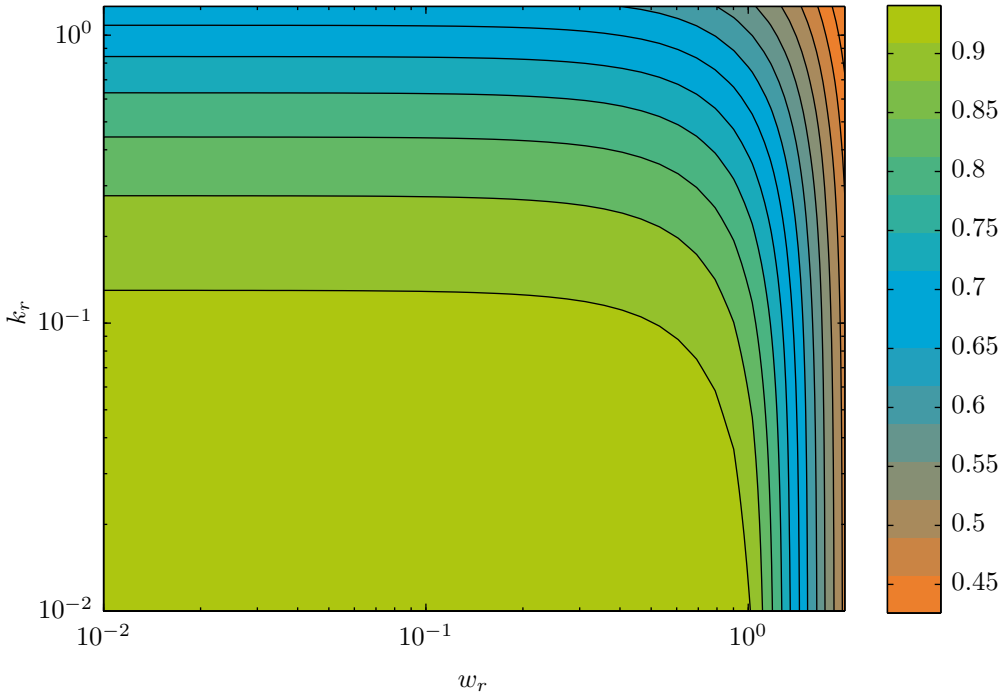

Figure 11.1: Relative change in eigenfrequency of the machine for different stiffness and frequency ratios

In this figure ω_r is defined as $\frac{\omega_m^{fixed}}{\omega_f}$ and k_r is defined as $\frac{k_m}{k_f}$. From this figure it follows that if the mounting stiffness is only a tenth or less than the floor stiffness and the eigenfrequency of the mounts is below the eigenfrequency of the floor, there will be almost no coupling and the machine will behave as if it is fixed. If this is not the case, then it is recommended to use the FBS technique to predict the coupling. This is for instance the case when a machine is placed on a floor which has a quite low eigenfrequency.

11.2.2 How to use the FBS method

When it is decided to use the FBS method, the most important decision is to define the number of coupling DOF. The number of coupling DOF may never exceed the number of possible deformations, because the FBS method depends on an inversion of the interface flexibility. It is even better if the number of coupling DOF is less then or equal to the number of deformations that will physically occur. Based on this, the following recommendations are given for both the machine model and the floor measurement.

- To reduce the number of coupling DOF in the model of the machine, equivalent

mounting points can be defined for parts of the machine that are rigid in the frequency range of interest.

- When the dynamic flexibility of the floor is available for all the physical mounting locations, the projection method as explained in section 7.1 should be used to obtain the dynamic flexibility on the coupling DOF.

- When the floor measurements are to be done, it is recommended to measure the coupling DOF directly, in stead of the full matrix for all the physical mounting locations. This reduces the measurement time significantly and it is shown in section 10.1 that this is still sufficient if only the translations are observed.

- When it is found that the rotations are also of importance, it is recommended to select three or four measurement locations around the coupling point and obtain the rotational information with the projection method from section 7.1.

- Because the off-diagonal terms in the dynamic flexibility matrix are as important as the driving points, a full matrix should always be measured. The only way to reduce the measurement time is to use as much sensors as possible simultaneously.

11.2.3 Further improvements

Coupling The FBS method is gaining more popularity and therefore a lot of research is already done and is being done by many others. In this thesis it is shown that the technique as it is known today can already be implemented successfully, so no further improvements are necessary for this technique.

There are however two things that might be worth investigating.

- For really large machines that are placed on floors with a lot of damping, especially slab on grade floors, the off-diagonal terms in the floor measurements might become less important. This will decrease the measurement time and therefore this technique can used in a much earlier stage of the design process. It would be nice if some guidelines are developed that give an indication of the importance of the off diagonal terms based on general floor properties.

- The damping in the floor will dissipate energy from the machine. The test case in this thesis was designed to have very little damping, but it turned out that the disc springs added a lot of damping. Even when the surfaces were smoothed and lubricated. Since the damping determines the height of the resonance peaks, it will influence the achievable accuracy of the machine. It is therefore recommended to perform an experimental verification with another test case which has very little damping.

It is also recommended to do a case study with some models of real machines that were already developed in the past. This will give a good indication for which type of machines this technique will typically yield a much better prediction of the coupled response.

Vibration transmission The proposed method to predict the vibration levels of the floor when the machine is placed, was not validated. There was not much control on the conditions for the experimental validation. The technique is however still very promising and it is therefore recommended to set up a much simpler experiment to validate the practical limitations of this technique. It is suggested that this experiment should not represent a machine on a floor, but that it consists of simple masses and springs. It is also important that one has full control over the imposed forces and/or displacements.

Bibliography

[1] M. Wilford and P. Young. *A Design guide for Footfall induced vibration.* The Concrete Centre, 2006.

[2] A.L Smith, S.J. Hicks, and P.J. Devine. *Design of floors for vibration: A new approach (SCI P354).* SCI, Ascot, Berkshire, revised edition edition, February 2009.

[3] H. Amick, S. Hardash, P. Gillett, and R.J. Reaveley. Design of stiff, low-vibration floor structures. *Proceedings of SPIE*, 1619:180–191, 1992. doi: 10.1117/12.56837.

[4] C. Gordon. The design of low-vibration buildings for microelectronics and other occupancies. *First International Conference on Vibration Control in Optics and Metrology, SPIE Proceedings*, 732, 1987.

[5] C.Q. Howard and C.H. Hansen. Vibration analysis of waffle floors. *Computers and structures*, 81:15–26, 2003. doi: 10.1016/S0045-7949(02)00348-6.

[6] *Slimdek Manual.* Corus, 2009.

[7] S. C. Kerr and N. W. M. Bishop. Human induced loading on flexible staircases. *Engineering Structures*, 23(1):37 – 45, 2001. ISSN 0141-0296. doi: 10.1016/S0141-0296(00)00020-1.

[8] J.E.A. Bertram and A. Ruina. Multiple walking speed-frequency relations are predicted by constrained optimization. *Journal of Theoretical Biology*, 209:445–453, 2001. doi: 10.1006/jtbi.2001.2279.

[9] S.C. Kerr. *Human induced loading on staircases.* PhD thesis, University Collage of London, Mechanical Engineering Department, 1998.

[10] Y. Matsumoto, S. Sato, T. Nishioka, and H. Shiojiri. A study on design of pedestrian over-bridges. *Transactions of Japan Society of Civil Engineers*, 4:50–51, 1972.

[11] S. Zivanovic, A. Pavic, and P. Reynolds. Vibration serviceability of footbridges under human-induced excitation: a literature review. *Journal of Sound and Vibration*, 279: 1–74, 2005. doi: 10.1016/j.jsv.2004.01.019.

[12] M. Willford, P. Young, and C. Field. Predicting footfall-induced vibration: Part 2. *Structures and Buildings*, 160:73–79, 2007.

[13] C.J. Middleton and J.M.W. Brownjohn. Response of high frequency floors: A literature review. *Engineering Structures*, 32:337–352, 2010. doi: 10.1016/j.engstruct.2009.11.003.

[14] A. Pavic and P. Reynolds. Vibration serviceability of long-span concrete building floors. part 1: Review of background information. *Shock and Vibration Digest*, 34: 191–211, 2002.

[15] C.G. Gordon. Generic criteria for vibration-sensitive equipment. *International Society for Optical Engineering (SPIE)*, 1619:71–85, 1992. doi: 10.1117/12.56826.

[16] H. Reiher and F. Meister. Die empfindlichkeit des menschen gegen erschtterungen. *Forschung im Ingenieurwesen*, 2:381–386, 1931. ISSN 0015-7899. doi: 10.1007/BF02578773.

[17] M. Gendreau H. Amick and, Todd Busch, and Colin Gordon. Evolving criteria for research facilities: Vibration. *Proceedings of SPIE*, 5933, 2005. doi: 10.1117/12.617970.

[18] J. Brownjohn and A. Pavic. Vibration control of ultra-sensitive facilities. *Proceedings of the ICE - Structures and Buildings*, 159(5):295–306, 2006. doi: 10.1680/stbu.2006.159.5.295.

[19] C.G. Gordon. Generic vibration criteria for vibration-sensitive equipment. *Proceedings of SPIE*, 3786:22–33, 1999. doi: 10.1117/12.363802.

[20] K. A. Ahlin. Response equivalent peak velocity: a new method for description of vibration environment for sensitive equipment in buildings. *Proceedings of SPIE*, 3786:118–125, 1999. doi: 10.1117/12.363788.

[21] E.E. Ungar and R.W. White. Footfall-induced vibrations of floors supporting sensitive equipment. *S V Sound and Vibration*, 13(10):10–13, 1979.

[22] I. Chowdhury and S.P. Dasgupta. *Dynamics of Structure and Foundation: Fundamentals*. Number 1 in Dynamics of Structure and Foundation: A Unified Approach. CRC Press, 2009. ISBN 978-0-415-47145-9.

[23] J. Ahn, G. Biscontin, and J.M. Roësset. Natural frequency and damping ratio of a vertically vibrated surface foundation. *Soil Dynamics and Earthquake Engineering*, 31(4):674–681, April 2011. doi: 10.1016/j.soildyn.2010.12.006.

[24] S. Haifeng, J. Liping, and M. Xianchun. Selection of artificial boundary condition on soil-structure dynamic interaction. *Key Engineering Materials*, 450:498–501, 2010. doi: 10.4028/www.scientific.net/KEM.450.498.

[25] B.M. Gur, C. Niezrecki, and P. Avitabile. Improvements in modal parameter extraction through post-processing frequency response function estimates. In *IMAC-XXVI: Conference & Exposition on Structural Dynamics*, 2008.

[26] E. Reynders, A. Teughels, and G. De Roeck. Finite element model updating and structural damage identification using omax data. *Mechanical Systems and Signal Processing*, 24(5):1306 – 1323, 2010. ISSN 0888-3270. doi: 10.1016/j.ymssp.2010.03.014. ¡ce:title¿Special Issue: Operational Modal Analysis¡/ce:title¿.

[27] P. Reynolds and A. Pavic. Impulse hammer versus shaker excitation for the modal testing of building floors. *Experimental Techniques*, 24:39–44, 2000. doi: 10.1111/j.1747-1567.2000.tb00911.x.

[28] R.R. Craig and M.C.C. Bampton. Coupling of substructures for dynamic analyses. *AIAA Journal*, 6(7):1313–1319, 1968. doi: 10.2514/3.4741.

[29] R.J. Guyan. Reduction of stiffness and mass matrices. *AIAA Journal*, 3(2):380, 1965. doi: 10.2514/3.2874.

[30] D. de Klerk, D.J. Rixen, and S.N Voormeeren. General framework for dynamic substructuring: History, review and classification of techniques. *AIAA Journal*, 46 (5):1169–1181, May 2008. doi: 10.2514/1.33274.

[31] D.J. Ewins. *Modal testing: theory, practice, and application*. Mechanical engineering research studies: Engineering dynamics series. Research Studies Press, 2000. ISBN 9780863802188.

[32] W. D'Ambrogio and A. Sestieri. A unified approach to substructuring and structural modification problems. *Shock and Vibration*, 11(3-4):295–309, 2004.

[33] B. Jetmundsen, R.L. Bielawa, and W. G. Flannelly. Generalized frequency domain substructure synthesis. *Journal of the American Helicopter Society*, 33(1):55–64, 1988. doi: 10.4050/JAHS.33.55.

[34] D. de Klerk, D.J. Rixen, and J. de Jong. The frequency based substructuring (fbs) method reformulated according to the dual domain decomposition method. In *IMAC-XXIV: Conference & Exposition on Structural Dynamics*, 2006.

[35] D. de Klerk, D.J. Rixen, S.N. Voormeeren, and F. Pasteuning. Solving the rdof problem in experimental dynamic substructuring. In *IMAC-XXVI: Conference & Exposition on Structural Dynamics*, 2008.

[36] K. Cuppens, P. Sas, and L. Hermans. Evaluation of the frf based substructuring and modal synthesis technique applied to vehicle fe data. In *ISMA 25: International Conference on Noise and Vibration Engineering*, pages 1143–1150, September 2000.

[37] D.J. Rixen. How measurement inaccuracies induce spurious peaks in frequency based substructuring. In *IMAC-XXVI: Conference & Exposition on Structural Dynamics*, 2008.

[38] D. Nicgorski and P. Avitabile. Experimental issues related to frequency response function measurements for frequency based substructuring. In *IMAC-XXVI: Conference & Exposition on Structural Dynamics*, 2008.

[39] D. Nicgorski and P. Avitabile. Condtioning of frf measurements for use with frequency based substructuring. In *IMAC-XXVII: Conference & Exposition on Structural Dynamics*, 2009.

[40] D. de Klerk and D.J. Rixen. Component transfer path analysis method with compensation for test bench dynamics. *Mechanical Systems and Signal Processing*, 24 (6):1693 – 1710, 2010. ISSN 0888-3270. doi: 10.1016/j.ymssp.2010.01.006.

[41] T.P. Dobrowiecki, J. Schoukens, and P. Guillaume. Optimized excitation signals for mimo frequency response function measurements. *Instrumentation and Measurement, IEEE Transactions on*, 55(6):2072 –2079, dec. 2006. ISSN 0018-9456. doi: 10.1109/TIM.2006.887036.

[42] M.H. Richardson and D.L. Formenti. Parameter estimation from frequency response measurements using rational fraction polynomials. In *IMAC-I: Conference & Exposition on Structural Dynamics*, 1982.

[43] N.M.M. Maia and J.M.M. Silva. *Theoretical and experimental modal analysis*. Mechanical engineering research studies: Engineering dynamics series. Research Studies Press, 1997. ISBN 9780863802089.

[44] A. Pavic, R. Pimentel, and P. Waldron. Instrumented sledge hammer impact excitation: Worked examples. In *IMAC-XVI Proceedings*, 1997.

Definition of Frequency Response Functions

For this thesis the terminology for the different FRFs as formulated by Ewins [31] are used. These are stated in table 1

Response	$\frac{\text{Response}}{\text{Force}}$	$\frac{\text{Force}}{\text{Response}}$
Displacement	Receptance Compliance Admittance Dynamic Flexibility	Dynamic Stiffness
Velocity	Mobility	Impedance
Acceleration	Accelerance Inertance	Apparent Mass

Table 1: Terminology for different FRFs

Fixed interface

The TPA method was used by de Klerk and Rixen [40] to analyse the transfer path from the gear force inside the differential to noise inside the car. From this example it is clear that it is quite difficult to measure these forces directly. To illustrate this method, the simple system as shown in figure 2 is used.

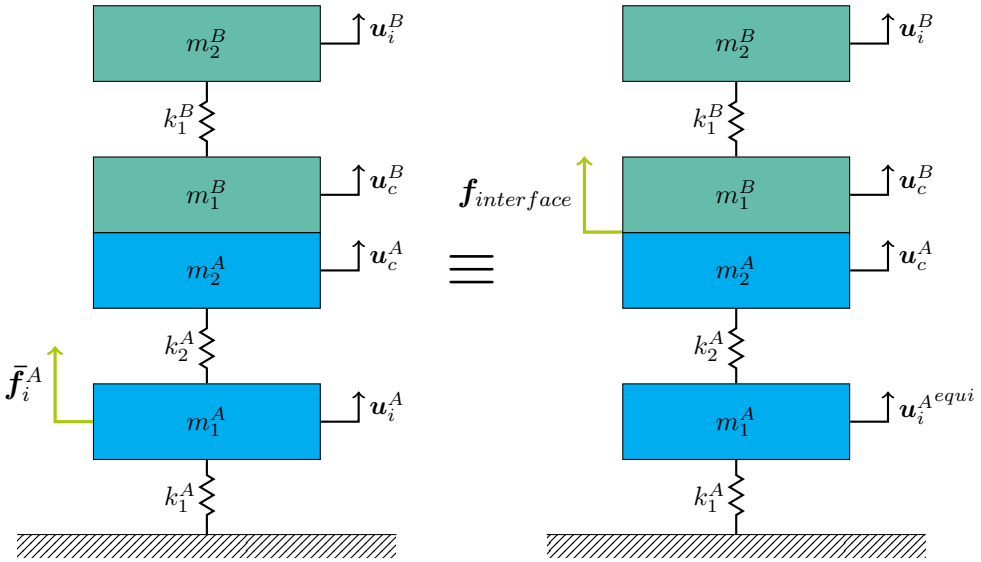

Figure 2: Original system (left) and the equivalent system (right)

This is a simple 3 DOF system that consists of two subsystems. In the original problem, the first DOF of substructure A is excited with an unknown force and the response of substructure B is of interest. It turns out that this is equal to an equivalent system, where the imposed excitation inside substructure A is substituted with an equivalent force on the interface. When using a primal assembly, the following representation is found

$$\begin{bmatrix} \boldsymbol{Z}_{ii}^A & \boldsymbol{Z}_{ic}^A & 0 \\ \boldsymbol{Z}_{ci}^A & \boldsymbol{Z}_{cc}^A + \boldsymbol{Z}_{cc}^B & \boldsymbol{Z}_{ci}^B \\ 0 & \boldsymbol{Z}_{ic}^B & \boldsymbol{Z}_{ii}^B \end{bmatrix} \begin{bmatrix} \boldsymbol{u}_i^A \\ \boldsymbol{u}_c \\ \boldsymbol{u}_i^B \end{bmatrix} = \begin{bmatrix} \bar{\boldsymbol{f}}_i^A \\ 0 \\ 0 \end{bmatrix} \tag{1}$$

where $\boldsymbol{u}_c = \boldsymbol{u}_c^A = \boldsymbol{u}_c^B$ in this example. The subscript $_i$ denotes the *internal* DOF and the subscript $_c$ denotes the *coupling* DOF. When $\boldsymbol{u}_1$ is eliminated from equation 1, the following equation is found

$$\begin{bmatrix} \boldsymbol{Z}_{cc}^A + \boldsymbol{Z}_{cc}^B - \boldsymbol{Z}_{ci}^A \boldsymbol{Z}_{ii}^{A\,-1} \boldsymbol{Z}_{ic}^A & \boldsymbol{Z}_{ci}^B \\ \boldsymbol{Z}_{ic}^B & \boldsymbol{Z}_{ii}^B \end{bmatrix} \begin{bmatrix} \boldsymbol{u}_c \\ \boldsymbol{u}_i^B \end{bmatrix} = \begin{bmatrix} -\boldsymbol{Z}_{ci}^A \boldsymbol{Z}_{ii}^{A\,-1} \bar{\boldsymbol{f}}_i^A \\ 0 \end{bmatrix} \tag{2}$$

Next, substructure A is separated from the total system and the interface is fixed. This results in the following equation

$$\begin{bmatrix} \boldsymbol{Z}_{ii}^{A} & \boldsymbol{Z}_{ic}^{A} \\ \boldsymbol{Z}_{ci}^{A} & \boldsymbol{Z}_{cc}^{A} \end{bmatrix} \begin{bmatrix} \boldsymbol{u}_i^{Afi} \\ \boldsymbol{0} \end{bmatrix} = \begin{bmatrix} \bar{\boldsymbol{f}}_i^{A} \\ \boldsymbol{f}_{interface} \end{bmatrix} \tag{3}$$

where the superscript ^{fi} denotes that this is the displacement for the fixed interface experiment and the force $\boldsymbol{f}_{interface}$ is the force at the interface. When $\boldsymbol{u}_i^{Afi}$ is eliminated from equation 3, the following expression for the interface force is obtained

$$\boldsymbol{f}_{interface} = \boldsymbol{Z}_{ci}^{A} \boldsymbol{Z}_{ii}^{A^{-1}} \bar{\boldsymbol{f}}_i^{A} \tag{4}$$

which is equal to minus the force acting on $\boldsymbol{u}_c^A$ in equation 2. It can be shown that the dynamic equation 1 with the unknown force $\bar{\boldsymbol{f}}_i^A$ is equivalent to

$$\begin{bmatrix} \boldsymbol{Z}_{ii}^{A} & \boldsymbol{Z}_{ic}^{A} & 0 \\ \boldsymbol{Z}_{ci}^{A} & \boldsymbol{Z}_{cc}^{A} + \boldsymbol{Z}_{cc}^{B} & \boldsymbol{Z}_{ci}^{B} \\ 0 & \boldsymbol{Z}_{ic}^{B} & \boldsymbol{Z}_{ii}^{B} \end{bmatrix} \begin{bmatrix} \boldsymbol{u}_i^{Aequi} \\ \boldsymbol{u}_c{}^{equi} \\ \boldsymbol{u}_i^{Bequi} \end{bmatrix} = \begin{bmatrix} 0 \\ -\boldsymbol{f}_{interface} \\ 0 \end{bmatrix} \tag{5}$$

for what concerns substructure B. This proves that $\boldsymbol{u}_c$ and $\boldsymbol{u}_i^B$ from equation 1 are equal to $\boldsymbol{u}_c{}^{equi}$ and $\boldsymbol{u}_i^{Bequi}$ from equation 5. Physically this means that minus the measured interface forces should be applied as external forces, acting on the interface between substructure A and B.

So the dynamic response of substructure B can be obtained by solving the equivalent problem in equation 5, which only needs the interface forces that in most cases are much easier to measure than the internal forces.

The equations are now written with the dynamic stiffness of the structure. This made deriving this method much easier, because of the zero entries in the total dynamic stiffness matrix. For most real applications the dynamic flexibility is measured. Obtaining the dynamic stiffness from dynamic flexibility measurements can sometimes cause numerical problems, because it involves an inversion of the measurements. It is much easier to rewrite equation 5 in the dynamic flexibility form, which yields

$$\begin{bmatrix} \boldsymbol{Y}_{11} & \boldsymbol{Y}_{12} & \boldsymbol{Y}_{13} \\ \boldsymbol{Y}_{21} & \boldsymbol{Y}_{22} & \boldsymbol{Y}_{23} \\ \boldsymbol{Y}_{31} & \boldsymbol{Y}_{32} & \boldsymbol{Y}_{33} \end{bmatrix} \begin{bmatrix} 0 \\ -\boldsymbol{f}_{interface} \\ 0 \end{bmatrix} = \begin{bmatrix} \boldsymbol{u}_i^{Aequi} \\ \boldsymbol{u}_c \\ \boldsymbol{u}_i^{B} \end{bmatrix} \tag{6}$$

Technical Drawings

In this appendix the technical drawings are shown as given to the machine shop. They were produced within the given tolerances.

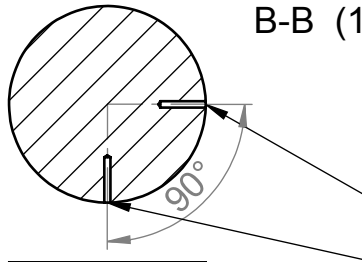

B-B (1 : 5)

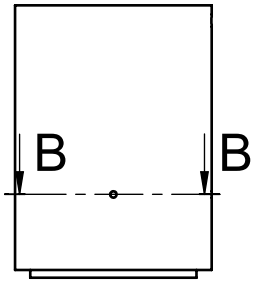

2 keer M5x30 tapgat
Haaks ten opzichte van elkaar

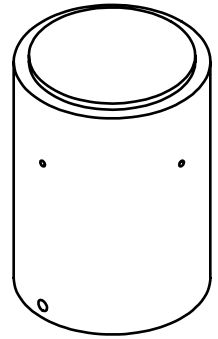

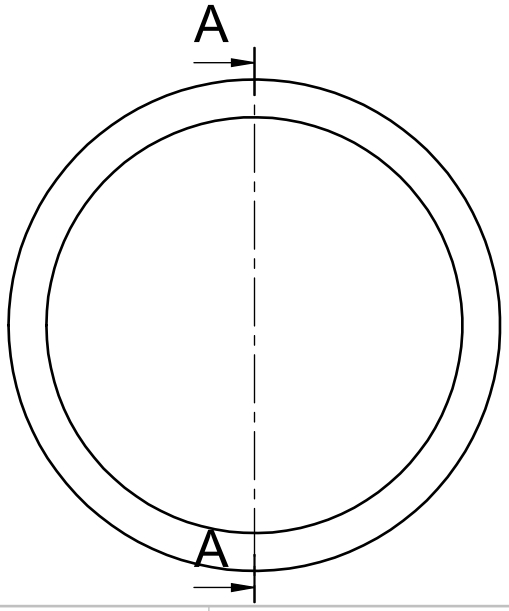

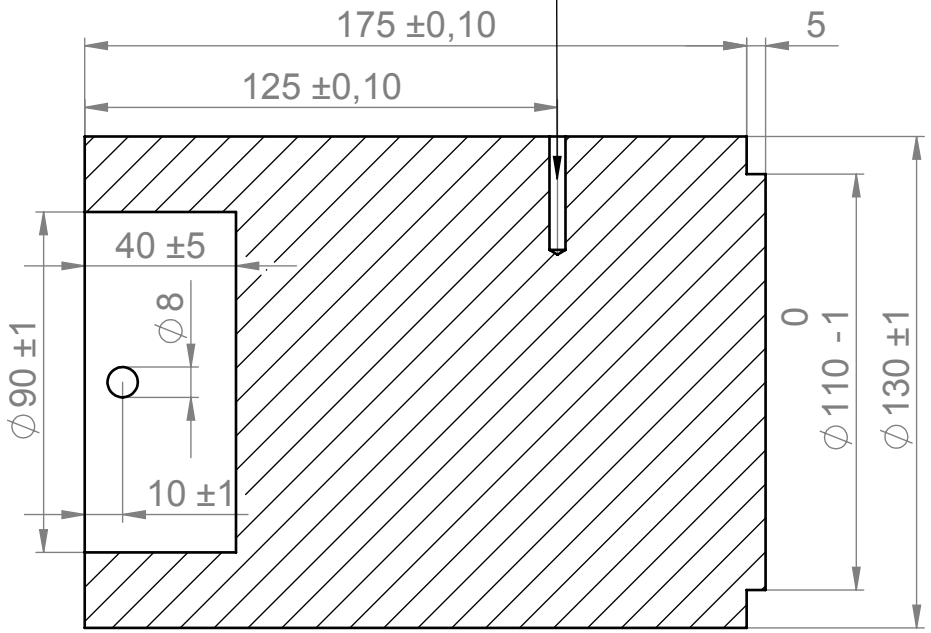

A-A

TU Delft Industrial Design Engineering	benaming **stand** uit standaard automaten staal Mag45 code: 0122 016 00 667	datum 19-12-2011	maateenheid mm
		schaal 1:2 / groep <<groep>> / formaat **A4**	tekeningnummer 1
		getekend Anthonie Boogaard	

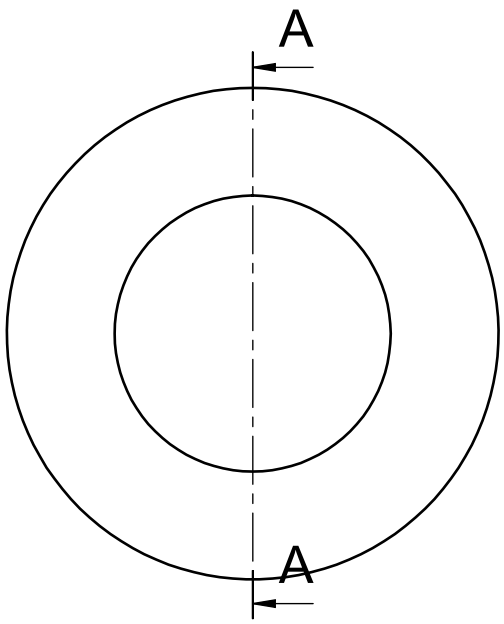

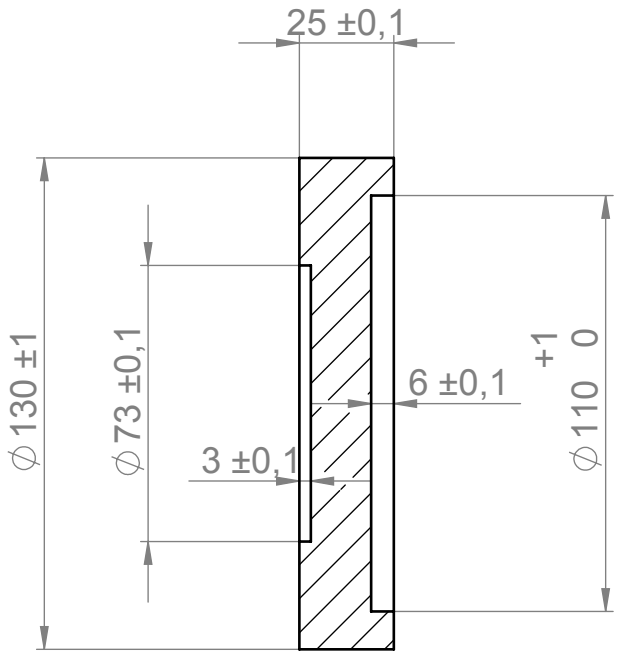

A-A

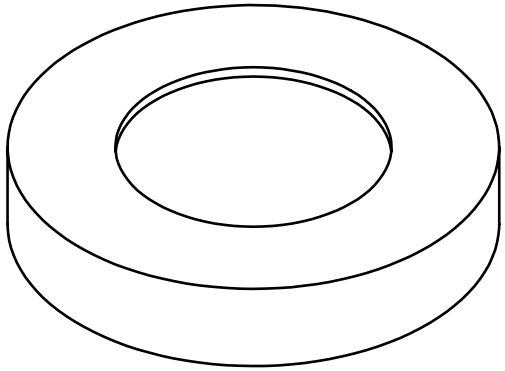

TU Delft Industrial Design Engineering	benaming **Base** uit gehard staal Mag45 code: 0122 038 00 108	datum 19-12-2011	maateenheid mm
		schaal 1:2 / groep <<groep>> / formaat **A4**	tekeningnummer 2
		getekend Anthonie Boogaard	

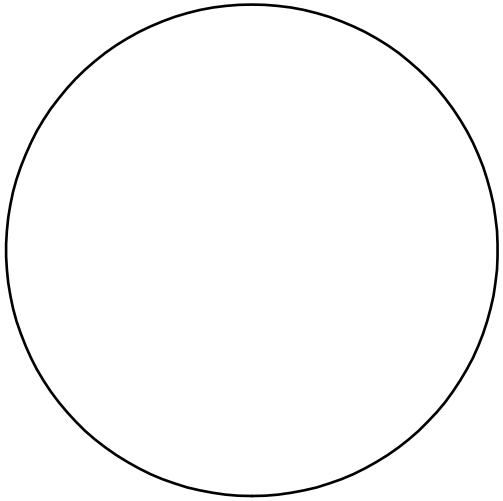

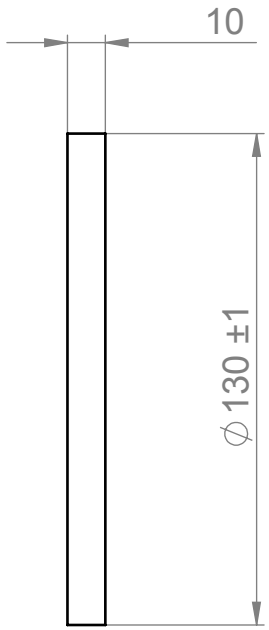

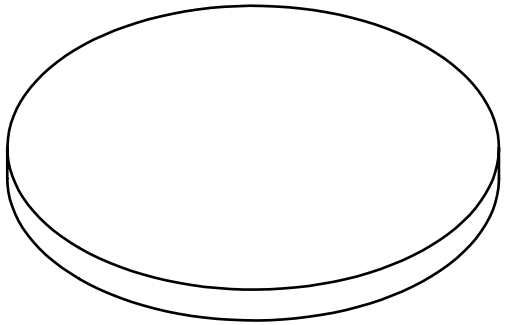

TU Delft Industrial Design Engineering	benaming top uit gehard staal Mag45 code: 0122 038 00 108	datum 19-12-2011	maateenheid mm
		schaal 1:2 / groep <<groep>> / formaat A4	tekeningnummer 3
		getekend Anthonie Boogaard	

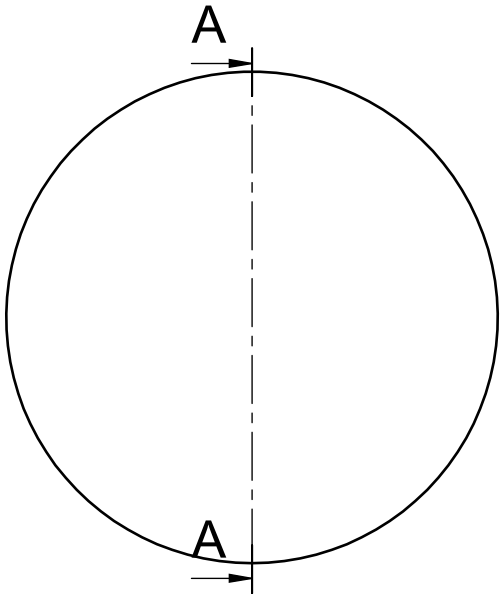

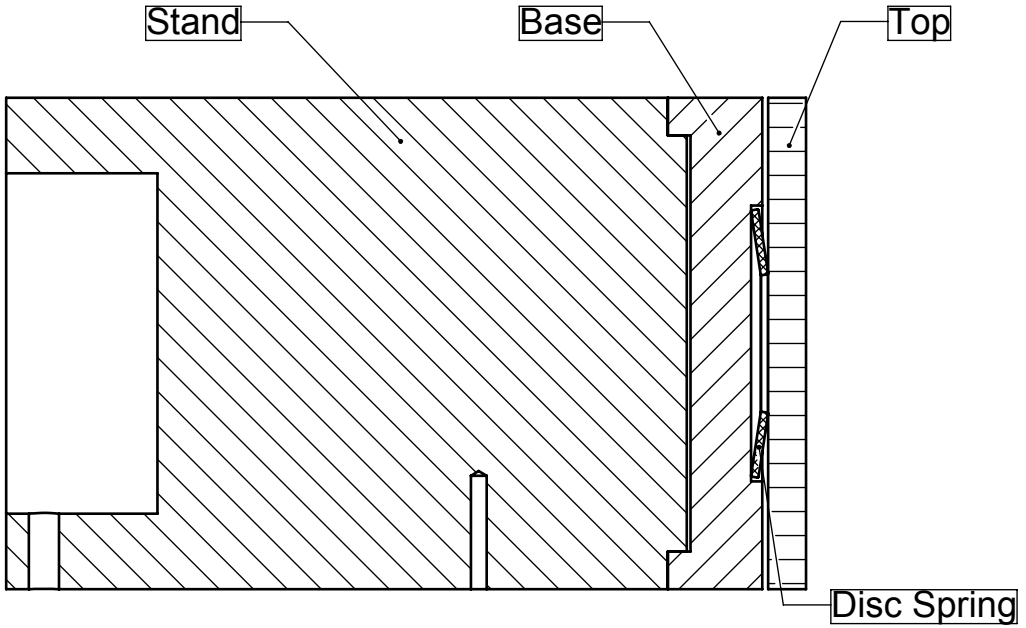

A-A

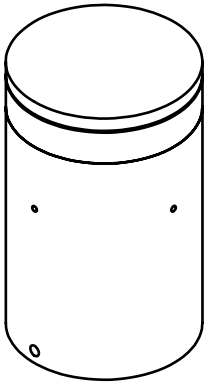

TU Delft Industrial Design Engineering	benaming totaal		datum 19-12-2011	maateenheid mm
		schaal 1:2	groep <<groep>>	formaat A4
		getekend Anthonie Boogaard		tekeningnummer 4

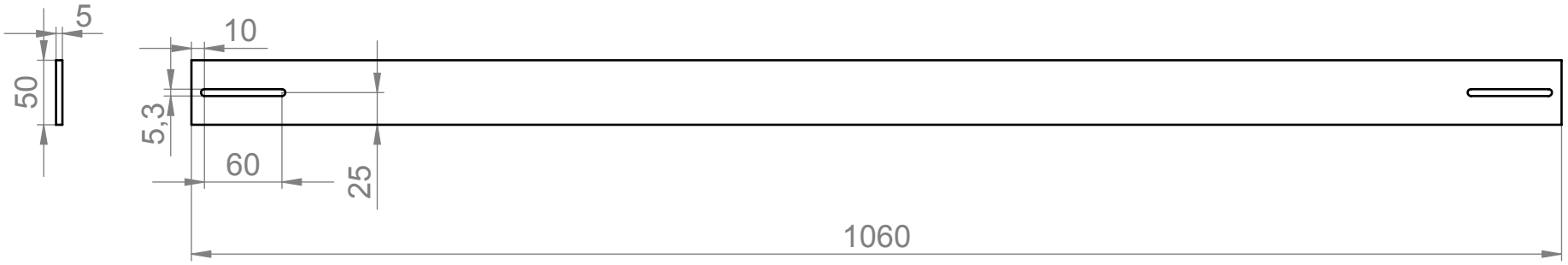

TU Delft Industrial Design Engineering	benaming **spacer** Uit standaard plat staf mag45 code 0112 026 25 119		datum 19-12-2011	maateenheid mm
		schaal 1:5	groep <<groep>>	formaat **A4**
		getekend Anthonie Boogaard		tekeningnummer 5

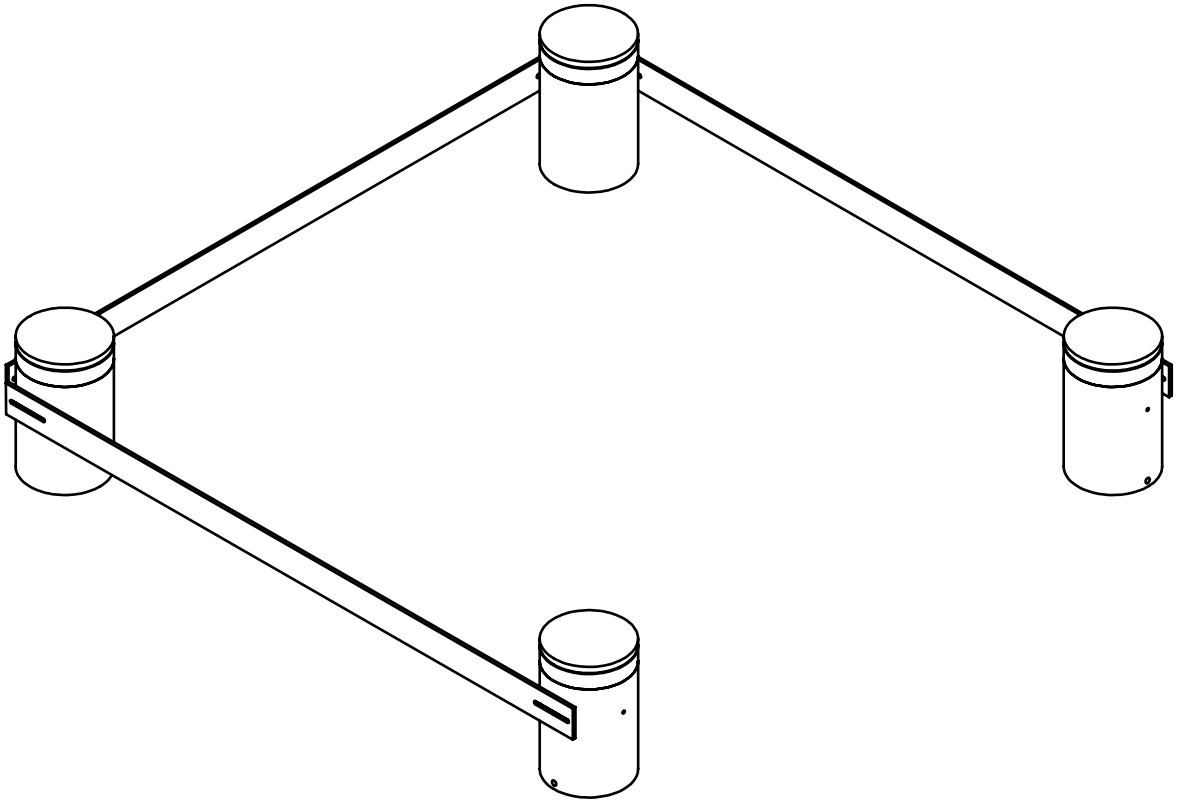

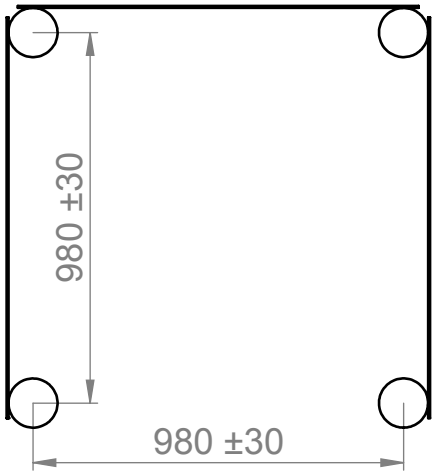

TU Delft Industrial Design Engineering	benaming totaal2		datum 19-12-2011	maateenheid mm
		schaal 1:10	groep <<groep>>	formaat A4 / tekeningnummer 6
		getekend Anthonie Boogaard		

Measurement set up

Impact hammer The measurement hardware is mainly selected on availability. Because the system is quite big, the biggest hammer available is used, which is a PCB 086D50. The specifications are given in tabel 2. With the soft tip, this will excite frequencies up to 200 Hz. The signal is conditioned by a battery powered signal conditioner from PCB, type 480C02.

	PCB 086D50
Sensitivity (± 15 %)	0.23 mV/N
Measurement range	± 22,240 N pk
Weight	5.5 kg

Table 2: Specifications PCB 086D50

Floor response The accelerometers to measure the response of the floor are charge transducer from Brüel & Kjær, type 4379. The specifications are given in table 3. These accelerometers were mounted to a aluminium plate with a stud. This plate as only three small contact points, so local irregularities in the floor will not cause any wobble of the sensor. The signals of the sensors are fed through a Nexus four-channel charge conditioning amplifier also from Brüel & Kjær, type 2692. The amplifier is set to 1 V/ms^{-2}.

	BK 4379
Sensitivity	31.6 pC/ms^{-2}
Measurement range	0.2 to 2800 Hz
Dynamic range	$0.1 \cdot 10^{-3}$to $5 \cdot 10^{3}$ ms^{-2}
Transverse sensitivity	¡ 4%

Table 3: Specifications BK 4379

Data acquisition The data acquisition system is a four channel Siglab system. As explained in section 8.1, not the Dynamic Signal Anlyzer (VNA) is used, but the time traces are captured with the Long Record Capture (VCAP) function. The bandwidth is set to 200 Hz and the block length is 8 seconds. The trigger is set on every frame and the

delay is 1 %. 5 frames are captured for every impact. The dynamic range for the input is set to 2.5 V and for the output to 10 V.

In the post processing, only 4 seconds of the signal is used. The other 4 seconds can be used later if a higher frequency resolution is needed. Because the pre-trigger was 1 % of 8 seconds, this should also be compensated. The window is a block exponential window. The block is 0.2 seconds and the magnitude at the end of the measurement block is .1 %.

Floor vibrations To measure the vibrations of the floor, Endevco type 86 accelerometers are used. This is an *ultra low-noise* piezoelectric accelerometer, which is designed to measure low frequency vibrations on structures. The specifications are given in table 4. This sensor is an Isotron sensor, which needs a constant current to work properly. These sensors are therefore connected to a Nexus four-channel DeltaTron conditioning amplifier from Brüel & Kjær, type 2693. Again the time traces are captured with the VCAP function of Siglab. This time, without a trigger a continuous time trace of 1600 seconds is captured.

	Endevco 86
Sensitivity	10 V/g
Measurement range ($\pm$1 dB)	0.0052 to 100 Hz
Dynamic range	$\pm 0.5g$

Table 4: Specifications Endevco 86